

NMR Resonance Assignments and Secondary Structure of a Mutant Form of the  
Human KCNE1 Channel Accessory Protein that Exhibits KCNE3-like Function

By

Cheryl Lynn Law

Dissertation

Submitted to the Faculty of the  
Graduate School of Vanderbilt University

In partial fulfillment of the requirements

For the degree of

DOCTOR OF PHILOSOPHY

In

Biochemistry

May 10th, 2019

Nashville, Tennessee

Approved by

Charles R. Sanders, Ph.D.

Walter J. Chazin, Ph.D.

Lauren P. Jackson, Ph.D.

Jens Meiler, Ph.D.

Kevin L. Schey, Ph.D.

## DEDICATION

I dedicate this dissertation to my loving and inspirational family. To my parents who showed unwavering support, and my whole life told me ‘You can change what you want to be every day as long as you strive for greatness.’ When I was stressed, they made me laugh. When I lost focus, they kicked me back on track. When I had successful days, they were my biggest cheerleaders. There is no amount of thanks that will show my true appreciation for them. To my brother, Tony, who gave me the inspiration to go into science. His brilliant mind always challenged me to strive for new challenges and to have fun with it. To my sister-in-law, Courtney, who has given my inspiration above and beyond graduate school. To my amazing husband, Kendall, who showed me a world that I never knew existed and believed in me when I thought it was impossible. For his patient and steadfast support of me, especially during our first years of marriage being hundreds of miles apart. I can’t wait to grow, learn, and travel the rest of the world with you. To all my friends, family, in-laws, Wine Chap friends, MegaLab friends, and Junior League friends, thank you for being amazing friends and influences in my life.



## ACKNOWLEDGMENTS

This dissertation work would not be possible without funding from IMSD, the NIH through RO1 grants to Chuck Sanders, and the Biochemistry department. I have been tremendously fortunate that have worked under the tutelage of Dr. Charles R. Sanders (Chuck) during my graduate school career. His guidance and support have been invaluable in my development as a scientist and personal development throughout the years.

I must give great thanks to past and present members of the Sanders' lab and the MegaLab for your friendship, scientific development, aid in my project development and talking through my ideas. A special thanks to former Sanders lab member Keenan for his tremendous amount of expertise in just about everything, having the patience and unhesitant willingness teach and help me at any time, and giving me the courage (whether he knew it or not) to be positive and push forward. Other special thanks to former Sanders member, Dungeng Peng, for mentoring me, great conversations, his infectious positivity, and knowing I was capable despite my insecure.

Thank you to Linda Sealy and the entire IMSD for allows supporting and encouraging me the entire time and teaching me to advocate for myself.

To my mentors outside of the science field, Ben Rosenblum, Alex Cate, Gary Rawlings, and Michelle Lane who have helped me develop and identify career goals.

To all my committee members who gave guidance and encouragement throughout my scientific career and helped me grow.

## Acknowledgment of Funding

This work was funded by the National Institute of Health (RO1 HL122010 and RO1 DC007416) awarded to Dr. Charles R. Sanders.

## Publications

The contents of Chapter 3 are published in *Biomolecular NMR Assignments* (Law, 2019).

1. Peng D, Kim J, Kroncke BM, **Law CL**, Xia Y, Droege KD, Van Horn WD, Vanoye CG, Sanders CR (2014) Purification and structural study of the voltage-sensor domain of the human KCNQ1 potassium ion channel. *Biochem* 53 (12), 2032-2042.
2. Mittendorf KF, Marinko JT, Hampton CM, Ke Z, Hadzieselimovic A, Schleich JP, **Law CL**, Li J, Wright JL, Sanders CR, Ohi MD (2017) Peripheral myelin protein 22 alters membrane architecture. *Science Advances* 3(7),e1700220.
3. **Law CL**, Sanders CR (2019) NMR resonance assignments and secondary structure of a mutant form of the human KCNE1 channel accessory protein that exhibits KCNE3-like function. *Biomolecular NMR Assignments*.  
<https://doi.org/10.1007/s12104-018-09867-6>.

## Table of Contents

	Page
TITLE PAGE.....	i
DEDICATION.....	ii
ACKNOWLEDGMENTS.....	iii
ACKNOWLEDGMENT OF FUNDING.....	iv
PUBLICATIONS.....	iv
LIST OF FIGURES.....	viii
LIST OF SUPPLEMENTARY FIGURES.....	x

### Chapter

1. Introduction.....	1
1.1 Membrane Proteins.....	1
1.2 Potassium Channels.....	1
1.3 Kv Voltage-Gated Channels.....	4
1.4 KCNQ1 Function and Relation to Human Disease.....	5
1.3 KCNE Family.....	7
1.5 Mechanism of KCNQ1 Opening.....	8
1.6 KCNE1 and KCNE3 Functional Regions.....	10
2. Methods and Materials.....	13
2.1 Reagents and Materials.....	13
2.2 Cloning of KCNE1 <sub>FTL→TVG</sub> (E1 <sub>FTL→TVG</sub> ).....	13
2.3 Overexpression of KCNE1 <sub>FTL→TVG</sub> .....	14
2.4 Purification of E1 <sub>FTL→TVG</sub> into LMPG Detergent Micelles.....	14
2.4.1 Solubilizing Inclusion Bodies with KNCE1 <sub>FTL→TVG</sub> .....	14
2.4.2 Purification and Buffer Exchange of E1 <sub>FTL→TVG</sub> .....	15
2.4.3 SDS Polyacrylamide Gel Electrophoresis of E1 <sub>FTL→TVG</sub> .....	17
2.5 NMR Sample Preparation and NMR Spectroscopy.....	16
2.6 Isotopic Labeling of E1 <sub>FTL→TVG</sub> and NMR Resonance Assignments.....	17
2.6.1 Uniformly <sup>13</sup> C, <sup>15</sup> N, isotopically-labeled E1 <sub>FTL→TVG</sub> .....	17
2.6.2 Inverse Labeling of E1 <sub>FTL→TVG</sub> .....	17
2.6.3 Specific Amino Acid Labeling of E1 <sub>FTL→TVG</sub> .....	17
2.6.4 Experiments for Assignments, Single Amino Acid Labeling, and Inverse Labeling.....	18
2.7 T <sub>1</sub> and T <sub>2</sub> <sup>15</sup> N Relaxation Measurements.....	18
2.8 Gd-DTPA 16-DSA.....	18

2.9 Clean-EX PM of E1 <sub>FTL→TVG</sub> and E1 Wild-type.....	19
3 Results of Cloning, Characterization, and Assignments of KCN E1 <sub>FTL→TVG</sub> .....	20
3.1 Introduction.....	20
3.1.1 NMR Assignments: Background.....	20
3.2 Results.....	22
3.2.1 Cloning of E1 <sub>FTL→TVG</sub> .....	22
3.2.2 Overexpression of the E1 <sub>FTL→TVG</sub> Protein.....	24
3.2.3 Purification of KCN E1 <sub>FTL→TVG</sub> into Detergent Micelles.....	25
3.2.4 NMR Sample Preparation and Spectroscopy.....	27
3.2.5 Uniform Isotopic Labeling and Sample Preparation.....	28
3.2.6 3D TROSY Backbone Experiments for Making Resonance Assignments.....	34
3.3 Single and Inverse Amino Acid Labeling.....	41
3.3.1 Single Amino Acids Labeling.....	41
3.3.2 Inverse Isotopic Labeling of Specific Amino Acids.....	44
3.4 Chemical Shift-Based Secondary Structure Analysis.....	47
4 Preliminary Data, Discussion and Future Directions.....	50
4.1 Purification Data and Discussion.....	50
4.1.1 Purification.....	50
4.1.2 Assignments.....	50
4.1.3 Secondary Structure of E1, E3, and E1 <sub>FTL→TVG</sub> .....	52
4.2 Additional Preliminary Data and Discussion.....	52
4.2.1 T <sub>1</sub> and T <sub>2</sub> Relaxation.....	52
4.2.2 Amide Hydrogen Exchange Measurements.....	56
4.2.3 Comparison of E1, E3, and E1 <sub>FTL→TVG</sub> .....	58
4.3 Secondary Structure of E1, E3, and E1 <sub>FTL→TVG</sub> .....	60
4.3.1 Paramagnetic Probe Access Experiments.....	60
4.3.2 Structural Restraints.....	61
Appendix	
A. Supplementary Figures.....	57
REFERENCES.....	68

## List of Figures

Figure 1: Potassium Ion Flow Into Channel.....	3
Figure 2: Topology of Kv potassium channel single alpha unit. ....	4
Figure 3: Mutations In KCNQ1 That Lead To Human Disease. ....	6
Figure 4: Schematic of KCNQ1.....	7
Figure 5: Conductance of KCNQ1 Channel When Bound to Ancillary Subunits.....	8
Figure 6: Models of KCNQ1 Bound to KCNE1 in Open and Closed Conformation.....	9
Figure 7: Electrophysiology of KCNE1 and KCNE3 With Select Residues Switched.....	11
Figure 8: Schematic of the pET16b Cloning Vector.....	23
Figure 9: Sequence Results Confirming All Mutations and Sequencing Were Correct..	24
Figure 10: Purification Gel of WT E1 With Native C106.....	25
Figure 11: Purification of E1 <sub>FTL→TVG</sub> in LMPG Micelles.....	27
Figure 12: 2D <sup>1</sup> H, <sup>15</sup> N-TROSY Spectrum of E1 <sub>FTL→TVG</sub> .....	28
Figure 13: Triple Labeled Sample of E1 <sub>FTL→TVG</sub> .....	29
Figure 14: Overlay of the Double-labeled Samples with 2 Versus 4 Grams of <sup>13</sup> C <sub>6</sub> - glucose.....	31
Figure 15: Overlay of <sup>15</sup> N-E1 <sub>FTL→TVG</sub> and <sup>13</sup> C, <sup>15</sup> N-E1 <sub>FTL→TVG</sub> containing 4 grams of <sup>13</sup> C <sub>6</sub> - glucose.....	32
Figure 16: Overlay of WT KCNE1 and E1 <sub>FTL→TVG</sub> . ....	33
Figure 17: Schematic of 3D Experiments.....	35
Figure 18: Triple Resonance Experiment HNCA.....	36
Figure 19: Triple Resonance Experiment HNCACB.....	37
... Figure 20: 3D Experiment HNCO.....	38
Figure 21: K70 Overlapping Peaks Identified in HCNO.....	39

Figure 22: Sequential Backbone Walking of Five Residues in an HNCA Spectrum.....	40
Figure 23: SDS PAGE Gel of E1 <sub>FTL→TVG</sub> Samples Labeled with One of 5 Specific Amino Acids.....	42
Fig 24: Single Amino Acid Label Sample for Val.....	43
Figure 25: Inverse Labeling of Thr.....	45
Figure 26: Resonances Assignments of E1 <sub>FTL→TVG</sub> .....	46
Figure 27: Topology of Missing E1 <sub>FTL→TVG</sub> Residues.....	47
Figure 28: Chemical Shift Analysis Plot using TALOS-N.....	49
Figure 29: T <sub>2</sub> Relaxation Data for E1 <sub>FTL→TVG</sub> . ....	53
Figure 30: T <sub>2</sub> Relaxation Data for Wild Type KCNE1.....	54
Figure 31: T <sub>2</sub> Relaxation Data for Wild Type KCNE3.....	54
Figure 32: CLEANEX-PM 25ms Data for WT E1.....	58
Figure 33: CLEANEX-PM 25ms Data for E1 <sub>FTL→TVG</sub> .....	58
Figure 34: Experimentally Determined KCNE1 and KCNE3 and Topology of E1 <sub>FTL→TVG</sub> .....	59

## List of Supplementary Figures

Supplemental Figure 1: Specific Amino Acid Labeling of Ala.....	65
Supplemental Figure 2: Specific Amino Acid Labeling of Leu.....	66
Supplemental Figure 3: Specific Amino Acid Labeling of Phe.....	67
Supplemental Figure 4: Specific Amino Acid Labeling of Met.....	68
Supplemental Figure 5: Specific Amino Acid Labeling of Ile.....	69
Supplemental Figure 6: $T_1$ and $T_2$ of $E1_{FTL \rightarrow TVG}$ Decay Curves.....	70
Supplemental Figure 7: $E1_{FTL \rightarrow TVG}$ Spectrum of Y74C Mutation.....	71
Supplemental Figure 8: $E1_{FTL \rightarrow TVG}$ Spectrum of Y65C Mutation.....	72
Supplemental Figure 9: $E1_{FTL \rightarrow TVG}$ Spectrum of S64C Mutation.....	73
Supplemental Figure 10: $E1_{FTL \rightarrow TVG}$ Spectrum of Y46C Mutation.....	74
Supplemental Figure 11: $E1_{FTL \rightarrow TVG}$ Spectrum of A44C Mutation.....	75

## Chapter 1

### Introduction

#### **1.1 Membrane Proteins**

Membrane proteins, while often difficult to study biochemically, play a crucial role in the dynamic and diverse cell membrane. Of all human genes, about  $\frac{1}{3}$  of these genes encode for membrane proteins [1] and of this subset only 3% have known 3D structures [2]. While many scientists are interested in studying membrane proteins as pharmacological targets, they present several challenges that have slowed their characterization. One of the main challenges is that membrane proteins often express in very low levels, making them difficult to study biochemically. Another factor relates to the fact that these proteins have both hydrophobic and hydrophilic regions that need to be satisfied by the surrounding solvent. This requires either studying the protein in the native membrane or isolation into a model membrane environment such as bilayered lipid vesicles or micelles that will satisfy both the hydrophobic transmembrane region and also its hydrophilic loops [3]. Solubilizing proteins into membrane mimetics like micelles can be a valuable tool when subjecting membrane proteins for biochemical and structural studies, which can provide the basis for better understanding membrane proteins.

#### **1.2 Potassium Channels**

Potassium channels are a class of integral membrane proteins that exist in virtually all species in both excitable and non-excitable cells [4]. These potassium channels are responsible for transporting specifically  $K^+$  ions from in the extracellular space to the intercellular space separated by the plasma membrane. Potassium channels are broken down into 3 classifications based on the channels structure and functions. One class is the inward rectifying channel ( $K_{ir}$ ) that contains 2 transmembrane helices and is regulated by intercellular factors. Another is the tandem-pore domain channel ( $K_{2P}$ ) that consist of

4 transmembrane helices. Lastly is the voltage-gated Kv channel which consist of 6 transmembrane helices and is activated by the change in membrane depolarization [5, 6] The classes are divided into 2 parts: pore-forming and regulatory. Pore-forming domain allows the passage of  $K^+$  ions through the plasma membrane. This domain is highly conserved throughout most potassium channels and many scientist have created models of this domain [6]. The regulator domain is structurally different throughout the potassium channels categories but its role is to detect diverse stimuli within the cell like membrane potential. This regulator domain is often what differentiate  $K^+$  channels [6].

One element that connects most potassium channels is the highly conserved pore domain and how it functions. The pore domain consist of 2 alpha helical transmembrane regions that are connected by a flexible unstructured region, the p-loop. The P-loop acts as the selectivity filter and has a highly conserved TVGYG sequence that plays a critical role in selectively allowing potassium ions to pass through and prevents passage for all other ions.

This selectivity filter contains 4  $K^+$  binding sites (S1-S4) that are evenly spaces. These binding sites are formed by making a “cage” of 8 carbonyl  $O_2$  ions from the TVGYG conserved region. In order of  $K^+$  ions to pass through the small filter water molecules must be removed. The carbonyl  $O_2$  of the TVGYG motif satisfy the energetic cost associated with the dehydration of the  $K^+$  ions allowing them to pass through the selective filter where they are rehydrated when entering the water filled vestibule (Figure 1). Ions like  $Na^+$  are not able to pass through due to the smaller size of  $Na^+$  that does not bond strongly enough to the TVGYG motif [7, 8]. The MacKinnon group showed that only 2 potassium ions can occupy the 4 S1-S4 binding sites at a time, either at the S1 and S3 sites or the S2 and S4 sites. When concentration is high, ions move in an orchestrated manner from 1,3 - configuration to 2,4- configurations [8-11] (Figure 1). After rehydration in the water filled core, the  $K^+$  ion wait for the channel to open before it enters into the intracellular compartment.

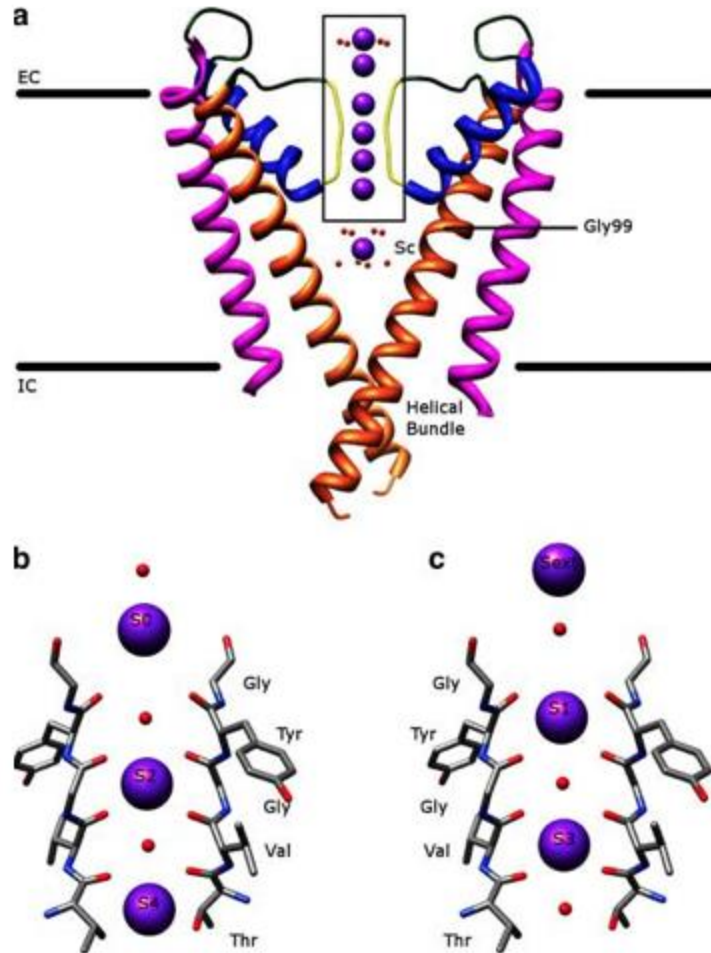


### Figure 1: Potassium Ion Flow Into Channel

This figure shows the transmembrane channel regions of potassium channel KcsA. Part a shows the experimentally determined structure of the pore region of KcsA. The magenta helix represents the outer helix. The pore helix is in blue, the inner helix is orange, and the selectivity filter is in yellow.  $K^+$  ions are represented in purple and water molecules in red in panels a, b, and c. Panel a shows  $K^+$  ions being dehydrated by the selectivity filter and rehydrated in the channel pore. Panel b and c show the 1,3- and 2,4-configuration of potassium passing through the TVGYG selectivity filter. Figure from reference 6.

### 1.3 Kv Voltage-Gated Channels

Kv voltage-gated channels are a diverse group that is split into 12 main families (K1-K12) [12] and contribute to several cellular processes from excitable cells, apoptosis [13], cell growth and differentiation [14], and cardiac activity [15]. Kv channels are unique from other potassium channels in that they are activated differently and have a more sophisticated transmembrane topology compared to other K<sup>+</sup> channels. When compared to KcsA channels, Kv channels are activated by membrane voltage creating a depolarized cell while KcsA is activated by lowered pH [16, 17] and Kv has a 6 transmembrane topology while KcsA has a more simple 2 transmembrane topology [18]. The 6 transmembrane helices single unit form a tetramer to form the full channel with two independent domains. Helices S1-S4 make up the voltage sensing domain (VSD) and undergoes conformational changes when charges residues on the S4 helix detect changes in membrane potential. Helices S5 and S6 make up the pore domain (PD) that allows K<sup>+</sup> ions to flow through. Like other potassium channels, S5 and S6 are connected by a p-loop or selectivity filter that is discussed in more detail in section 1.2 (Figure 2). The VSD and the pore-domain are connected by an S4-S5 linker that plays an important role in channel opening.

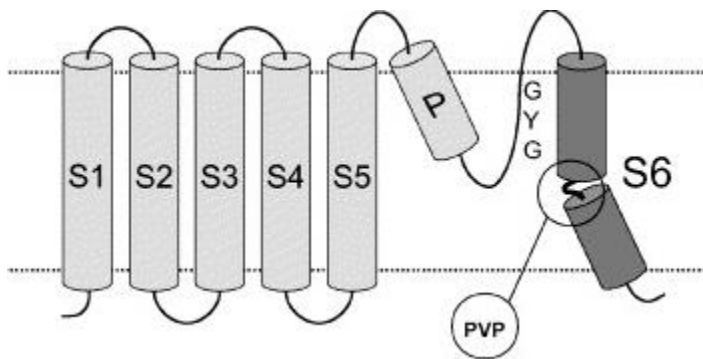


**Figure 2: Topology of Kv potassium channel single alpha unit.**

This figure shows the topology of a single alpha unit of a Kv channel where S1-S4 make up the voltage sensor domain and S5 and S6 make up the pore domain. S5 and S6 are connected by the p-loop containing the GYG motif that coordinates K<sup>+</sup> ions and provides selectivity for the channel. S6 helix displays the PVP conserved motif that leads to a kinked S6 helix. Figure from reference 19.

Models and simulation of an isolated S6 helix suggest that the helix is kinked right at the highly conserved PVP motif and allows this hinge region to undergo dynamic changes [20-22]. Experimental studies have shown that, while less flexible, S6 PVP region still remains kinked when in its tetrameric form [23, 24] and may be important for gating. The S4 helix, a part of the S1-S4 VSD, contains 4 positively evenly spaced charged Arg residues. In response to changes in the action potential, S4 helix undergoes an rotational and upwards movements. This S4 movement causes conformational changes within the entire VSD. This conformational change of the VSD is connected to the pore domain and leads to channel open. Upon depolarization, all Kv channels transition from a closed, to intermediate, then open conformational state where ions are only conducted in the open state. KCNQ1, the first of 5 discovered in the KCNQ subfamily, is unique from other Kv channel and within its KCNQ subfamily because it has the ability to be voltage dependent and voltage independent.

#### **1.4 KCNQ1 Function and Relation to Human Disease**

KCNQ1 (Q1), a member of the Kv channel family, is a 676 amino acid voltage-gated potassium channel that forms functional homotetramers in the plasma membranes of vertebrates. It is expressed in several tissues throughout the body including the heart, lungs, and intestine. Mutations in this channel can have a significant and distinct effect on human health. A unique property of the normally voltage-gated KCNQ potassium channel family is that, when associated with certain ancillary proteins, they can be activated independent of changes in transmembrane voltage and thus can serve as “leak” channels [25]. Because Q1 is widely expressed, both gain-of-function and loss-of-function mutations in the Q1 channel or its ancillary proteins can lead to health issues such as atrial fibrillation [26], deafness [27] and cardiac arrhythmias, such as long QT syndrome, leading to cardiac arrest. More mild health issues like poor balance and abnormalities in the inner ear [28] and intestines [29] have also been noticed in KCNQ1 mutant mice (Figure 3). The fascinating relationships between Q1 function and its binding partners and their implications for human health have made this channel and its binding partners the targets of many studies.

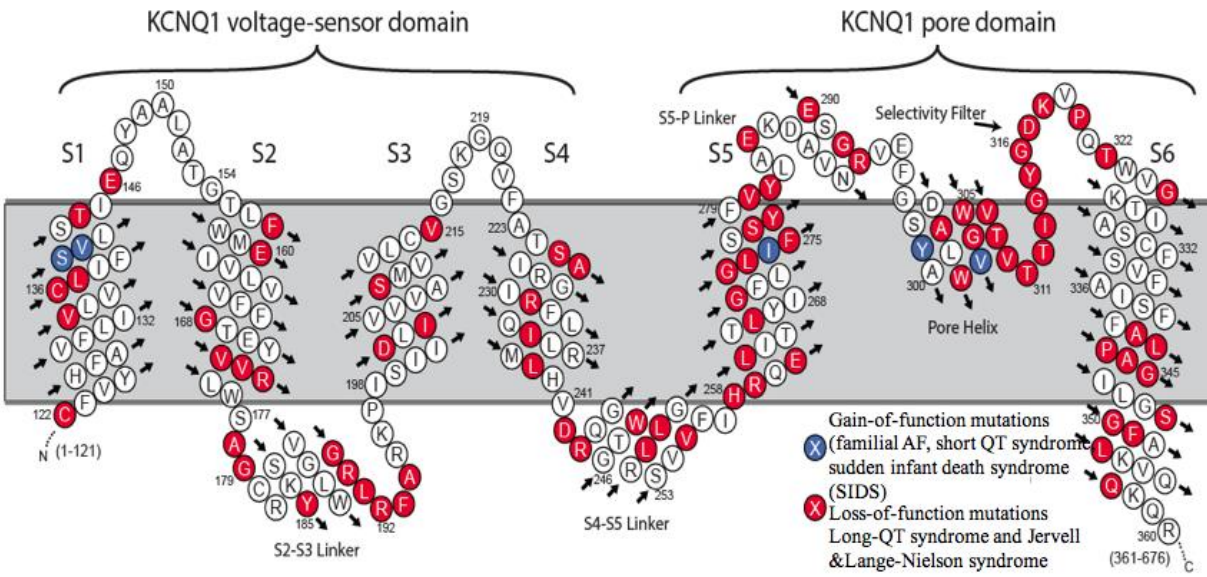


**Figure 3: Mutations In KCNQ1 That Lead To Human Disease.**

This figure depicts several mutations in KCNQ1 that lead to human disease. Many of these mutations are loss-of-function mutations (red sites), while fewer are gain-of-function mutations (blue sites). These mutations are spread throughout both the voltage-sensor (S1-S4) and pore domain and cause disease with varying degrees of severity.

Q1 has six transmembrane segments, with the first four (S1-S4) comprising the voltage sensor domain and the last two (S5, S6) contributing to the pore that forms the ion conduction pathway (Figure 3, Figure 4). When in its functional, homotetrameric form, the VSD domains form 4 nodules on the outside of the pore domain. The transmembrane S4 helix of the voltage sensory domain (S1-S4) contains four positively charged residues that can sense the electrical potential of the membrane and undergo a conformational change from its resting configuration to the activated state when the transmembrane electrical potential transitions from a negative to a positive value during the action potential. The activation of the voltage sensor domain is coupled via the S4-S5 connector to the opening of the channel gate in the pore domain, resulting in activation of potassium ion conduction by the channel. The pore domain includes a “P-loop” between S5 and S6 helices that provides the  $K^+$  ion selectivity of the channel [30, 31] (Figure 4).

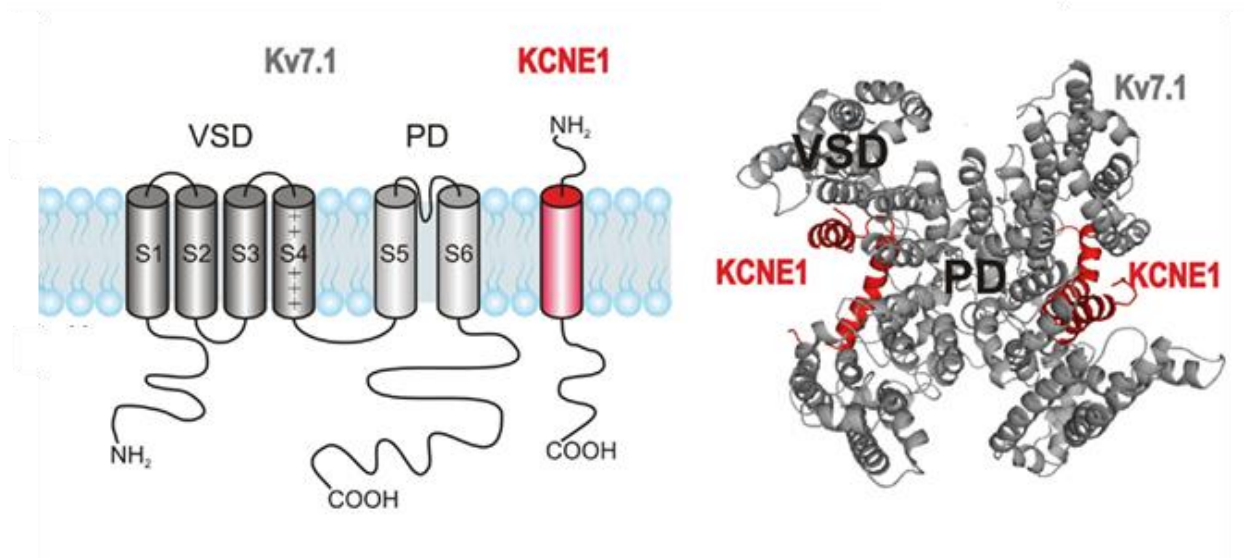


**Figure 4: Schematic of KCNQ1**

(Left) S1-S4 make up the voltage sensor domain while S5 and S6 make up the pore domain. These two domains are coupled by the S4-S5 linker. S4 has multiple positive charges that sense the voltage, triggering channel opening. (Right) This panel shows the channel homotetramer with one of Q1's binding partners, KCNE1, bound to the clefts between two VSD. The figure is from reference 32.

## 1.5 KCNE Family

Under physiological conditions, Q1 can be modulated by any member of the KCNE family, with KCNE1 (E1) and KCNE3 (E3) being the most well-studied. Members of the KCNE family have a single TM alpha helix and bind homotetrameric Q1 to form a complex, possibly with a 4:2 KCNQ1:KCNE subunit stoichiometry [33]. While some studies suggest the KCNQ1:KCNE complex forms in a 4:4 ratio [34, 35], several other studies observed steric clashes in a 4:4 complex and propose an alternative 4:2 KCNQ1:KCNE ratio [36-39]. It is believed that the KCNE site is located between the VSD nodules right above the S4-S5 linker [40, 41, 42]. While E1 and E3 are homologs, their tissue localization and channel modulatory effects are strikingly distinct. The Q1/E1 complex is expressed in cardiomyocytes where the complex results in delayed channel activation and an increase open state conductivity (Figure 5). The Q1/E1 complex provides the repolarizing IKs current of the cardiac action potential of cardiomyocytes [43, 44] and is essential for heart muscle contraction. On the other hand, the Q1/E3 complex is found in epithelial cells of the colon, stomach, and kidney, where association of E3 with Q1 leads to a constitutively active “leak” channel that is critical for the secretion of potassium and chloride ions in

epithelial cell fluid and salt homeostasis [30, 31, 45] (Figure 5). While less studied, KCNE4 is mainly expressed in the uterus, where it binds to the Q1 channel to inhibit the channel from opening when in the presence of calmodulin [46]

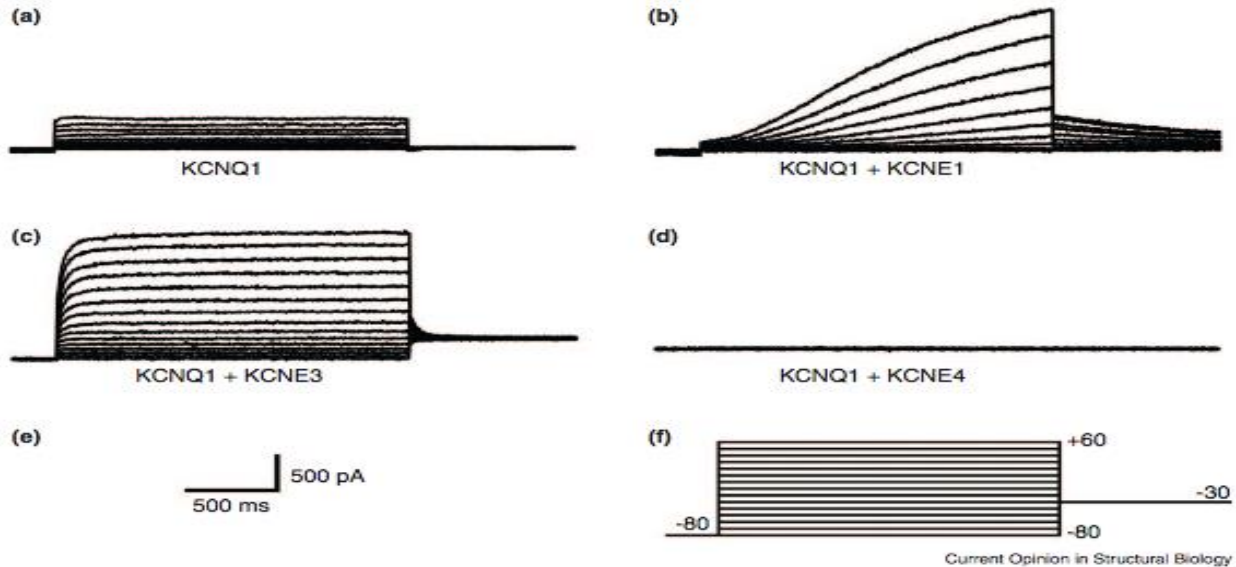


**Figure 5: Conductance of KCNQ1 Channel When Bound to Ancillary Subunits**

This figure shows the conductance of the KCNQ1 channel in the absence of ancillary subunits and when bound to KCNE1, KCNE3, and KCNE4. (a) shows a homotetrameric KCNQ1 channel in the absence of any ancillary proteins. This figure shows a channel that opens rapidly but has very low conductance. (b) depicts the current from the KCNQ1/KCNE1 complex. Much higher conductance can be seen in the channel, but also delayed activation. (c) shows current for the KCNQ1/KCNE3 complex, exhibiting increased conductivity and constitutive activation: “leak” channel behavior. (d) KCNQ1/KCNE4 is shown to be a completely inhibited channel. This figure is adapted from reference 42.

## 1.6 Mechanism of KCNQ1 Opening

Our current understanding of how the Q1 channel opens begins with the S4 helix. The positively charged residues on S4 sense the hyperpolarized potential of the cell and undergo an upward rotational conformational change. The helix movement causes a lateral pull on the S4-S5 linker that couples the VSD and pore domain via the S6 helix and thus leads to channel opening. The E1 TM C-terminal and N-terminal domains have extensive interactions with the Q1 channel and this may play a critical role in the delayed activation of the channel. The critical E1 functional residues T58 and L59 are thought to interact with S338, F339, and F340 of S6 in Q1 [32, 47, 48, 41]. E1 has been proposed

to sit between the VSD nodules right on top of the S4-S5 linker [41, 42] and is believed to impede channel opening but not the S4 movement. The N-terminal end of the E1 TM domain interacts with residues at the top of the Q1 S1 helix in a “gain-of-function cleft” while the C-terminal end of E1, specifically H73, S74, and D76, interacts with residue H363 in the S6 Q1 helix, and is believed to contribute to the channel’s increased conductivity upon opening, as well as to delayed opening [46]. At high transmembrane voltage potentials, the S4 helix senses the elevated voltage and undergoes a conformational and position change that leads to an intermediate, yet closed channel state under conditions where E1 is bound and inhibits the coupling of the S4 helix to the S6 helix of the pore domain. The channel will not open and conduct completely until all S4 helices are in the fully active conformation [53, 47, 42] (Figure 6).

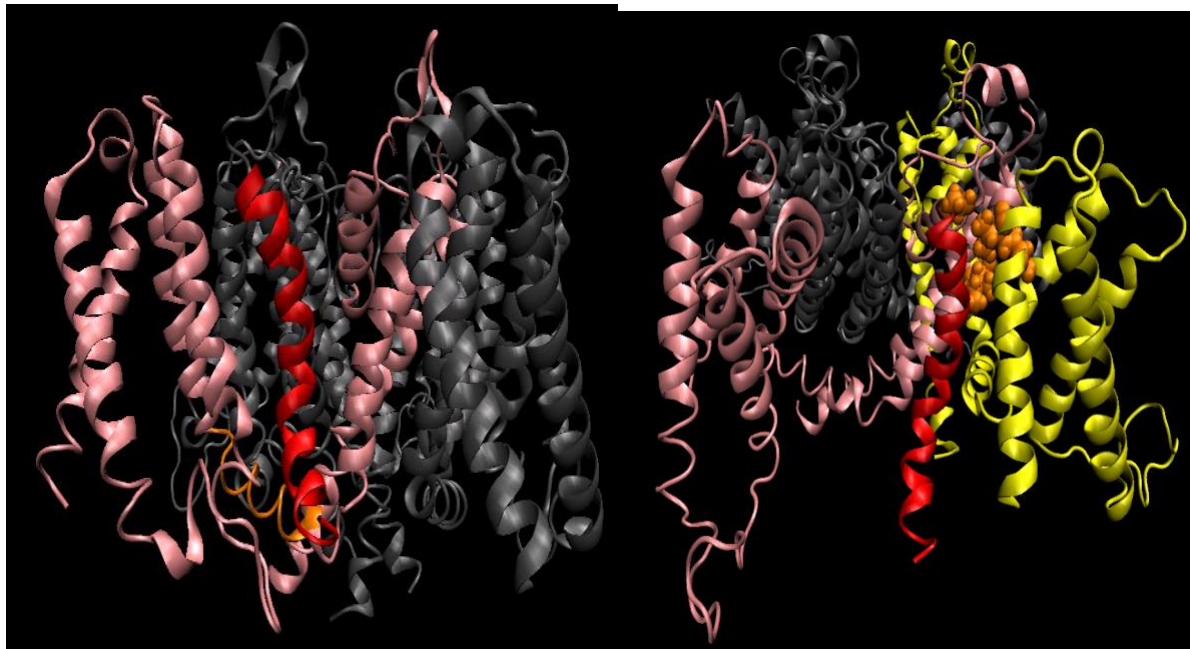


**Figure 6: Models of KCNQ1 Bound to KCNE1 in Open and Closed Conformation**

This figure shows models of the open (left panel) and closed (right panel) states of the homotetrameric KCNQ1 channel bound to KCNE1. The left panel shows E1 sitting on top of the gating S4-S5 linker in the closed position. During full activation, the E1 protein rotates and pulls away from the S4-S5 linker and associates with a series of residues that, when mutated, lead to gain of function of Q1. This is called the gain of function cleft that is located between the sensor and pore domains.

E3 has 2 critical acidic residues juxtamembrane at the N-terminal end, D54 and D55, that contain electrostatic interaction with Q1 residue R237 in the S4 helix. This interaction promotes to the channel's voltage independent and stabilizes the channel in a constitutively open state [44]. E3 also makes extensive contact with the S4-S5 linker [53, 47]. While the structures of E1 and E3 TM regions exhibit curved structures, they interact with Q1 through different mechanisms. Their distinct interactions lead to E1 contributing to both the S4 helix movement and channel gating, while E3 primarily affect the S4 movement [47].

### **1.7 KCNE<sub>1</sub> and KCNE<sub>3</sub> Functional Regions**

Studies have shown the transmembrane region of both E1 and E3 is necessary for their unique functions when bound to Q1. More specifically, amino acids F57, T58, and L59 of E1 and T71, V72, and G73 of E3, both in the center of their respective TM helices, are critical to determining their functional differences. Studies indicate that when these sites in E1 are swapped in the corresponding wild type sites in E3 to generate the E3<sub>TVG→FTL</sub> mutant, this modulates Q1 in a manner that closely resembles modulation by wild type E1. In particular, delayed Q1 channel activation is induced by binding of the E3<sub>TVG→FTL</sub> mutant to the channel, which now affects both Q1 channel S4 movement and gating. Conversely, swapping in the E3 triplet motif into E1 to generate E1<sub>FTL→TVG</sub> leads to E3-like constitutive activation of the Q1 channel [54, 55; 47] (Figure 7).

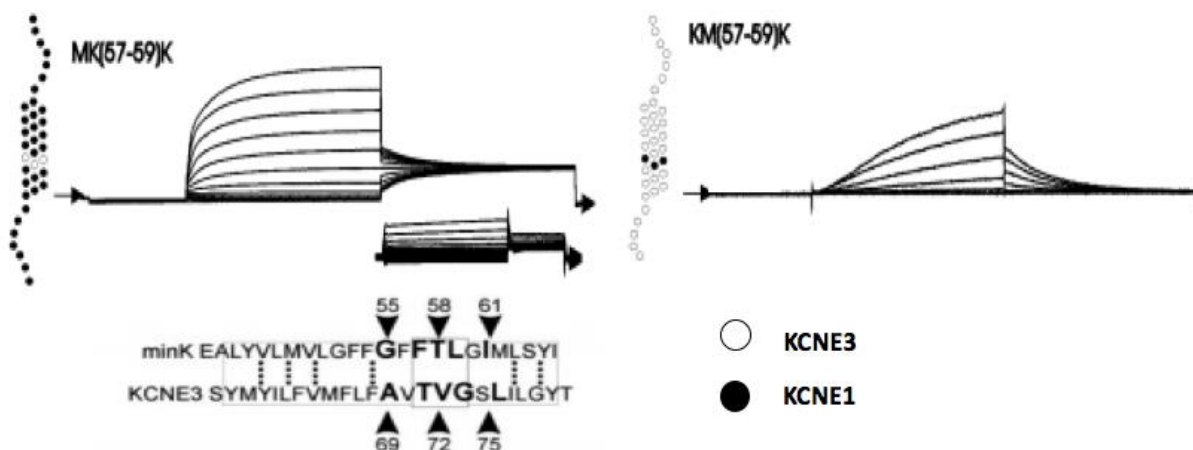


**Figure 7: Electrophysiology of KCNE1 and KCNE3 With Select Residues Switched**

This figure represents the transmembrane regions of KCNE3 with open circles and KCNE1 with closed black circles. The left panel indicates a majority KCNE1 with 3 TM KCNE3 residues that behaves similarly to KCNE3 as a constitutively active channel. The right panel shows a majority KCNE3 protein with 3 residues inserted from KCNE1. This mutation leads to a KCNE3 channel that exhibits delayed activation, similar to KCNE1. This figure was adapted from reference 54 and 55.

It is clear from these results that the triplet motifs located near the middle of the E1 and E3 TM segments are critical to defining how E1 and E3 exert their distinct effects on Q1 function. However, little information is known about how these motifs alter the structures and/or dynamics of each KCNE subunit or how these changes result in altered channel interaction and functional modulation. I hypothesize that the TVG motif leads to a structural change of the transmembrane helix of KCNE1 which may lead to E1<sub>FTL→TVG</sub> interacting with Q1 in a different fashion than E1.

This study details the cloning and subsequent purification of a uniform isotopically labeled E1<sub>FTL→TVG</sub> to make NMR resonance assignments by using a suite of 3D experiments and specific isotopic labeling techniques. The chemical shift data from these assignments were used to determine the secondary structure of the protein, providing the basis for comparison to both wild type E1 and E3. With assignments in hand, it is possible to move forward with other NMR-based structural experiments to better elucidate how the E1<sub>FTL→TVG</sub> mutation differs from wild type E1 and E3. These NMR-based structural

experiments give way to determine the structure of E1<sub>FTL→TVG</sub> to provide additional insight and to provide the basis for possible docking studies to the Q1 channel.

## Chapter 2

### Methods and Materials

#### 2.1 Reagents and Materials

The QuickChange II site-directed mutagenesis kit and QIAprep spin mini-prep kit were purchased from Qiagen (Foster City, CA). XL1-Blue, BL21(DE3) CodonPlus PR, and CT19 *E coli* competent cells were prepared at the Vanderbilt University MegaLab (Nashville, TN). MEM (100x) vitamins were purchased from Sigma-Aldrich (St. Louis, MO). (LPMG detergent was purchased from Anatrace (Maumee, OH). Ni-NTA was purchased from ThermoFisher Scientific (Waltham, MA). Precast SDS-PAGE gels were purchased from ThermoFisher Scientific (Waltham, MA). Analytical grade imidazole was purchased from Sigma-Aldrich (St. Louis, MO). Protein markers for SDS PAGE gels were purchased from ThermoFisher Scientific (Waltham, MA). The 800MHz and 900MHz NMR spectrometers used were Bruker Avance III.

#### 2.2 Cloning of KCNE1<sub>FTL→TVG</sub> (E1<sub>FTL→TVG</sub>)

cDNA encoding full-length human E1<sub>FTL→TVG</sub> was created from the wild type E1 template using the QuickChange mutagenesis kit from Qiagen consisting of Pfu polymerase and Dpn1, and cloned into a pET16b expression vector according to a published protocol [56]. The E1<sub>FTL→TVG</sub> mutant construct employed in this study includes not only the wild type E1 residues 71-73 (FTL) replaced with the corresponding residues of E3 (TVG), but also includes mutation of the single wild type cysteine (residue 106) to serine and an N-terminal HHHHHHG- purification tag (136 residues, with tag). The DNA was then transformed into XL1-Blue competent cells and plated on an agar gel plate with appropriate antibiotics and incubated overnight at 37°C. Single colonies were picked and used to inoculate LB medium for 6-8 hours at 37°C before being mini-prepped using a

Qiagen QIAprep Spin kit. The mini-prepped samples were submitted for sequencing to confirm that the mutations were correctly inserted.

### **2.3 Overexpression of KCNE1<sub>FTL→TVG</sub>**

The vector encoding His<sub>6</sub>-E1<sub>FTL→TVG</sub> was transformed into BL21(DE3) CodonPlus RP competent cells using a heat-shock technique, and the cells were plated on agar with the appropriate antibiotics overnight at 37°C. Single colonies were picked and added to LB medium with appropriate antibiotics, then agitated at 37°C for 6-8 hours or until solutions were turbid. 2-3 mL of this starter culture was added to 1L of <sup>15</sup>N-M9 media (0.1 mM CaCl<sub>2</sub>, 1 mM MgSO<sub>4</sub>, 0.4% glucose, 10 mL 1X MEM vitamins, 100ug/ml of ampicillin, and 34 ug/ml of chloramphenicol). This was followed by rotary shaking at 25°C for 16-18 hours until the optical density (OD<sub>600</sub>) was between 0.7 and 1.0. Cell expression was induced using 1 mM IPTG, followed by continued rotary shaking at 37°C for 6 hours. The cells expressing recombinant E1<sub>FTL→TVG</sub> were harvested at 6,000 X g in 4°C, flash frozen, and stored at -80°C until ready for purification.

### **2.4 Purification of E1<sub>FTL→TVG</sub> into LMPG Detergent Micelles**

Because E1<sub>FTL→TVG</sub> and wild-type E1 are membrane proteins, they need a membrane mimetic to aid in purification and proper folding of the protein. Various detergent micelles and bicelle conditions were tested, and lyso-myristoylphosphatidylglycerol (LMPG) micelles proved to yield an NMR spectrum that was well dispersed [56] indicating that it was well folded under these micelle conditions. LMPG micelles were used throughout the entire project unless otherwise stated.

#### **2.4.1 Solubilizing Inclusion Bodies with KCNE1<sub>FTL→TVG</sub>**

Frozen cell pellets containing overexpressed E1 were thawed and resuspended in lysis buffer (75 mM Tris-base, 300 mM NaCl, 0.2 mM EDTA, pH 7.8) at 20 mL per gram of

cell pellet. Added to the dissolved cell pellets were 2  $\mu$ L of LDR solution (100mg/mL lysozyme, 10 mg/ml DNase, 10 mg/mL RNase, 10% glycerol) per mL of lysis buffer. To complete cell lysis conditions, the protease inhibitor PMSF was added to a final concentration of 1 mM and magnesium acetate to a final concentration of 5 mM. This solution was tumbled for 30 minutes at 4°C. The solution was then probe-sonicated on ice for five minutes with an alternating 5-second pulse and 5-second rest cycles. The lysed cells were centrifuged for 20 minutes at 20,000 x g at 4°C. The supernatant was discarded, and the inclusion body pellet was homogenized in lysis buffer. The homogenized pellet was sonicated on ice and centrifuged using the same conditions as listed above, before being resuspended in 10mL of an 8M urea and 0.2% lauroyl sarcosine solution per gram of wet cells. This solution was tumbled overnight at 4°C.

#### **2.4.2 Purification and Buffer Exchange of E1<sub>FTL→TVG</sub>**

The dissolved inclusion bodies were centrifuged at 30,000 x g for 45 minutes at 4°C to remove debris. This supernatant was mixed with 1.2 mL of Ni-NTA resin per gram of wet cell pellet and tumbled at 4°C for 1 hour. The solution was transferred to a gravity-flow column, allowing the supernatant to pass through, leaving the resin with bound protein. The resin was washed with 10 column volumes of a wash buffer (20 mM tris, pH 7.8, 150 mM NaCl, 0.2% lauroyl sarcosine) to remove urea. The resin was then washed with 10 column volumes of a buffer exchange solution (20 mM tris, pH 7.8, 150 mM NaCl, 30 mM imidazole, 0.2% LMPG) to exchange in the non-denaturing detergent LMPG and to elute loosely bound impurities. The protein was eluted with 300 mM analytical grade imidazole at pH 7.8 with 0.2% LMPG to a final volume of 10ml. The protein concentration was determined by measuring light absorption at 280nm using an extinction coefficient of 1.29 OD per mg/mL per cm. An SDS-PAGE gel was used to assess if the target protein was present, the presence of impurities in the sample, the presence of oligomers, and the presence of degradation or cleavage products. By SDS-PAGE E1<sub>FTL→TVG</sub> exhibited an apparent molecular weight of 15.4 kDa for. This purification approach yielded approximately 2.5 mg of pure protein per liter of medium.

### **2.4.3 SDS Polyacrylamide Gel Electrophoresis (SDS-PAGE) of E1<sub>FTL→TVG</sub>**

10% precast Tris-SDS PAGE gels were loaded with 1:4 ratio of diluted KCNE1<sub>FTL→TVG</sub> to loading dye. The gel was run at 100V in a 1X running buffer and included a lane with SeeBlue prestained protein marker used to evaluate the apparent molecular weight of the protein. Following electrophoresis, the gel was removed from the casket and washed with milli-Q water, then heated using a microwave for 45 seconds, then put on a slow rotary shaker for 5 minutes. Water was removed from the gel and replaced with Simply Blue stain, heated in a microwave for 45 seconds, then incubated using rotary shaking until protein bands appeared. Distaining of the gel was done by removing the stain solution and replacing it with dH<sub>2</sub>O and 1-2 Kimwipes until the blue stain is removed and bands are clearly observed on the gel. Sample bands were compared to the SeeBlue prestained marker to determine the apparent molecular weight.

### **2.5 NMR Sample Preparation and NMR Spectroscopy**

Uniformly <sup>15</sup>N-labeled His<sub>6</sub>-E1<sub>FTL→TVG</sub> was exchanged from the elution buffer listed above into an NMR buffer (10% D<sub>2</sub>O, 50 mM imidazole, 50 mM NaCl, 2 mM EDTA, 0.05% LMPG, pH 6.5) using a 10 kDa molecular weight cut-off Amicon Ultra-15 centrifugal filter. Using the same centrifugal filter method, E1<sub>FTL→TVG</sub> was concentrated to 1 mM, and 200 uL was carefully transferred to a 5 mm NMR tube. Using a Bruker 800 MHz or 900 MHz spectrometer, 2-dimensional <sup>1</sup>H,<sup>15</sup>N-TROSY(transverse relaxation-optimized spectroscopy) spectra of U-<sup>15</sup>N- E1<sub>FTL→TVG</sub> were collected at 45°C. 256 x 512 points were collected in the <sup>15</sup>N dimension and <sup>1</sup>H dimension, respectively, and the spectra were processed in TopSpin and analyzed using NMRFAM-Sparky from the National Magnetic Resonance Facility at the University of Wisconsin-Madison.

## **2.6 Isotopic Labeling of E1<sub>FTL→TVG</sub> and NMR Resonance Assignments**

All experiments were conducted using either an 800MHz or 900 MHz Bruker Avance III NMR spectrometer using a TROSY or HSQC based pulse sequences. The spectra from these experiments were processed using TopSpin and analyzed using NMRFAM-Sparky.

### **2.6.1 Uniformly <sup>13</sup>C,<sup>15</sup>N, isotopically-labeled E1<sub>FTL→TVG</sub>**

Uniformly <sup>13</sup>C,<sup>15</sup>N, isotopically-labeled E1<sub>FTL→TVG</sub> was prepared and purified using the methods listed above, with the addition of 4 g of <sup>13</sup>C<sub>6</sub>-glucose instead of 2 <sup>12</sup>C-glucose to the minimal medium.

### **2.6.2 Inverse Labeling of E1<sub>FTL→TVG</sub>**

Inverse labeling (unlabeled Thr or Ser in otherwise <sup>15</sup>N-labeled protein) of E1<sub>FTL→TVG</sub> was expressed in <sup>15</sup>N-enriched-M9 medium with the addition of 1g of an unlabeled <sup>14</sup>N amino acid of choice. Inverse labeled E1<sub>FTL→TVG</sub> was purified using the standard method.

### **2.6.3 Specific Amino Acid Labeling of E1<sub>FTL→TVG</sub>**

To express protein labeled with a specific <sup>15</sup>N amino acid (<sup>15</sup>N-labeled Ala, Val, Phe, Leu, Met, Ile, or Thr in otherwise unlabeled protein), CT19 cells containing unlabeled-E1<sub>FTL→TVG</sub> were grown in LB medium until OD<sub>600</sub> reached 0.5, then gently spun down and washed. Washed cell pellets were resuspended in unlabeled-M9 medium with specific antibiotics, 0.5g of each of the 7 unlabeled amino acids (Val, Ala, Phe, Leu, Ile, Tyr, Asp), 0.1g of unlabeled Trp and 0.5g of the specific <sup>15</sup>N-labeled amino acid of choice (per liter of culture). When <sup>15</sup>N labeling one of the 7 unlabeled amino acids listed above, the unlabeled amino acid was replaced with the <sup>15</sup>N-labeled version at 0.5g. These cells were induced, harvested, and the specifically <sup>15</sup>N-labeled E1<sub>FTL→TVG</sub> protein was purified using the methods listed above.

#### **2.6.4 3D Experiments for Assignments, Single Amino Acid Labeling, and Inverse Labeling**

Uniformly  $^{13}\text{C}$ ,  $^{15}\text{N}$ , isotopically-labeled  $\text{E1}_{\text{FTL}\rightarrow\text{TVG}}$  was prepared and purified using the methods listed above, with the addition of 4 g of  $^{13}\text{C}_6$ -glucose instead of 2 g of  $^{12}\text{C}$ -glucose to the minimal medium. To make resonance assignments, the following experiments were used: 3D TROSY-based pulse sequences (HNCACB, HNCO, HNCA, HNCACO, HNCB), inverse labeling (unlabeled Thr or Ser in otherwise  $^{15}\text{N}$ -labeled protein), and specific amino acid labeling ( $^{15}\text{N}$ -labeled Ala, Val, Phe, Leu, Met, Ile, or Thr in otherwise unlabeled protein).

#### **2.7 $T_1$ and $T_2$ $^{15}\text{N}$ Relaxation Measurements**

Uniformly  $^{15}\text{N}$ -labeled  $\text{E1}_{\text{FTL}\rightarrow\text{TVG}}$  was expressed and purified as described above. The same sample was used for both  $T_1$  and  $T_2$  experiments, which were performed on a Bruker 900MHz spectrometer at 323 K. 2D inversion recovery spectra used for determining  $T_1$  values were collected using a TROSY-based pulse sequence. Relaxation delay times were 15, 30, 50, 100, 200, 400, 800, 1200, 1600, 2000, and 4000 ms.  $T_2$  correlation spectra were collected using a 2D TROSY version of the Carr-Purcell-Mieboom-Gill sequence using delay times of 3.38, 8.48, 16.96, 33.92, 50.88, 67.84, 84.80, 101.76, 135.86, and 169.60 ms. The delay time between scans used in both relaxation experiments was 3.6 ms.

#### **2.8 Gd(III)-diethylenetriaminepentaacetic acid (Gd-DTPA) and 16-doxyl-stearic acid (16-DSA)**

To make matched  $\text{E1}_{\text{FTL}\rightarrow\text{TVG}}$  NMR samples for 16-DSA, Gd-DTPA, and a reference sample, 2L of cells were grown and purified as a single sample using the protocol described above. This was split into 3 samples; the paramagnet-free reference, the 16-DSA-containing sample, and the Gd-DTPA-containing sample. All samples were in NMR buffer at pH 6.5 and contained 0.5 mM of U- $^{15}\text{N}$ -labeled  $\text{E1}_{\text{FTL}\rightarrow\text{TVG}}$  and an LMPG

concentration of 8%. 200ul of this sample were placed in a 3 mm NMR tube and then subjected to NMR spectroscopy on a Bruker 900 MHz spectrometer at 323 K.

The aqueous probe, Gd-DTPA, was added to a final concentration of 20 mM from a 2.5mg/ml stock to a sample containing 0.5 mM E1<sub>FTL→TVG</sub> and 10 mM EDTA in NMR buffer. Both this sample and the reference sample were incubated for 1 hour at room temperature then 5 minutes at 323K in the spectrometer before running 2D <sup>1</sup>H,<sup>15</sup>N-TROSY experiments. The spectrum from the Gd-DTPA-containing sample was superimposed on the matched reference sample (collected with the exact same spectral acquisition parameters) for comparison. This data was analyzed by measuring the intensity ratio for each peak between the probe-containing sample and the reference sample.

To make the lipophilic probe stock sample, 16-DSA was dissolved in methanol to a final concentration of 2.5mg/ml. 113uL of the stock was added to an empty Eppendorf tube and the methanol was evaporated by gently blowing nitrogen over the sample until a thin residue of 16-DSA was left. 200uL of E1<sub>FTL→TVG</sub> in NMR buffer with 8% LMPG was then added to solubilize the dried 16-DSA in the 1.5ml Eppendorf, and the sample was incubated for 16 to 18 hours at 37°C, then transferred to a 3 mm NMR tube. This sample was used to collect a 2D <sup>1</sup>H,<sup>15</sup>N-TROSY spectrum that was compared to that of the matched reference sample using the same method as used for the Gd-DTPA experiment.

## **2.9. Clean-EX PM of E1<sub>FTL→TVG</sub> and E1 Wild-type**

<sup>15</sup>N-E1<sub>FTL→TVG</sub> and <sup>15</sup>N-E1 were both expressed and purified using the standard methods described above and buffer-exchanged into NMR buffer. 2D CLEANEX-PM HSQC pulse sequences were run at 323K on both samples with exchange delays of 25ms and 100ms on a 900MHz spectrometer. Peak intensities in the Clean-EX spectra were quantitated and compared to the peak intensities of the reference HSCQ [57, 58].

## Chapter 3

### Results of Cloning, Characterization, and Assignments of KCNE1<sub>FTL→TVG</sub>

#### 3.1 Introduction

Membrane proteins make up approximately 1/3 of all proteins and many are related to human health, disease, and even cancer, yet they can often be challenging to study biochemically and structurally, in part because they are hard to overexpress and purify [2, 59, 60]. Many biochemists study membrane proteins produced using *E. coli* overexpression systems. *E. coli* overexpression methods can be inexpensive, robust, and sometimes allow large protein yields and uniform isotopic labeling of membrane protein. This previously proved to be the case for wild-type human KCNE1 [56] and other proteins within our lab including the unique KCNE1/KCNE3 mutant used for this project.

It is known that switching transmembrane residues FTL of KCNE1 (E1) and TVG of KCNE3 (E3) results in a KCNQ1/KCNE1 complex that behaves as if it were the KCNQ1/KCNE3 complex. I hypothesize that this is due to changes in flexibility in the transmembrane helix of E1 when the TVG triple mutation is introduced in place of the native FTL sequence. To investigate this hypothesis, I used NMR techniques to assign E1<sub>FTL→TVG</sub> and determine structural differences between E1<sub>FTL→TVG</sub>, E1 and E3.

##### 3.1.1 NMR Assignments: Background

A central benefit of NMR protein investigation is the possibility of monitoring proteins at residue-specific resolution over multiple time-scales. While the 2D TROSY experiment gives some information, such as insight into whether the protein is properly folded, 3D NMR TROSY and other isotopically label experiments provide a route to site-specific resonance assignments that enable characterization of specific residues within the

protein. This includes determining (“assigning”) which residue in the protein gives rise to each TROSY contour peak, making each peak a reporter of residue-specific information. 3D TROSY experiments allow for a “sequential walk” through the protein backbone that provide the basis for residue assignment of both the amide  $^1\text{H}/^{15}\text{N}$  peaks and also the backbone  $^{13}\text{C}(\alpha)$ ,  $^{13}\text{C}(\text{carbonyl})$ , and  $^{13}\text{C}(\text{beta})$  peaks. Using a combination of experiments, I can identify and assign each residue in the sequence.

Many of the 2D and 3D TROSY experiments used to make assignments require the protein to be isotopically enriched. There are two types of isotopic labeling, uniform and selective. Non-selective labeling involves the enrichment of all amino acids with  $^{13}\text{C}$ ,  $^{15}\text{N}$ , and/or  $^2\text{H}$ . Selective labeling involves isotopic labeling of only a single residue type. There are also “inverse labeling” techniques that allow for the labeling of all other residues except one type of amino acid. Because  $^1\text{H}$  is the only NMR isotope that is found naturally in high abundance in proteins, others ( $^2\text{H}$ ,  $^{13}\text{C}$ , and  $^{15}\text{N}$ ) must be enriched artificially [61, 62]. Isotopic labeling can be accomplished by providing cells with the selected isotope so that it substitutes natural isotopes and incorporates the otherwise rare isotope into the protein [61]. Isotopic labeling is an essential tool for biomolecular NMR for all but the simplest of proteins. Once a protein is labeled, this paves the way for experiments that enable resonance assignments and to spectral parameters that convey structural information.

In this chapter I describe the expression and purification of isotopically-labeled  $\text{E1}_{\text{FTL}\rightarrow\text{TVG}}$  in mg quantities in order to make protein NMR assignments and to study its structural elements. I describe the results of our efforts to clone the cDNA for  $\text{E1}_{\text{FTL}\rightarrow\text{TVG}}$  into a suitable *E. coli* expression vector. The ability to purify membrane proteins like  $\text{E1}_{\text{FTL}\rightarrow\text{TVG}}$  requires the protein to be solubilized into complexes containing lipids or detergents, which allows them to be studied in solution [63]. This purification in to detergent micelles is described in this chapter. Last, isotopically labeling will allow for NMR studies and the assigning of  $\text{E1}_{\text{FTL}\rightarrow\text{TVG}}$  using a series of 2D and 3D NMR based experiments. These  $\text{E1}_{\text{FTL}\rightarrow\text{TVG}}$  studies will be compared to those of the previously studied  $\text{E1}$  [41] and  $\text{E3}$  [53] in the hope of elucidating the structural and dynamic

differences of wild type E1 and the E3-like E1<sub>FTL→TVG</sub> mutant. The data results of this chapter based on the published data of Law 2019 [64].

## **3.2 Results**

### **3.2.1 Cloning of E1<sub>FTL→TVG</sub>**

The cDNA for E1<sub>FTL→TVG</sub> was created from a WT E1 cDNA template using site-directed mutagenesis to replace the F57, T58, and L59 WT residues with T, V, and G, respectively (corresponding to wild type E3 residues 71-73). Also, because previous members of our lab determined that the C106 residue near the C-terminus causes the formation of disulfide-linked dimers under our purification conditions, this lone cysteine residue was mutated using quick change mutagenesis to generate C106S. The E1<sub>FTL→TVG</sub> template was cloned into the ampicillin-selective pET16b expression vector, which contains a readily-inducible T7 promoter that facilitates the expression of recombinant proteins [65, 66]. This vector also contains 3 cloning sites and an in-frame sequence that encodes an N-terminal His<sub>6</sub>-tag to facilitate purification (Figure 8) [56, 67].

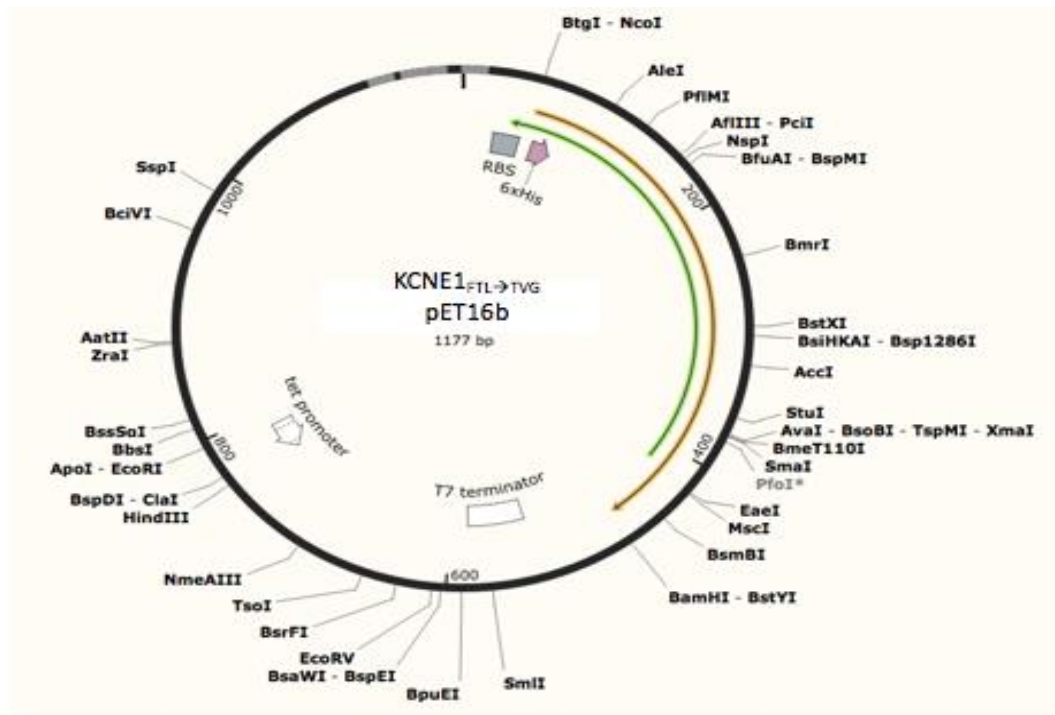


**Figure 8: Schematic of the pET16b Cloning Vector**

The cDNA for E1<sub>FTL→TVG</sub> was cloned into an 1177 base pair pET16b vector. The yellow line indicates where the cDNA was cloned into the expression vector in-frame with the His<sub>6</sub>-tag sequence in the small pink arrow. This figure was created from GenHunter when E1<sub>FTL→TVG</sub> cloning was confirmed.

The E1<sub>FTL→TVG</sub> containing plasmid was transformed into a competent *E. coli* XL-1 Blue strain for expression because this strain lacks *endA* and *recA*, which improves miniprep results and increases insert stability. Transformation onto agar plates containing ampicillin for selectivity resulted in several single colonies after a 16-18 hour incubation period at 37°C. Five single colonies were selected for inoculation in LB media and then later mini-prepped to isolate the E1<sub>FTL→TVG</sub> DNA. The mini-prepped sample was submitted to the company GenHunter for sequencing to confirm that the DNA sequences encoded the TVG mutation, as well as the C106S mutation. Sequencing data determined that both mutations had been appropriately incorporated (Figure 9).

```

      10          20          30          40          50          60
HHHHHHGMIL SNTTAVTPFL TKLWQETVQQ GGNMSGLARR SPRSSDGKLE ALYVLMVLGF

      70          80          90          100         110         120
FGFTVGGMIL SYIRSKKLEH SNDFPNVYIE SDAWQEKDKA YVQARVLESY RSYVVENHL

      130
AIEQPNTLHP ETKPSP

```

**Figure 9: Sequence Results Confirming All Mutations and Sequencing Were Correct**

DNA sequencing confirmed the correct cloning of the E1<sub>FTL→TVG</sub> sequence, which encodes the amino acid sequence as shown. This sequence included a His<sub>6</sub>-tag and a correctly inserted TVG mutation. The lone cysteine (site 106) residue was deleted, and a serine residue was added in its place. The mutations introduced are highlighted in red boxes. The WT length is 129 residues and, with the His<sub>6</sub>-tag and flexible Gly linker, our total construct contains 136 residues. This image is from GenHunter to confirm site directed mutations were correct when cloning.

**3.2.2 Overexpression of the E1<sub>FTL→TVG</sub> Protein**

To determine the best *E. coli* strain for expression, protein expression tests were carried out in the following strains of competent cells: XL10-Gold, Rosetta C43(DE3) [49], and BL21(DE3) CodonPlus RP [56]. I tested XL10-Gold cells because of its high transformation efficiency while Rosetta C43(DE3) is generally good at expressing toxic proteins like membrane proteins. The BL21(DE3) CodonPlus RP cell line was selected because it contains extra copies of genes that encode tRNAs that recognize rare arginine and proline codons and has occasionally has high expression levels for membrane proteins. Of the 3 strains, the transformation of BL21(DE3) CodonPlus RP yielded several healthy single colonies and the highest expression levels of His<sub>6</sub>-E1<sub>FTL→TVG</sub>. Accordingly, for all following experiments, BL21(DE3) CodonPlus RP was used unless stated. LB media and <sup>15</sup>NH<sub>4</sub>Cl M9 media were used to grow and induce <sup>15</sup>N-His<sub>6</sub>-E1<sub>FTL→TVG</sub> expression and yielded approximately 2.5g of cells per liter of culture. Cells from a liter of culture usually yielded 2.5-4mg/mL of pure E1<sub>FTL→TVG</sub> .

### 3.2.3 Purification of KCNE1<sub>FTL→TVG</sub> into Detergent Micelles

I first started by repeating the purification of WT E1 [56] and subsequent NMR. In my hands, this yielded poor spectral quality, suggestive of an unfolded E1 protein. Through adjusting several purification conditions, including replacing SDS with LS (at concentrations above the CMC), the new purification process yielded high-quality spectra for WT KCNE1. Using this new protocol, I then repeated the purification of E1<sub>FTL→TVG</sub> and collected 2D TROSY NMR spectra. An SDS-PAGE gel of purified E1<sub>FTL→TVG</sub> protein showed that it formed both monomer and dimer, possibly due to disulfide bond formation involving the single cysteine residue located in the C-terminal tail (Figure 10). For this reason, I mutated C106S and observed that this eliminated dimer formation (Figure 11). Our construct for all subsequent studies contained the C106S mutation.

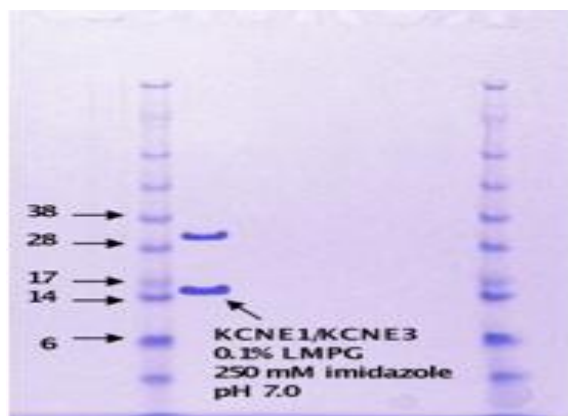


**Figure 10: Purification Gel of WT E1 With Native C106**

Purification gel for E1<sub>FTL→TVG</sub> with native C106 shows two bands around 15kDa and 30kDa. 15kDa and 30kDa are the expected molecular weights for monomer and dimer, respectively. There appears to be an equal amount of dimer as there is monomer in this sample. Unpublished data performed by postdoctoral researcher, Congbao Kang.

Like many toxic and membrane proteins that often do not incorporate well into the *E. coli* plasma membrane, His<sub>6</sub>-<sup>15</sup>N- E1<sub>FTL→TVG</sub> was found to be expressed in inclusion bodies [56, 68] and solubilized as mentioned in chapter 2 before purification into membrane mimetic.

Attempts were also made to purify E1<sub>FTL→TVG</sub> into lipodisq nanoparticles (LDNP) using the amphipathic polymer (poly(styrene-co-maleic acid); SMA) to solubilize DMPC and DMPG lipids [69, 71]. With this method, I hoped to purify E1<sub>FTL→TVG</sub> into a more native-like environment, lipodisqs. E1<sub>FTL→TVG</sub> was eluted into LDNP, but the polymer solution was viscous, even after dilution. When examined using NMR, no peaks were detected due to slow tumbling in solution.

To summarize, attempts to purify E1<sub>FTL→TVG</sub> in LDNP lipodisqs failed. Because micelles are relatively small and well suited for NMR [72] LMPG detergent micelles will be used in all further studies. This detergent was previously identified [56] as being optimal for wild type E1. LMPG is a lipid-like anionic detergent that is generally regarded as being relatively mild and non-denaturing.

For purification of E1<sub>FTL→TVG</sub> into LMPG micelles, I added 10 mM and 30 mM imidazole column rinse steps to exchange buffer from LS into LMPG detergent micelles and to remove loosely bound impurities on resin. Imidazole competes with the His-tag bound protein-ligand sites on the nickel resin [73, 83]. An elution buffer containing 300 mM of analytical grade imidazole was used to elute the His-tagged protein from the resin. All fractions were collected and then subjected to electrophoresis on a 10% Tris-SDS PAGE gel to determine the purity of the sample. This optimized protocol and the C106S mutation appeared to eliminate dimerization in micelles (Figure 11).

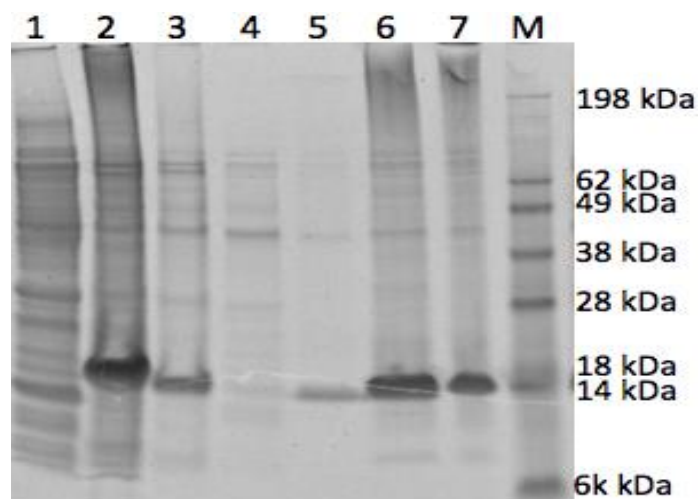


**Figure 11: Purification of E1<sub>FTL→TVG</sub> in LMPG Micelles**

The figure illustrates the purification of the protein via an SDS PAGE gel to show the purity of collected fractions. Lane 1: supernatant Lane 2: Flow-through from gravity packing Lane 3: LS wash to remove urea with 0.2% LS Lane 4: 10 mM Imidazole wash with 0.2% LMPG Lane 5: 30 mM imidazole wash in 0.2% LMPG Lane 6: 300 mM imidazole wash 0.2% LMPG Lane 7: Ni(II)-NTA resin Lane M: Simply Blue stain marker. Lane 6 shows reasonably pure E1<sub>FTL→TVG</sub> and no dimer or oligomer formation.

### 3.2.4 NMR Sample Preparation and Spectroscopy of E1<sub>FTL→TVG</sub>

Most of my studies to gain structural information rely heavily on nuclear magnetic resonance (NMR) methods to probe the properties E1<sub>FTL→TVG</sub> at the atomic level. 1D spectra are usually not useful in this regard because of excessive signal overlap, obscuring useful information. Multidimensional NMR was used to disperse resonances in multiple dimensions, allowing access to a wealth of information. For many multidimensional NMR experiments, the protein must be enriched with NMR-active <sup>15</sup>N and/or <sup>13</sup>C isotopes [74]. 2D heteronuclear single quantum correlation (HSQC) or transverse relaxation-optimized spectroscopy (TROSY) [75, 76] pulse sequences was used to correlate backbone amide nitrogen-15 resonances to the resonances from the attached amide protons. After transforming the data and plotting as a <sup>15</sup>N x <sup>1</sup>H plot, each contour peak represents a single amino acid. Each peak will have a unique combination of <sup>15</sup>N and <sup>1</sup>H chemical shifts, which are sensitive to the local environment of the amide group. E1<sub>FTL→TVG</sub> solubilized in LMPG detergent micelles forms a large complex. When the molecule or complex under study is relatively large, 2D TROSY is preferable to 2D HSQC because it yields sharper peaks, leading to enhanced resolution

and, in some cases, signal-to-noise. Shown in Figure 12 is the TROSY NMR spectrum of E1<sub>FTL→TVG</sub> in LMPG micelles, a spectrum that displays well dispersed and sharp peaks (Figure 12).

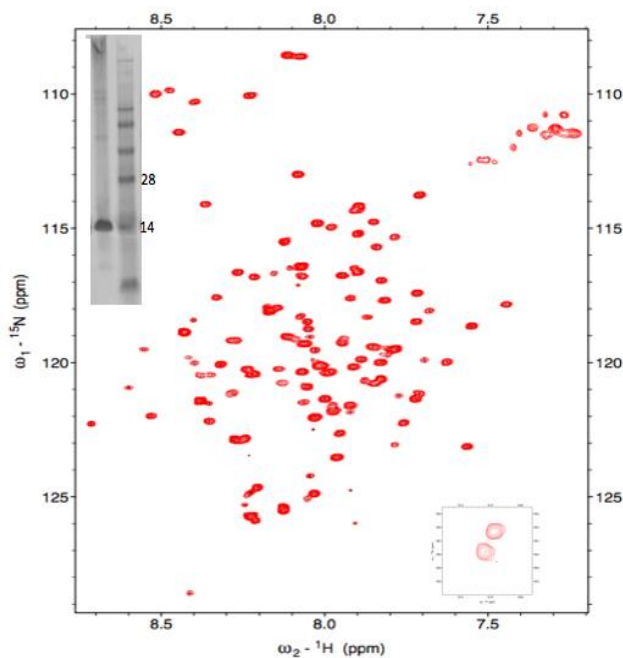


**Figure 12: 2D <sup>1</sup>H, <sup>15</sup>N-TROSY Spectrum of E1<sub>FTL→TVG</sub>**

2D TROSY NMR spectra of <sup>15</sup>N-E1<sub>FTL→TVG</sub> in LMPG micelles. 116 of the expected 122 peaks can be identified, and the spectral resolution is high. Both tryptophan indole side chain NH resonances can be seen in the lower right inset. Of the 122 expected peaks, 116 peaks can be identify. The inset in the top left corner shows the purification gel illustrating sample purity and monomeric E1<sub>FTL→TVG</sub>. This figure is from reference 64.

### 3.2.5 Uniform Isotopic Labeling and Sample Preparation

Uniform isotopic labeled proteins using <sup>2</sup>H, <sup>13</sup>C, <sup>15</sup>N isotopes allow for elucidation of backbone resonance assignments via 3D NMR experiments. I first tried uniform, triple-isotope labeling to generate U-<sup>2</sup>H, <sup>15</sup>N, <sup>13</sup>C-E1<sub>FTL→TVG</sub>. Cells were grown in media containing increasing percentages of D<sub>2</sub>O up 100% and also supplemented the media with <sup>15</sup>NH<sub>4</sub>Cl and <sup>13</sup>C<sub>6</sub>-glucose. The same protocol used for purifying <sup>1</sup>H, <sup>15</sup>N-E1<sub>FTL→TVG</sub> was used. Ideally, I would hope to see the same quality spectra as observed for the <sup>15</sup>N-labeled-only <sup>1</sup>H, <sup>15</sup>N-E1<sub>FTL→TVG</sub> samples. Unfortunately, cells in 100% D<sub>2</sub>O-based media exhibited limited growth and prevented growth to a sufficient optical density before cells

began to show evidence of death. Cells grew well in 70% D<sub>2</sub>O and so were therefore grown in 2L of media in 70% D<sub>2</sub>O-containing M9 media in hopes that this condition would result in sufficient quantities for an NMR sample. This yielded a sample that was purified to approximately 0.1 mM and yielded a 2D TROSY spectrum following 12 hours of spectra acquisition. However, the quality of the spectrum from U- <sup>2</sup>H, <sup>15</sup>N, <sup>13</sup>C-E1<sub>FTL→TVG</sub> in 70% D<sub>2</sub>O (Figure 13) indicates that under our conditions, the triple labeled E1<sub>FTL→TVG</sub> sample showed several missing peaks and poor resolution, concluding that it was not properly folded under these conditions and was therefore not amenable for further NMR studies.

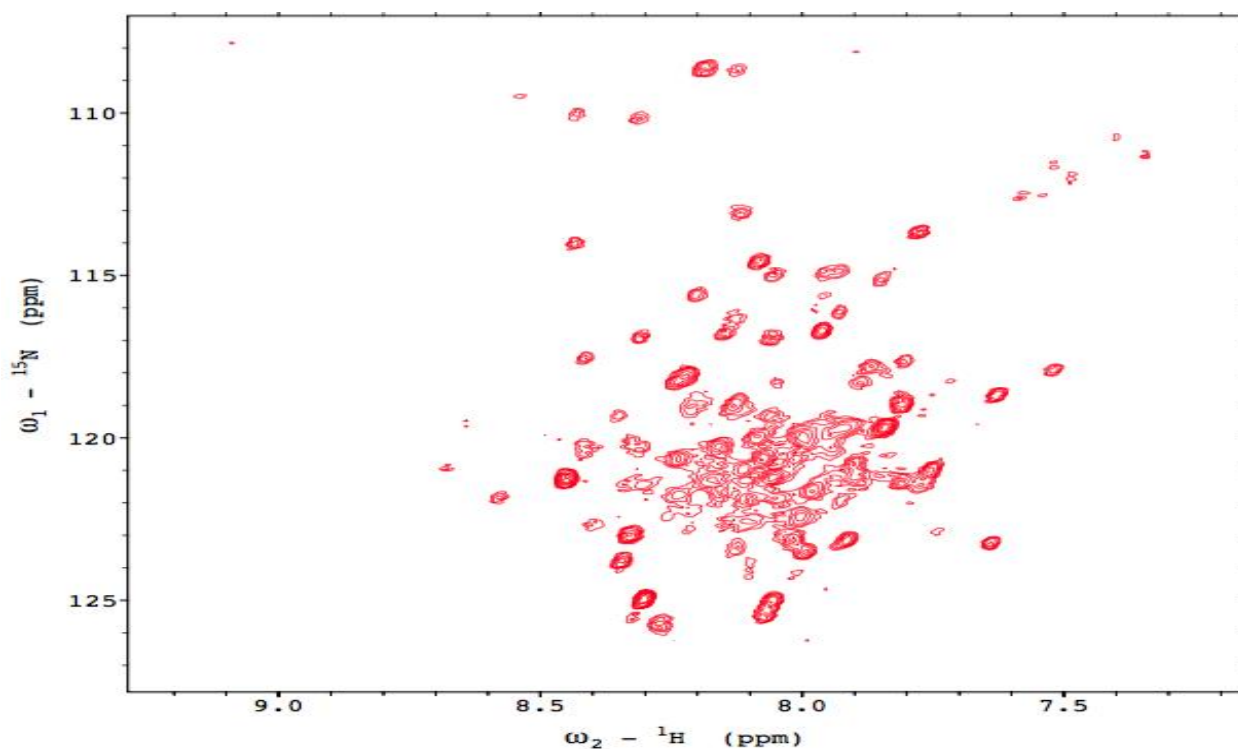


**Figure 13: Triple Labeled Sample of E1<sub>FTL→TVG</sub>**

TROSY spectrum of <sup>2</sup>H, <sup>15</sup>N, <sup>13</sup>C-E1<sub>FTL→TVG</sub> in 70% D<sub>2</sub>O run on a 900MHz spectrometer for 12 hours at 318.2K. The final sample contained 30 mM imidazole, 8% LMPG, 0.1 mM protein at a pH of 6.5. Several peaks are missing and not well resolved. This spectrum is indicative of a protein that is not well folded and not amenable for assignment experiments.

Since triple labeling E1<sub>FTL→TVG</sub> was not successful at providing a sufficient quantity of protein or spectra of the high quality spectra required for assignments, a uniformly isotopically double labeled sample, U-<sup>13</sup>C,<sup>15</sup>N-E1<sub>FTL→TVG</sub>, was generated by substituting D<sub>2</sub>O with standard H<sub>2</sub>O in the medium. This sample was created using the protocol of growing cells in <sup>15</sup>N-M9 media with the alteration of 2 grams of <sup>12</sup>C<sub>6</sub>-glucose for 2 grams <sup>13</sup>C<sub>6</sub>-glucose. Sample growth was normal. Purification and NMR TROSY spectroscopy followed the standard protocol, yet yielded spectra that were poorly resolved and missing several peaks suggestive of a poorly folded protein. I attempted to increase the temperature from 318.2K to 323.2K in hopes of obtaining a better resolution but to no avail. However, it was found that increasing the amount of <sup>13</sup>C<sub>6</sub>-glucose used per liter from 2g to 4g per liter of culture increased the yield dramatically, allowing preparation of a 1 mM protein sample in 8% LMPG. This TROSY spectrum demonstrated that 4g yielded a well-dispersed spectrum (Figure 14).

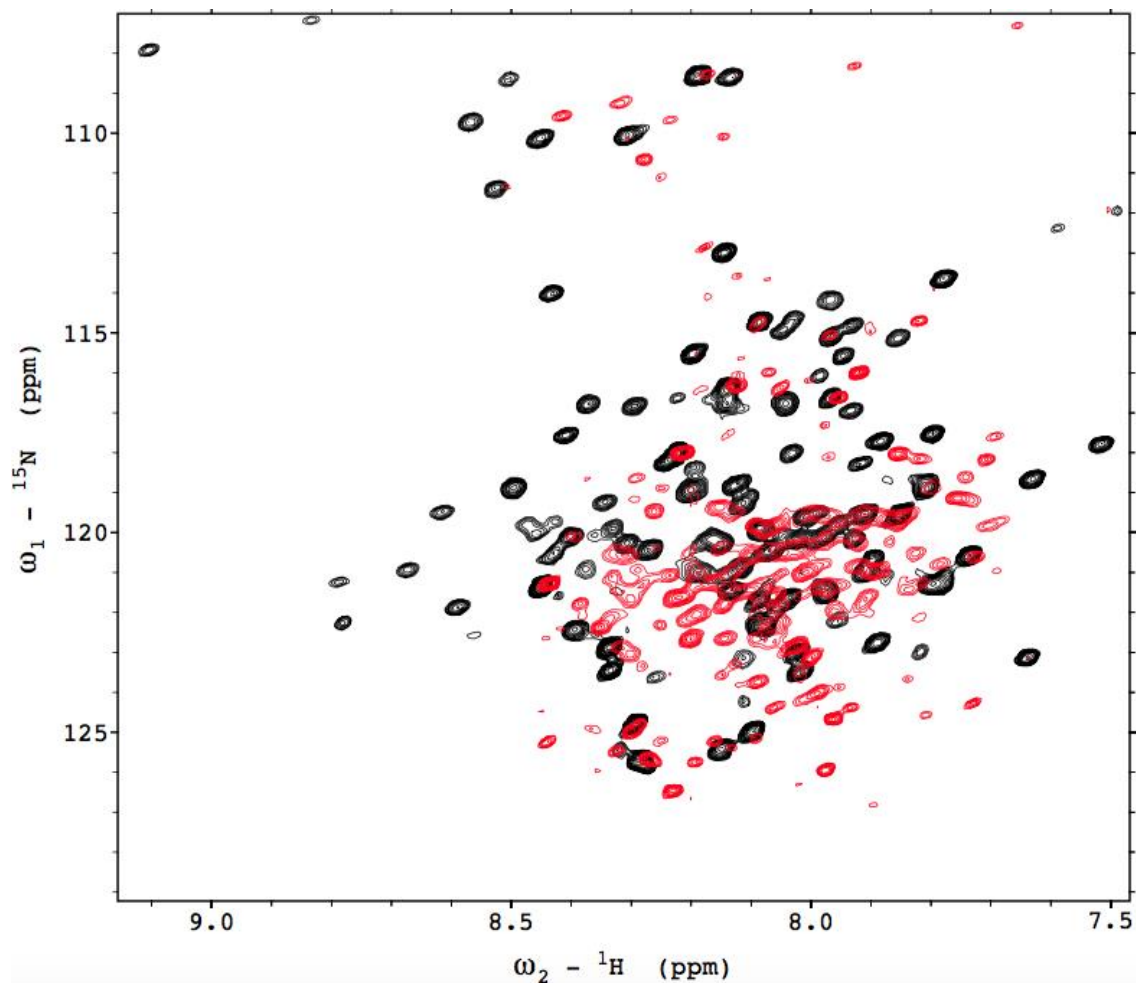


**Figure 14: Overlay of the Double-labeled Samples with 2 Versus 4 Grams of  $^{13}\text{C}_6$ -glucose**  
 Overlay of  $^{13}\text{C}, ^{15}\text{N}$ , E1<sub>FTL</sub>→TVG spectra with 2g (red) and 4g (black) of  $^{13}\text{C}_6$ -glucose.  $^{13}\text{C}, ^{15}\text{N}$ - E1<sub>FTL</sub>→TVG grown in 4g glucose produced well-dispersed spectra.  $^{13}\text{C}, ^{15}\text{N}$ , E1<sub>FTL</sub>→TVG grown in 2g glucose is missing several peaks, does not align well with the 4-gram sample, and not resolved well enough to make assignments.

The  $^1\text{H}, ^{15}\text{N}$ -TROSY spectrum from a  $^{13}\text{C}, ^{15}\text{N}$ , E1<sub>FTL</sub>→TVG sample prepared with 4g of glucose per liter of culture was compared to that of the  $^{15}\text{N}$ -E1<sub>FTL</sub>→TVG prepared with  $^{12}\text{C}_6$ -glucose to determine if peaks overlay. The two samples were prepared and purified side by side and the two spectra aligned well, with only a few minor shifts (Figure 15). This was a strong indicator that the sample could be used for 3D experiments to make assignments.

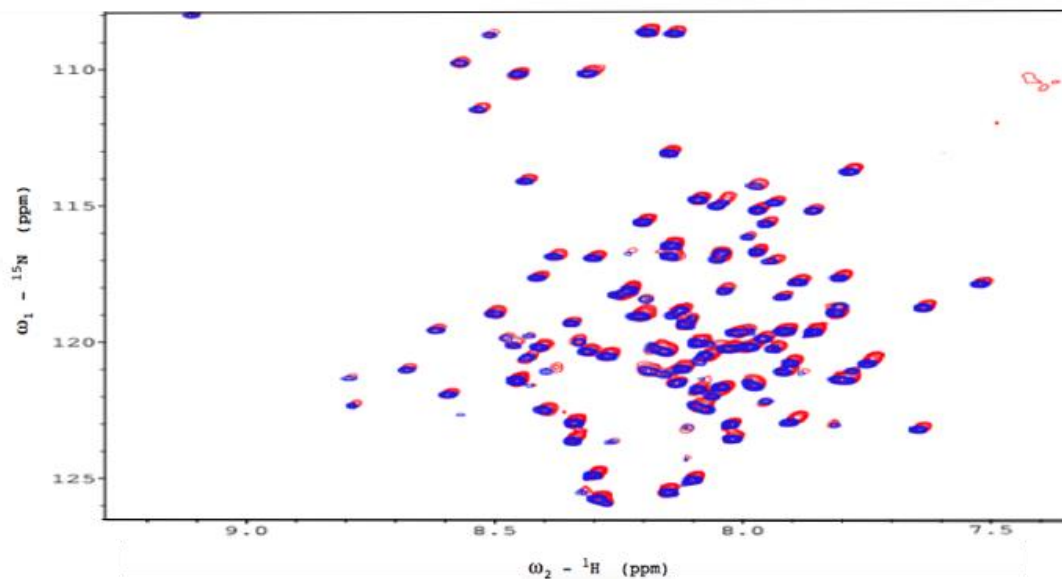


**Figure 15: Overlay of  $^{15}\text{N-E1}_{\text{FTL}\rightarrow\text{TVG}}$  and  $^{13}\text{C},^{15}\text{N-E1}_{\text{FTL}\rightarrow\text{TVG}}$  containing 4 grams of  $^{13}\text{C}_6$ -glucose**  
 The red peaks represent  $^{15}\text{N-E1}_{\text{FTL}\rightarrow\text{TVG}}$ . The blue peaks show  $^{13}\text{C},^{15}\text{N-E1}_{\text{FTL}\rightarrow\text{TVG}}$ . Both samples were prepared and purified side by side under the same conditions and processed using the same parameter. Both samples contained 1 mM  $\text{E1}_{\text{FTL}\rightarrow\text{TVG}}$ , 8% LMPG, 30 mM imidazole and 10%  $\text{D}_2\text{O}$  at pH 6.5. There are a few subtle shifts but there are no peaks missing or significantly shifted seen in the spectrum from the double-labeled sample.

Our lab has previously studied WT KCNE1 and has published its assignments and structure [56]. Since  $\text{E1}_{\text{FTL}\rightarrow\text{TVG}}$  was created by QuikChange Mutagenesis from WT KCNE1 and thus has a very similar sequence, I wanted to determine if the mutations induced a significant change in chemical shifts from that of WT E1. This would mean that the addition of mutations did not significantly disrupt the structure or fold of the protein. The overlay of the  $^{13}\text{C},^{15}\text{N-E1}_{\text{FTL}\rightarrow\text{TVG}}$  and the WT  $^{15}\text{N-E1}$  spectra (Figure 16) indicates that  $^{13}\text{C},^{15}\text{N-E1}_{\text{FTL}\rightarrow\text{TVG}}$  has very similar chemical shifts to that of the published and assigned WT  $^{15}\text{N-E1}$ .

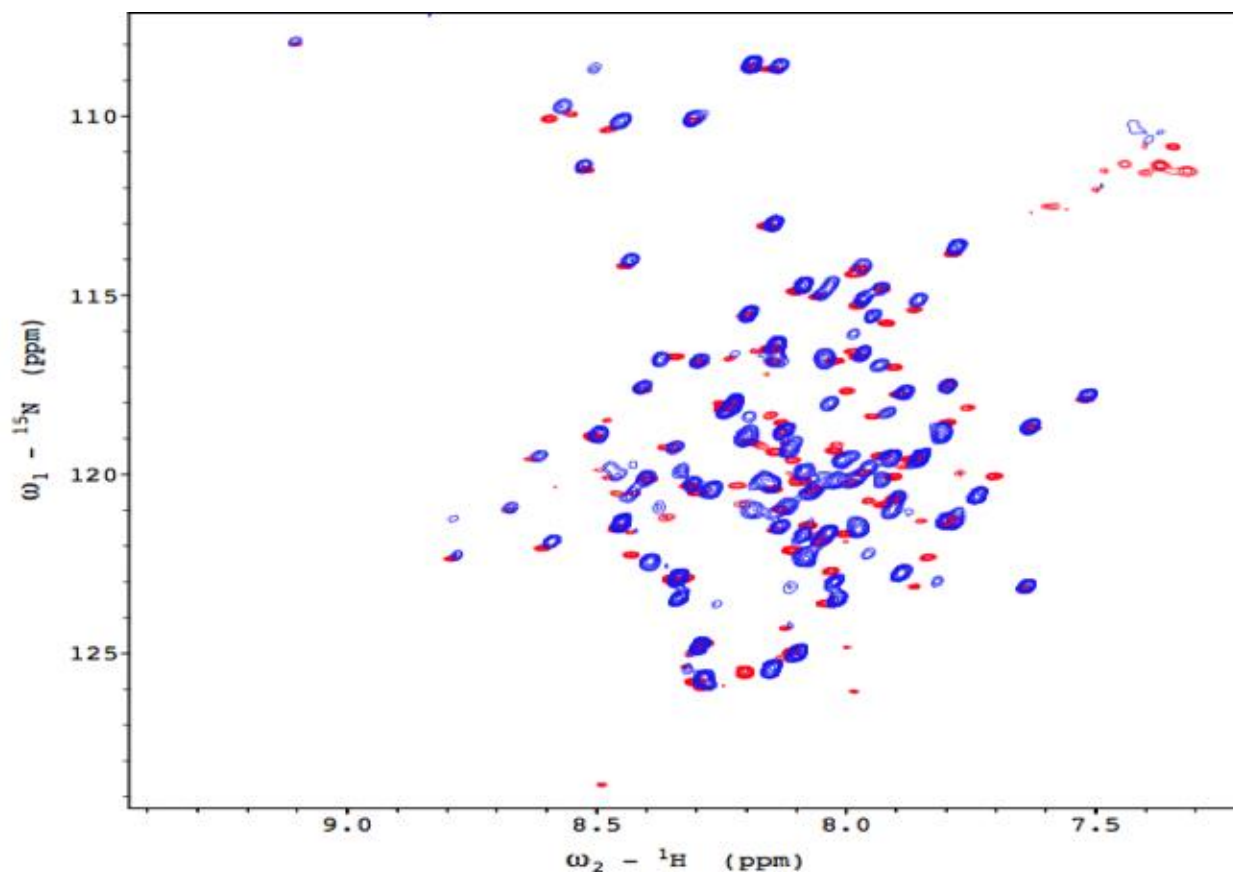


**Figure 16: Overlay of WT KCNE1 and E1<sub>FTL→TVG</sub>.**

Red peaks are from WT <sup>15</sup>N-E1. Blue peaks are from <sup>13</sup>C, <sup>15</sup>N- E1<sub>FTL→TVG</sub>. A few peaks are missing due to them being removed by mutations or by peak broadening. Other peaks can be seen in blue that have no red counterpart. This may be due to the mutations introduced or peaks being better resolved in the mutant sample. Overall the two spectra indicate that the folds of the two proteins are very similar.

While there are a few peaks that have shifted, disappeared, or are now present, the overall appearance of the spectra are similar. This was useful when making assignments for E1<sub>FTL→TVG</sub> due to our ability to transfer many resonance assignments from the published WT E1 study [56]. Even prior to starting any 3D TROSY experiments, approximately 65% of assignments could be transferred. It was also observed that <sup>13</sup>C, <sup>15</sup>N-E1<sub>FTL→TVG</sub> contained some additional peaks that were not present in the published spectrum of WT E1. A number of peaks not seen for WT E1 are now present in the E1<sub>FTL→TVG</sub> spectrum. Of the 4 substituted peaks (F57T, T58V, L59G, C106), 2 of them can easily be observed. Due to the unique chemical shift ranges for the Thr and Gly peaks, T57 and G59 were easily identifiable. Additional peaks not in the

original assigned and published spectrum were observed in new E1<sub>FTL→TVG</sub> spectrum. For the E1<sub>FTL→TVG</sub> spectrum, roughly 10 resonances that could not be assigned or observed in the original WT E1 spectrum were now observable. To confirm the identity of transferred peaks and to continue to make additional assignments for the mutant form, additional 3D TROSY experiments were used.

### **3.2.6 3D TROSY Backbone Experiments for Making Resonance Assignments**

Making backbone assignments is the process of identifying and assigning the nuclei of an amino acid in a protein peptide that is observed in the NMR spectra. The peaks in the <sup>1</sup>H-<sup>15</sup>N spectra map to each HN of each amino acid in the E1<sub>FTL→TVG</sub> sequence. In order to complete and confirm our assignments and to sequentially walk along the protein backbone, a series of 3D backbone experiments on uniformly <sup>13</sup>C,<sup>15</sup>N-labeled E1<sub>FTL→TVG</sub> in a high field magnet were utilized. The experiments used were TROSY versions of HNCACB, HNCO, HNCA, HN(CA)CO, and HNCB.

A simple way to visualize how a 3D TROSY experiment works can be seen below (Figure 17). I start with taking a 2D <sup>1</sup>H, <sup>15</sup>N TROSY spectra. All peaks in the 3D spectra can be mapped back to an individual peak in the 2D spectra, allowing for assignments to be made. The 3D experiments take the peaks from the 2D spectra and add a third dimension represented by the <sup>13</sup>C plane and z-slices into the <sup>15</sup>N plane can be made. While moving through the z-planes and also move through the <sup>15</sup>N axis of the 2D spectra will provide us with important information that facilitates the sequential walking of the backbone.

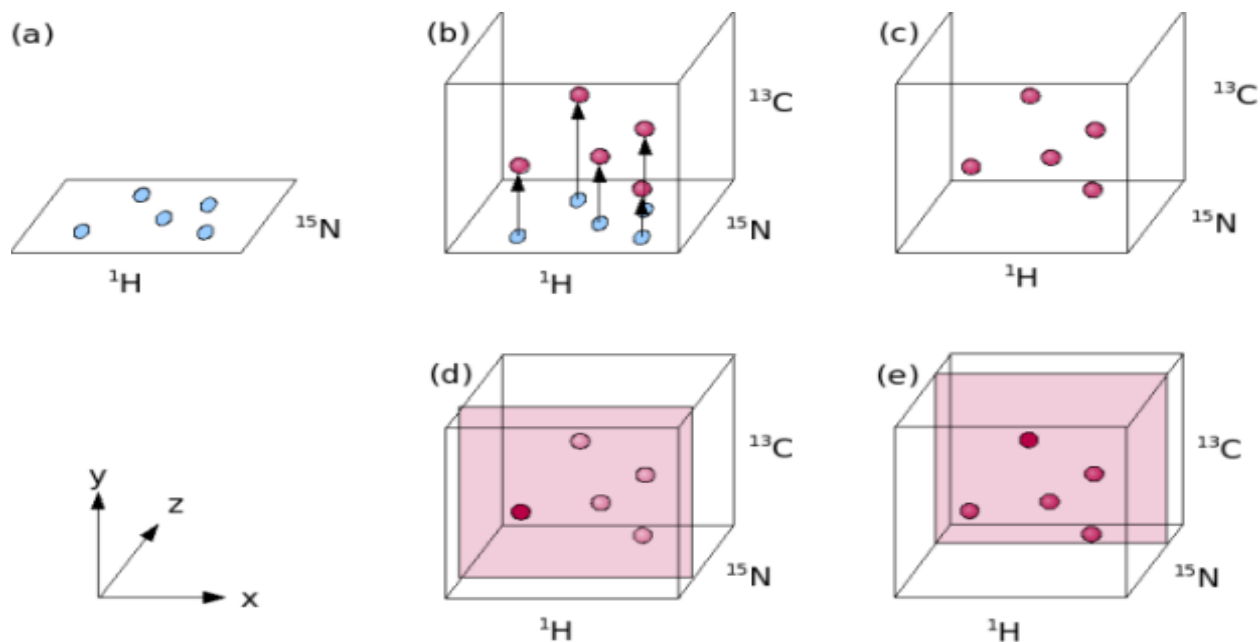


**Figure 17: Schematic of 3D Experiments**

This schematic depicts an overview of the basics of a 3D NMR spectrum. (a) 2D plane showing proton and nitrogen dimension. Each peak corresponds to a backbone amide  $^1\text{H}$ - $^{15}\text{N}$  pair in the sequence. (b) The 2D plane is expanded in a third (i.e., carbon) dimension. (c) A model of peaks in a 3-dimensional space. (d) The pink shade represents a z-slice through the nitrogen plane. (e) The z-slice moving through the nitrogen plane, each showing different peaks that correlate back to the 2D plane seen in (a). This figure is from Victoria A. Higman, modified October 2012 on website <https://www.protein-nmr.org.uk/solution-nmr/assignment-theory/visualising-3d-spectra/>

I first tested 1D, 2D TROSY and a 3D projection of the HNCACB experiment to show that the protein would produce high-quality 3D spectra before moving forward. These experiments indicated that the protein was present in sufficient quantities and that  $\text{E1}_{\text{FTL} \rightarrow \text{TVG}}$  peaks in the 2D TROSY and 3D TROSY projection were well resolved, leading to the continuation of further 3D TROSY experiments. The simplest and most sensitive of the 3D TROSY experiments used for sequential backbone walking is HNCA (Figure 18). In this experiment, the proton of residue  $i$ ,  $\text{H}(i)$ , is excited. This magnetization is transferred to the connecting nitrogen ( $\text{N}(i)$ ), then to the Ca connected to  $\text{H}(i)$  ( $\text{Ca}(i)$ ) and the Ca carbon of the previous residue  $\text{Ca}(i-1)$  [77]. The transfer of magnetization allows for correlation of peaks from one residue to those from the previous residue, enabling a sequential walk of the protein backbone (Figure 18, inset). When looking at a single nitrogen slice of the HNCA spectra, two aligned peak were

observed in the proton dimension in a single column. These peaks can be directly mapped back to the 2D  $^1\text{H} \times ^{15}\text{N}$  TROSY spectra. The more intense peak represents the  $\text{Ca}(i)$  and the less intense peak reveals the  $\text{Ca}(i-1)$  [78]. The peaks not aligned with any another peak in its column are likely  $\text{Ca}(i)$  from different nitrogen slices. Moving through nitrogen slices allows observation of the matching  $\text{Ca}(i-1)$  peak. In this figure, 4 sets of  $\text{Ca}(i)$  and  $\text{Ca}(i-1)$  within this one z-slice can be observed. Our data indicate the HNCA spectra is well resolved and allows us to see many  $\text{Ca}(i)$  and connecting  $\text{Ca}(i-1)$ . The majority of  $\text{Ca}$  assignments were able to be made through this HNCA data, which aided interpretation of our other 3D data.

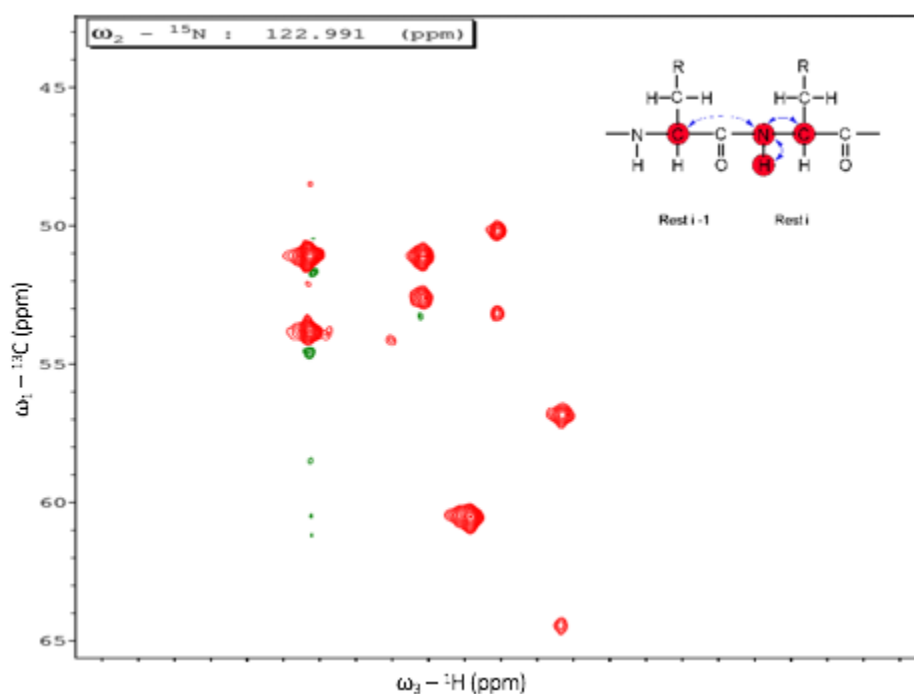


**Figure 18: Triple Resonance Experiment HNCA**

The figure displays an HNCA  $^{15}\text{N}$  slice. 4 sets of different  $\text{Ca}(i)$  and  $\text{Ca}(i-1)$  pairings can be seen. The larger, more intense peaks are the  $\text{Ca}(i)$  because the transfer of magnetization is much closer than the smaller  $\text{Ca}(i-1)$  where the magnetization pass through CO of the  $i-1$  residue. The inset shows the excitation of  $\text{H}(i)$  and the transfer to the  $\text{N}(i)$ ,  $\text{Ca}(i)$ , and the  $\text{Ca}(i-1)$ . Inset adapted from Horst Joachim Schirra November 1996 on <http://www.cryst.bbk.ac.uk/PPS2/projects/schirra/html/trex.htm>.

Another important experiment is HNCACB. Similar to HNCA, it provides chemical shifts for  $\text{Ca}(i)$  and  $\text{Ca}(i-1)$ , and also for  $\text{C}\beta(i)$  and  $\text{C}\beta(i-1)$ . This allows us to sequentially walk the backbone and make  $\text{C}\beta$  assignments as well as  $\text{Ca}$  assignments. In this experiment,

H(i) is excited and the magnetization is transferred to N(i). The magnetization is transferred to C $\alpha$ (i), C $\beta$ (i), C $\alpha$ (i-1), and C $\beta$ (i-1) (Figure 19, Figure 19 inset). This allows us to detect C $\beta$ (i) and C $\beta$ (i-1), which enables us to sequentially walk the backbone. In some columns, not all 4 peaks are present. As a result of moving through the z-slices, a set of 4 peaks lined up along the  $^{13}\text{C}$  axis can be observed. C $\alpha$ (i) and C $\beta$ (i) are seen in the more intense red and green peaks while C $\alpha$ (i-1) and C $\beta$ (i-1) are the less intense red and green peaks. Some columns exhibit less than 4 peaks and some can show more than 4 peaks. This happens because the z-slice is not on the centers of the peaks and needs to be moved in either direction to find the peak center. Alternatively, some of the peaks broadened so much that they are not observable and assignments cannot be made with that peak. When analyzing our HNCACB data, it was more common to have C $\beta$  peaks broadened, possibly because of the number of atoms separating C $\beta$  from the amide proton sites of excitation.

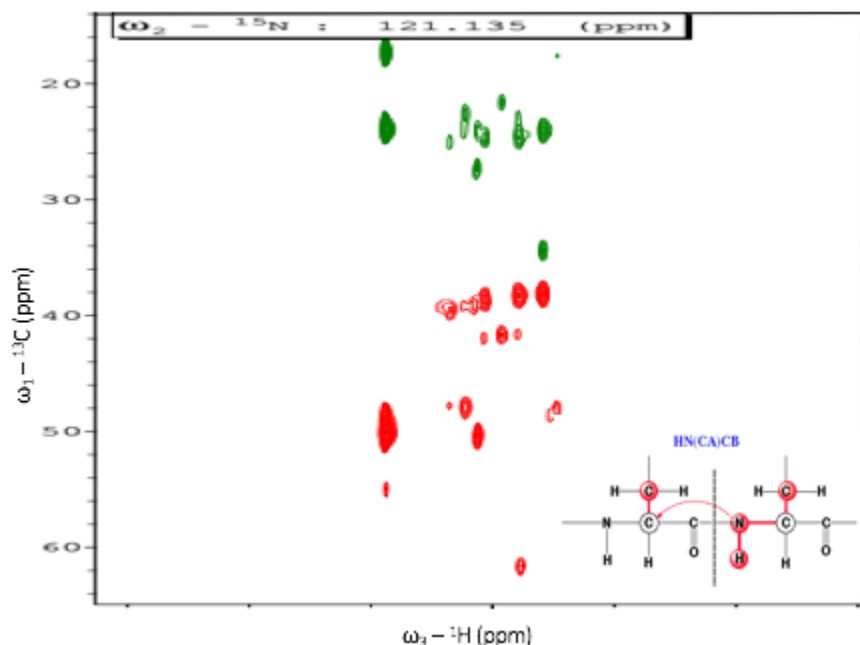


**Figure 19: Triple Resonance Experiment HNCACB**

The figure displays an HNCACB spectra  $^{15}\text{N}$  z-slice. The green peaks show C $\alpha$  peaks where C $\alpha$ (i) are more intense than C $\alpha$ (i-1). The red peaks show C $\beta$  peaks where C $\beta$ (i) and more intense than the C $\beta$ (i-1). The inset is a schematic of the transfer of magnetization pattern. Inset adapted from Horst Joachim Schirra November 1996 on <http://www.cryst.bbk.ac.uk/PPS2/projects/schirra/html/trex.htm>.

HNCO is the most sensitive of the 3D experiments (Figure 20), but it does not provide direct information for backbone walking. In this experiment, the magnetization is transferred to the CO(i-1). In figure 20, each peak represents the CO(i-1) associated with the nitrogen and proton of the i residue. Therefore, in any z-slice of the HNCO spectra, one would expect to see a single peak in a column while scanning through the z-slices. Two or more peaks in a  $^1\text{H}$  column would indicate that two or more peak have the same nitrogen and proton chemical shifts within the 2D TROSY spectrum. The HNCO spectrum can become useful in resolving overlapping peaks in 2D TROSY spectra. For example, in the left panel of figure 21 a very intense peak labeled K70 is identified in the  $^1\text{H},^{15}\text{N}$  2D TROSY spectra. When looking at the corresponding peak in the HNCO spectra, 2 peaks can easily identify, indicating that the intense K70 peak seen in the  $^1\text{H},^{15}\text{N}$  2D TROSY spectra is actually 2 overlapping peaks. This aided in deconvoluting several overlapping peaks in the 2D TROSY spectra and in other 3D spectra.

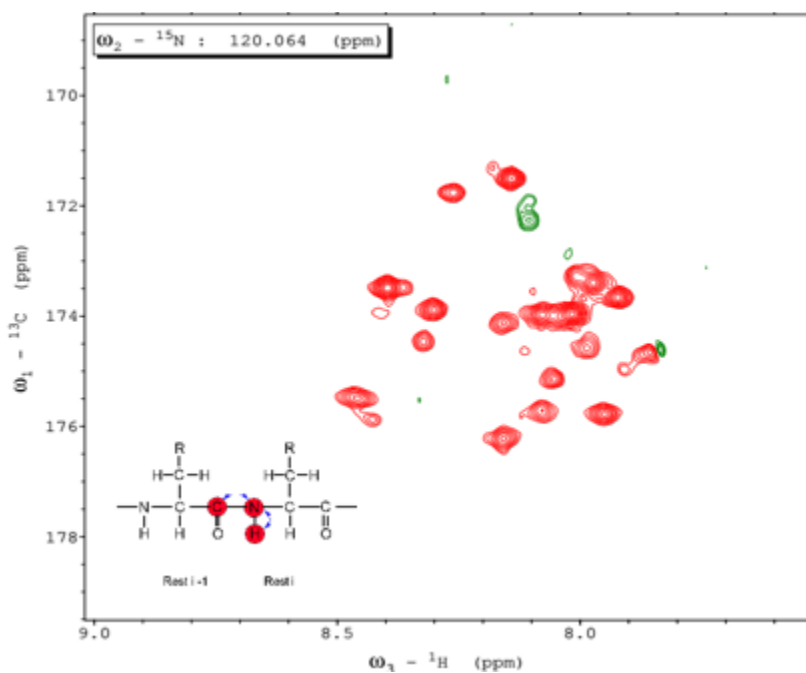


**Figure 20: 3D Experiment HNCO**

This figure depicts the HNCO spectra of E1<sub>FTL→TVG</sub>. The inset figure shows the CO(i-1) by transferring magnetization from the H(i) and N(i) to the CO(i-1). Each peak corresponds to a CO(i-1) that can be mapped back to the 2D TROSY. Inset adapted from Horst Joachim Schirra November 1996 on <http://www.cryst.bbk.ac.uk/PPS2/projects/schirra/html/trex.htm>.

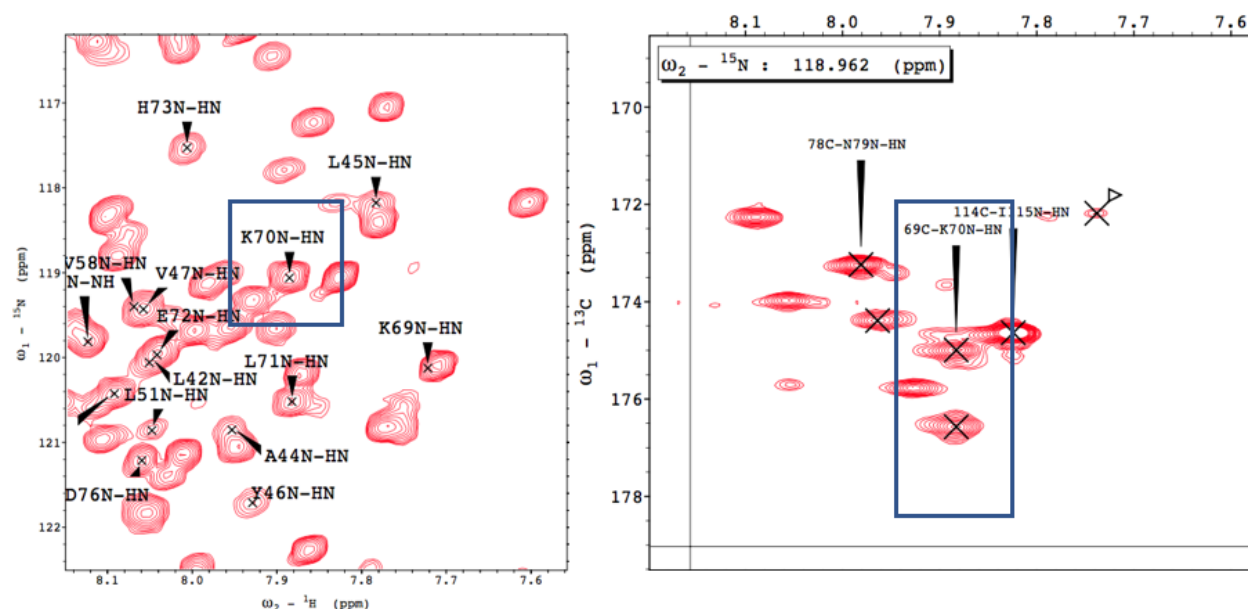


**Figure 21: K70 Overlapping Peaks Identified in HCNO**

The left panel shows a zoomed-in region of the 2D TROSY spectra. In this figure, I observe that K70 (left panel boxed in blue) is very intense. This peak can be mapped to peaks in the HNCQ spectra in the blue highlighted section in the right panel. The right panel shows 2 peaks aligned in the HNCQ spectrum, which correspond to two overlapped peaks in the TROSY spectrum. This figure is from reference 64.

3D-TROSY based experiments were used to confirm the assignments that were transferred, make assignments that could not be transferred, and to provide chemical shift data for CO, C<sub>alpha</sub>, C<sub>beta</sub>, H<sub>alpha</sub>, HN, and N. All spectra were collected using a 900MHz spectrometer under the same conditions mentioned in the Methods section. The data was processed in TopSpin and analyzed in NMRfam-SPARKY. Peaks were picked automatically than manually checked and edited by hand.

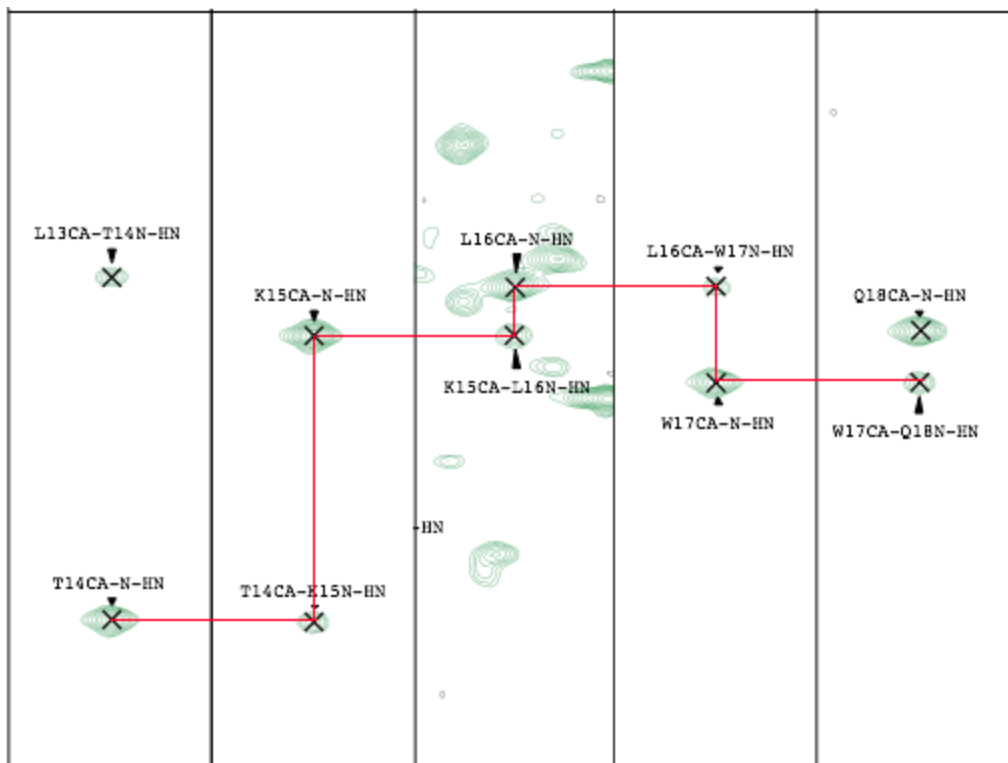


**Figure 22: Sequential Backbone Walking of Five Residues in an HNCA Spectrum**

In this figure, an example of sequential backbone walking from residues T14 to Q18 is shown. The red line indicates the  $C\alpha(i)$  connecting to the matching  $C\alpha(i-1)$ , then to the next residue,  $C\alpha(i+1)$ . Continuing in this manner, connections can be made to assign residues sequentially. This figure is from reference 64.

Combining all of these methods, I was able to connect, assign, and verify approximately 65% of the residues. It was useful to start with amino acids that have unique chemical shifts that are easy to identify, such as glycine, which does not have a  $C\beta$ , or alanine, that has  $C\alpha$  chemical shifts that exhibit much lower values than other amino acids. These 3D experiments provided data to correctly assign several misassigned peaks transferred from WT E1 and to confirm and make new assignments.

While these experiments provided a wealth of information to make assignments and sequentially walk through segments of the protein backbone, several assignments could not be completed using this data alone, particularly in the transmembrane regions (Figure 22). Other experiments, such as single and inverse amino acid labeling provided

excellent tools to fill in missing assignments. In the next section, I detail single and inverse labeling and the completion of assignments.

### **3.3 Single and Inverse Amino Acid Labeling**

#### **3.3.1 Single Amino Acid Labeling**

Specific amino acid labeling allows us to isotopically label all residues of one specific amino acid type in the entire sequence. Therefore, the spectrum will display peaks from only the amino acid type that was isotopically labeled. To begin single amino acid labeling, I selected 6 amino acids for which additional data were needed to complete missing assignments. Using CT19 cells in minimal medium, the  $^{15}\text{N}$ -amino acid of choice were spiked into the media towards the end of the standard growth protocol, just before IPTG induction. Both use of CT19 cells and the addition of  $^{15}\text{N}$ -labeled amino acids just before induction helps to reduce scrambling during the synthesis process. These samples were harvested and the E1<sub>FTL→TVG</sub> was purified to yield between 2.3-5 mg of pure protein per liter for each amino acid labeled (Figure 23). The amino acids that were labeled were Leu, Ala, Phe, Met, Ile, and Val. These amino acids were chosen because they were overrepresented among the remaining unassigned residues, the location of the residues on the sequence, and the relatively low price of the labeled amino acid in each case. 5 of 6 of the single amino acid labeled samples exhibited very little impurities, showed all or the majority of the peaks, and overlaid well with peaks seen in the TROSY spectrum of E1<sub>FTL→TVG</sub> TROSY (Figure 23, Figure 24, Supplemental Figures 1-5).

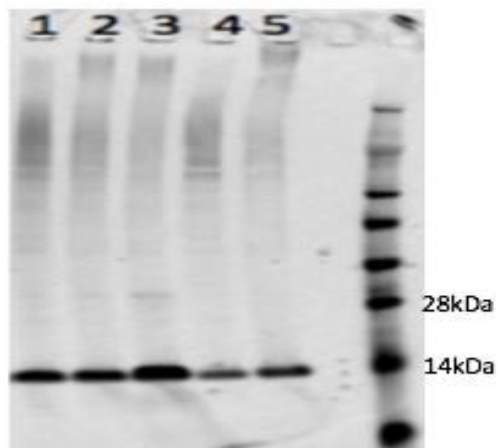


**Figure 23: SDS PAGE Gel of E1<sub>FTL→TVG</sub> Samples Labeled with One of 5 Specific Amino Acids**

Displayed above is a gel documenting the final purification state of E1<sub>FTL→TVG</sub> labeled with either <sup>15</sup>N-Met (lane 1), <sup>15</sup>N-Leu (lane 2), <sup>15</sup>N-Ala (lane 3), <sup>15</sup>N-Val (lane 4) and <sup>15</sup>N-Ile (lane 5) and two different concentrations. The last lane is a marker to show approximate molecular weight.

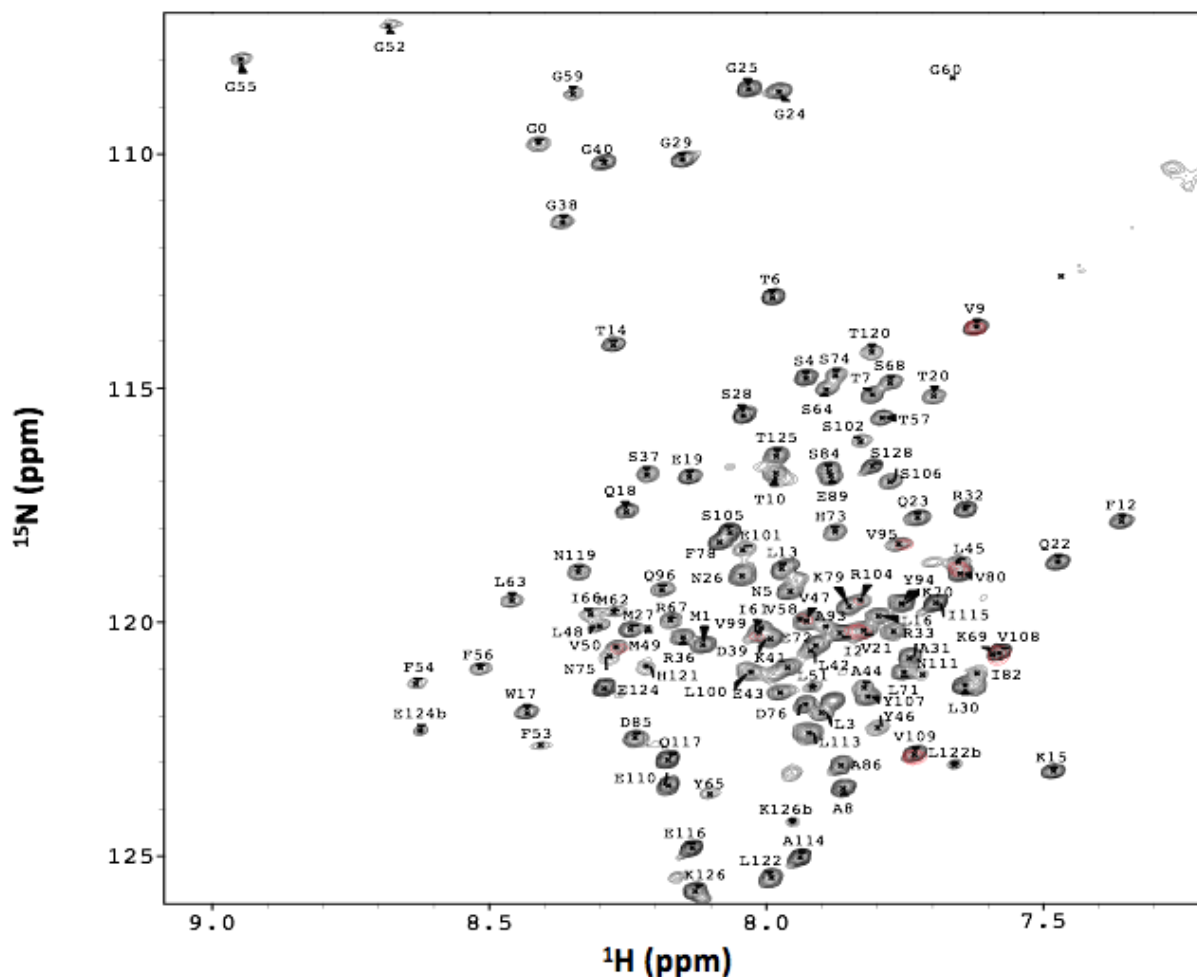


**Fig 24: Single Amino Acid Label Sample for Val**

This figure shows single  $^{15}\text{N}$ -amino acid labeling of Ala residues in red (top) and of Val residues in red (bottom). The blue (top) and black (bottom) peaks are from the 2D TROSY of E1<sub>FTL</sub>→TVG. This figure shows all 10 of the expected peaks for Val highlighted in red and align with the 2D TROSY spectra (in black) and the assigned Val residues.

The  $^{15}\text{N}$ -Met spectrum shows 4 peaks from a total of 4 residues. The Ala spectrum shows 6 out of the 7 expected peaks while the Leu spectrum show all 13 expected peaks. The Phe and Val spectra display 5 and 10 expected peaks, respectively, as expected. Specific labeling of selected amino acids provided a significant number of additional assignments.

### **3.3.2 Inverse Isotopic Labeling of Specific Amino Acids**

I also utilized the technique of “inverse labeling” which enabled us to isotopically label all residues in our sequence, with the exception of one selected amino. Peaks from that amino acid type are identified because they disappear from what is otherwise an ordinary TROSY spectrum.

While Ser and Thr have unique chemical shifts around 116 ppm in the nitrogen dimension, inverse labeled Thr (Figure 25) samples were created to better differentiate between the two amino acids. All 7 Thr peaks disappeared, which aided in completing assignments and confirming the T57 mutation. Amino acids Ser was also inversely labeled, but the spectra showed that the labeling was not effective and few peaks were seen to disappear.

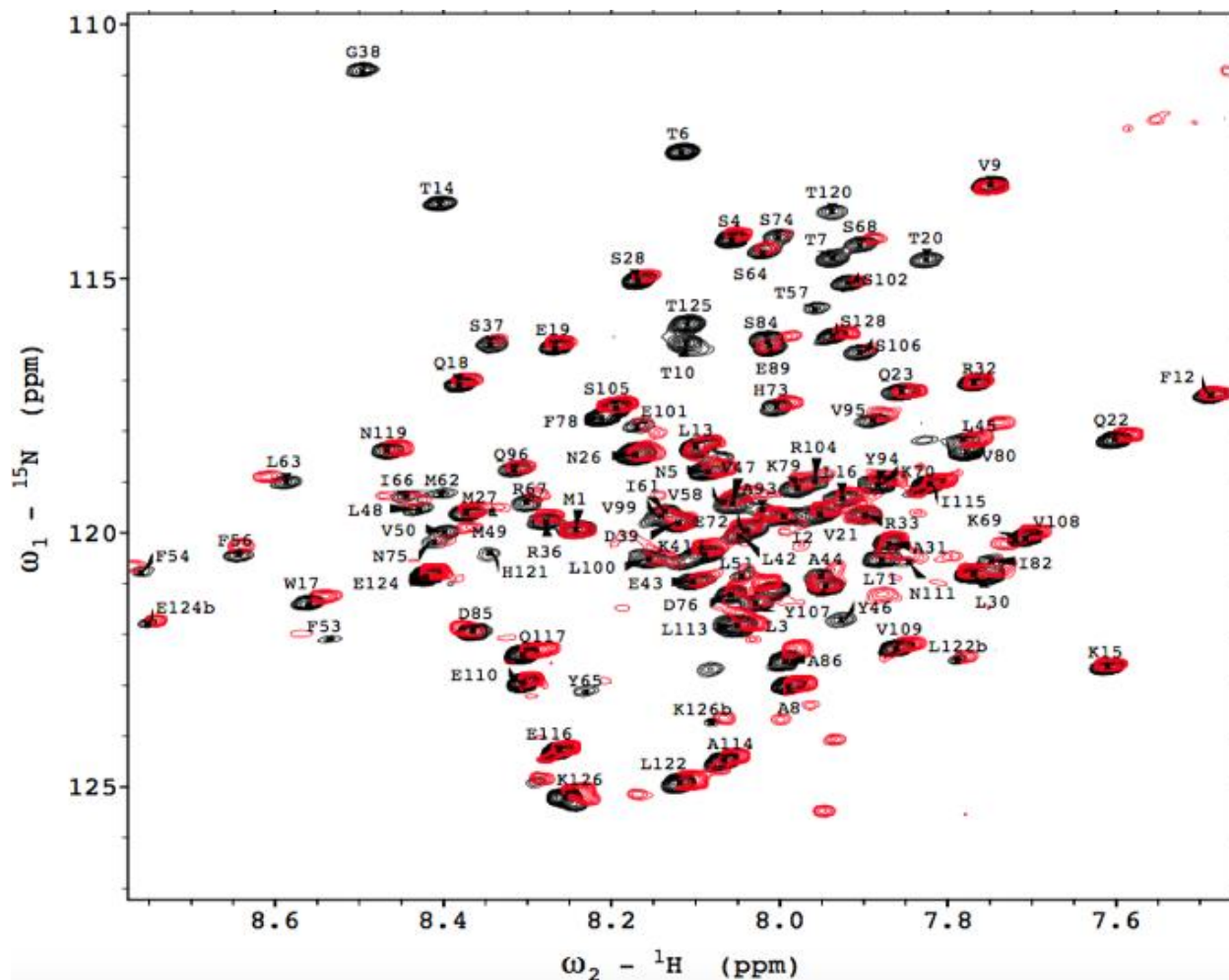


**Figure 25: Inverse Labeling of Thr**

The black peaks show the E1<sub>FTL→TVG</sub>. The red peaks show all the residues in the sequence with the exception of Thr. The black peaks that do not have an overlapping red peak are Thr residues. All 7 of the expected Thr peaks disappeared.

Using an iterative approach involving analyzing the 3D TROSY, as well as data from both specific labeled and inverse labeled samples, I were able to establish assignments for 86% of the peaks of the entire protein (Figure 26, Figure A) [64]. I also noticed that there are small number of residues (122, 125 and 126) that split into 2 individual peaks, perhaps arising from two slowly interconverting conformations. These peaks were also seen to be also be split in the published WT E1 spectra [56].

Since I believe that the major structural difference between WT E1 and E1<sub>FTL→TVG</sub> lies within the transmembrane, I exerted special focus to complete 95% of the assignments within the transmembrane and juxtamembrane regions (9 residues on each side of the TMR), including peaks for all 3 of the TVG mutations that were introduced. With these assignments in hand, I proceeded to collect and analyze relaxation and topology experiments to determine flexible regions of the protein and which regions of the protein are inserted in the membrane. While most of these missing peaks were dispersed throughout the protein, there is one small region in the C-terminal (Figure 27).

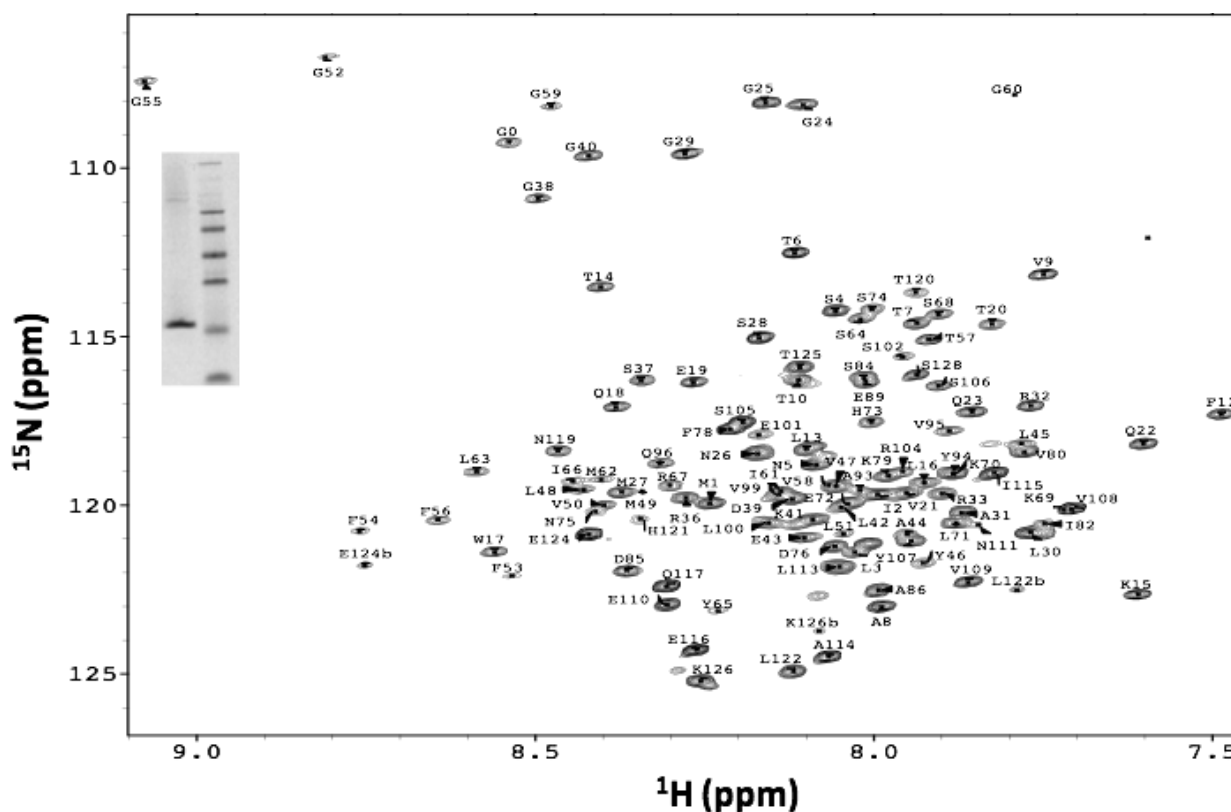


**Figure 26: Resonances Assignments of E1<sub>FTL→TVG</sub>**

This figure shows all the assignments that could be made using the experiments described in this chapter. The left inset shows the final purification for the <sup>13</sup>C, <sup>15</sup>N-E1<sub>FTL→TVG</sub> sample.

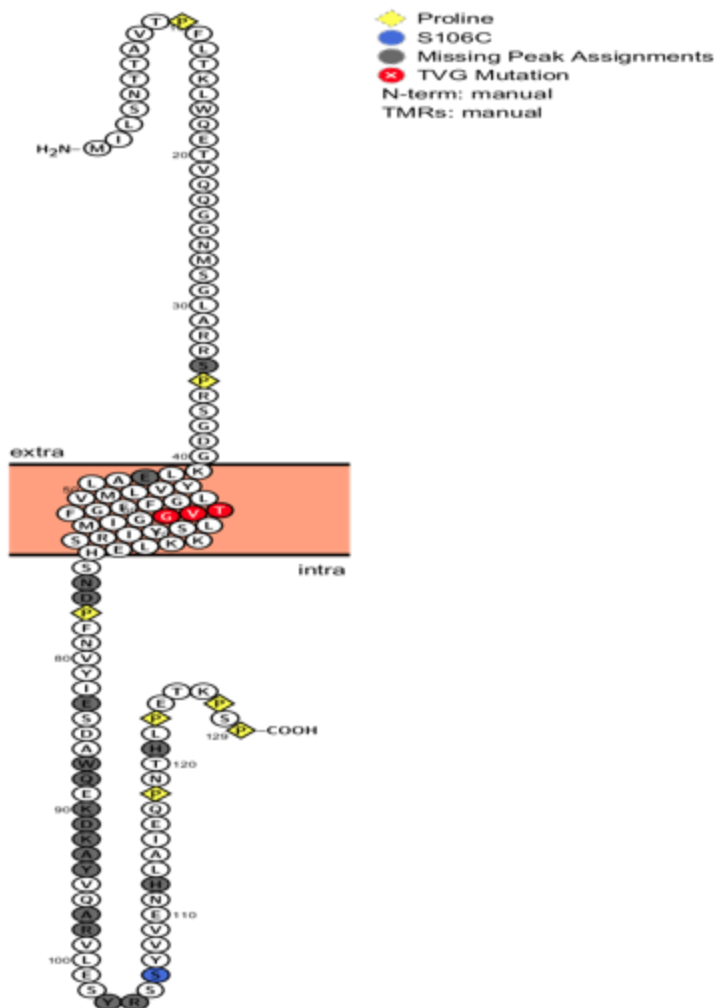


**Figure 27: Topology of Missing E1<sub>FTL→TVG</sub> Residues**

This figure depicts the topology of E1<sub>FTL→TVG</sub>. 7 prolines have been identified in yellow diamonds and the single Cys represented in blue. The TVG mutation can be seen in red within the tan transmembrane region. Peaks that could not be assigned are designated in gray. This figure was created using Protter - visualize proteoforms [79].

### 3.4 Chemical Shift-Based Secondary Structure Analysis

TALOS-N is an online resource that allows determination of the protein backbone and side-chain torsion angles based on measured backbone chemical shift (CS) data [80]. From our assignment data, I was able to use the chemical shifts for C, C $\alpha$ , C $\beta$ , N, and HN for each residue to predict the secondary structure E1<sub>FTL→TVG</sub> (Figure 28, middle panel). Residues that have TALOS-N helical probabilities close to or equal to 1.0

indicate the residue is part of an alpha-helix. Helical probability values that are close to 0 indicate random coil. The E1<sub>FTL→TVG</sub> TALOS-N plot predicts structured helical regions at both the N- and C-terminals around residues 9-22 and 87-104, and between residues 41 through 73, which contain the inserted TVG mutation. These helical regions are connected by flexible disordered regions. One notable characteristic of the E1<sub>FTL→TVG</sub> TALOS-N plot is seen at residue 58, the site of the T58V mutation, where a slight drop in helicity within the middle of the helix is observed. Also noticed, at residue 49, is a decrease in helical probability of about the same percentage as at residue 58.

To determine if the drop in helicity at residue T58V was due to the mutations introduced, I wanted to compare our E1<sub>FTL→TVG</sub> data to that of WT E1 and WT E3. Assignments for both E1 and E3 have been published by our lab [81, 53] and CS information has been deposited into the BMRB database that houses published CS data for proteins. When running WT E1 and E3 CS data through TALOS-N, I were able to see helical predictions that were similar to E1<sub>FTL→TVG</sub> but with some very notable differences (Figure 28, top and bottom panel). WT E1 CS data indicates helical structure spanning N-terminal residues 7-25, C-terminal residues 87-105, and the transmembrane region 42-71 that houses the functionally critical residues, FTL. Similar to E1<sub>FTL→TVG</sub>, in WT E1 a noticeable drop in helicity can be seen at residue 49 and at and around the FTL region, specifically for residues 59, 60, 61, and 62. One interesting difference between WT E1 and E1<sub>FTL→TVG</sub> is that WT E1 shows a much more intense drop in helicity at 4 transmembrane residues (site 59-62) while E1<sub>FTL→TVG</sub> only shows a mild decrease and only at one residue. (Figure 28, middle panel). In both WT E1 and E1<sub>FTL→TVG</sub>, residue 49 shows similar helical reductions. WT E3 CS data shows structured helical regions spanning residue N-terminal segments 9-26, C-terminal segments 90-97, and the TM segment 55-80, the latter of which contains the functionally important TVG motif. Unlike WT E1 and E1<sub>FTL→TVG</sub>, where a decrease in helicity around important or mutated regions is noticed, TALOS-N predicted strong helical structure for E3 between residue 55-80, including at and near the TVG motif (Figure 28, bottom panel). Interestingly, the percent of helical content of the mutated region of E1<sub>FTL→TVG</sub> is intermediate between that of WT E1 and E3. The decrease in helical content with the TVG mutation

introduced into E1 makes the transmembrane region of E1<sub>FTL→TVG</sub> more similar to E3 [64]. This increase in transmembrane helical structure for E1<sub>FTL→TVG</sub> relative to WT E1 may help us understand how E1<sub>FTL→TVG</sub> function is changed. Additional experiments detailed in Chapter 4 were conducted to confirm the TALOS-N prediction and give us more information about the mutated TVG region.

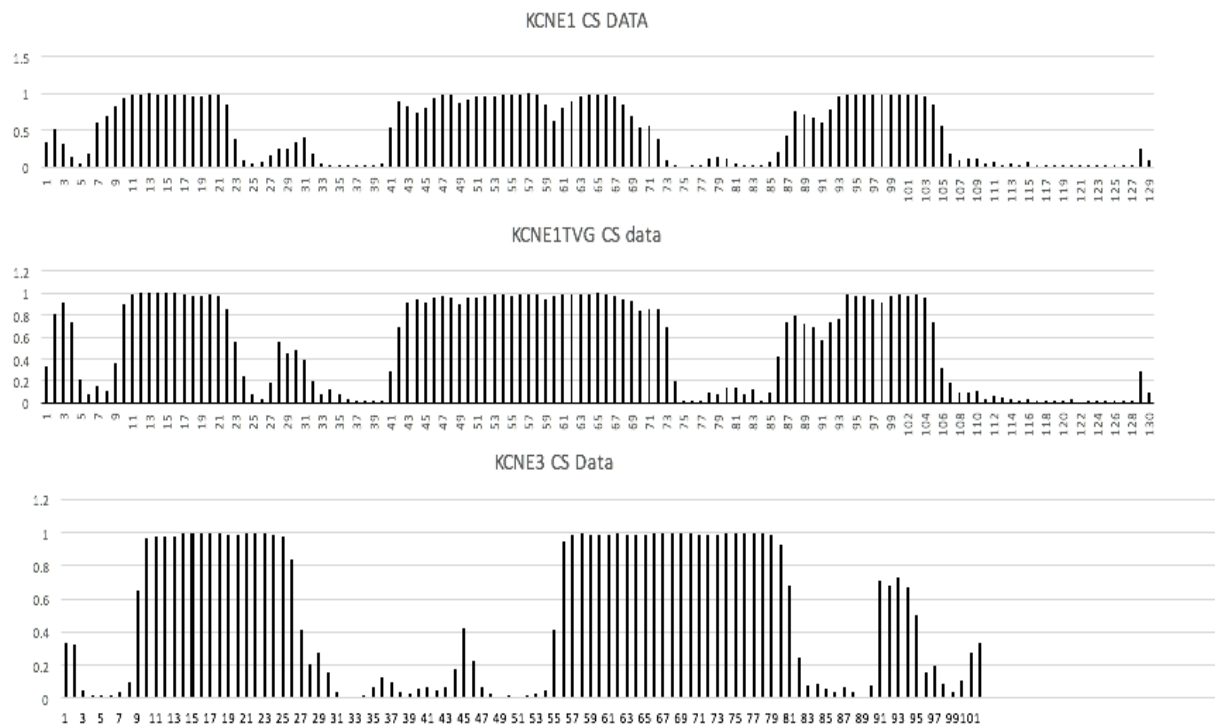


**Figure 28: Chemical Shift Analysis Plot using TALOS-N**

This figure shows helical and random coil regions for WT E1, WT E3, and E1<sub>FTL→TVG</sub>. Helical probabilities close to 1 indicated predicted helical structure while those close to 0 are predicted regions of random coil with no secondary structure. All 3 proteins were predicted to have 3 alpha helical segments that are connected by sections of random coil. This data has been obtained from reference 64.

## Chapter 4

### Preliminary Data, Discussion and Future Directions

#### 4.1 Published Data and Discussion

##### 4.1.1 Purification

The work of this dissertation represents the first step toward determining the E1<sub>FTL→TVG</sub> structure, its structural comparison to E1 and E3, and biochemical elucidation of how it interacts with the Q1 channel. Site-directed mutagenesis to mutate C106S and then F57T, T58V, and L59G was successful and paved the way to protein overexpression in *E. coli* in BL21 (DE3) CodonPlus RP competent cells. Healthy cell growth produced between 2.5 to 4 mg/ml of pure monomeric protein, a sufficient amount to perform high-quality NMR experiments. The pET16 expression vector added an N-terminal His<sub>6</sub>-tag, allowing us to purify pure monomeric <sup>15</sup>N-E1<sub>FTL→TVG</sub> into LMPG micelles using a nickel resin, enabling TROSY based NMR experiments. The dispersion of peaks seen in the TROSY spectra of E1<sub>FTL→TVG</sub> is typical for a reasonably well-behaved single-span membrane protein in detergent micelles and several of the previous assignments from wild type E1 could be transferred to E1<sub>FTL→TVG</sub> [56].

##### 4.1.2 Assignments

3D-TROSY based experiments were used to confirm the assignments that were transferred, make assignments that could not be transferred, and to provide chemical shift data for CO, C<sub>alpha</sub>, C<sub>beta</sub>, H<sub>alpha</sub>, HN, and N. Inverse labeling and specific amino acids labeling were used to fill in missing assignments not obtained by transferring or sequential backbone walking using 3D data. Leu, Ala, Phe, Met, Ile, Val were all selected for single amino acid labeling and Thr was inversely labeled. These amino acids were selected because Thr and Val are residues of the FTL→TVG triplet

substitution and these amino acids were common among the unassigned residues after 3D experiments. A total of 86 percent of the backbone resonances were assigned using these methods, with 95 percent assigned in the critical transmembrane and juxtamembrane regions. While I was not able to obtain 100% assignments, much of our studies were focused on the transmembrane region, specifically the FTL→TVG. Because of this, it was important to obtain a higher percent of assignments. This would allow us to gain more detailed information on how the FTL→TVG affected the transmembrane helical structure.

While some of the peaks from E1<sub>FTL→TVG</sub> aligned well with those from the <sup>1</sup>H,<sup>15</sup>N wild type E1, many others exhibited significant shifts in both resonances. The majority of these shifted peaks lie within the transmembrane regions, as might be expected given that this was the site of the triple substitution. Residues with the most highly shifted peaks (G52, F54, G55, F56, G60, L63) are each within 5 residues on either side of the TVG substitution, hinting that there might be structural changes from wild type E1 at and around the TVG mutation site. This suggests that these residues may undergo exceptional changes in the chemical environment around those residues. This could possibly be due to more or less flexibility or dynamics with the region due to the introduction of the TVG motif. Also of note, the TVG substitution added an additional Gly in a transmembrane region of WT E1 that is already Gly rich and also removed an aromatic Phe. Leu and Val are both nonpolar, branched amino acids and replacing one for the other might have little effect on function. However, Phe and Gly have different and unique structures. Phe has an aromatic ring, while Gly has only a single hydrogen for a side chain and typically allows backbone flexibility. While Gly is known as a helix breaker, it is quite commonly seen in transmembrane helices where it is believed to aid in helix-helix packing and facilitate tertiary and quaternary structure [82]. This additional Gly might play a role in stabilizing E1<sub>FTL→TVG</sub> packing and decreasing flexibility such that is it similar to that of KCNE3.

### 4.1.3 Secondary Structure of E1, E3, and E1<sub>FTL→TVG</sub>

The  $^{13}\text{CO}$ ,  $\text{C}_{\alpha}$ ,  $\text{C}_{\beta}$  H, HN, and N chemical shift values were input into the TALOS-N web server for secondary structure analysis. TALOS-N data showed 3 alpha helical regions located at the N- and C-termini and in the transmembrane domain, all connected by unstructured loops or strands. Unsurprisingly, E1<sub>FTL→TVG</sub> has a similar secondary structure as E1 and E3. However, while similar, all three proteins displayed a few noticeable differences. Both E1<sub>FTL→TVG</sub> and E1 exhibited a break in helicity in the TM region while E3 exhibits a continuous helix [53]. The TM segment of E1 exhibited a modest drop in helicity at and immediately after the wildtype FTL triplet that is critical for its unique function, located at residues 59-61 [41]. E1<sub>FTL→TVG</sub> showed a significantly smaller decrease in helicity and only at residue 59. This data supports the idea that TM segment in E1<sub>FTL→TVG</sub> is structurally more similar to E3 than it is wild type E1, possibly helping to explain why the triplet mutation converts E1<sub>FTL→TVG</sub> into a functionally similar protein to E3.

## 4.2 Addition Preliminary and Discussion

### 4.2.1 $T_1$ and $T_2$ Relaxation

To better understand if the break in helicity seen in E1 and E1<sub>FTL→TVG</sub> affects their flexibility, relaxation experiments were undertaken. Relaxation occurs when nuclear spins that have been excited in a magnetic field via application of a magnetic pulse return to their ground or equilibrium state. Dynamics and flexibility information can be extracted from these experiments due to the fact the transfer of energy from the excited nuclear state back to its ground state is mediated by molecular motions, both overall tumbling, and local flexibility. The  $T_1$  relaxation time is for relaxation of magnetization along the axis of the static magnetic field (designated z) and is called the “longitudinal” relaxation time.  $T_2$  is for relaxation of magnetization in the XY plane and is called the “transverse” relaxation time. Another relaxation experiment to measure dynamics and flexibility is the steady-state Nuclear Overhauser Effect (ss-NOE). ss-

NOE experiments measure NOE-based changes in the  $^{15}\text{N}$  signal intensity after saturating the proton signal, measurements that are useful for detecting local backbone motions [63].  $T_1$  and  $T_2$  experiments for membrane proteins are conducted by monitoring relaxation using a series of delay times through 2D TROSY- based NMR experiments [84]

NMR relaxation experiments have been implemented on  $^{15}\text{N}$ -E1<sub>FTL</sub>→TVG samples. Preliminary 1D and 2D recordings of  $T_1$  and  $T_2$  measurements have been executed using 11 and 10 delay times ( $\tau$ ), respectively, and in the following order: 15ms, 4000ms, 400ms, 30ms, 2000ms, 50ms, 1600ms, 100ms, 1200ms, 200ms, 800ms, for  $T_1$  and 3ms, 170ms, 8ms, 137ms, 17ms, 102ms, 34ms, 85ms, 51ms, and 68ms for  $T_2$ . In our preliminary data, spectra showed that at longer  $\tau$  times, E1<sub>FTL</sub>→TVG signals decayed for both  $T_1$  and  $T_2$  (Sup Figure 7). Signal decay corresponds to the spin state relaxing back to the ground state.

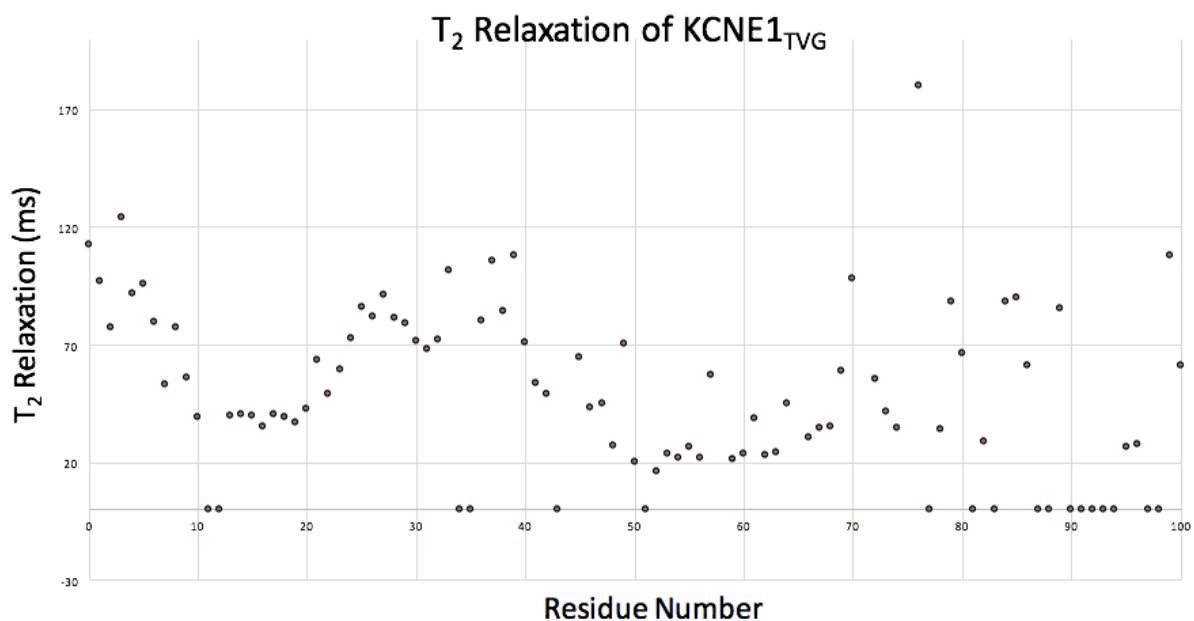


**Figure 29: T<sub>2</sub> Relaxation Data for E1<sub>FTL</sub>→TVG.**

This figure shows the  $T_2$  relaxation data for E1<sub>FTL</sub>→TVG in ms. Data points at 0 indicate missing assignments or missing data. The amino acid residues are on the x-axis and the relaxation times in ms are on the y-axis.

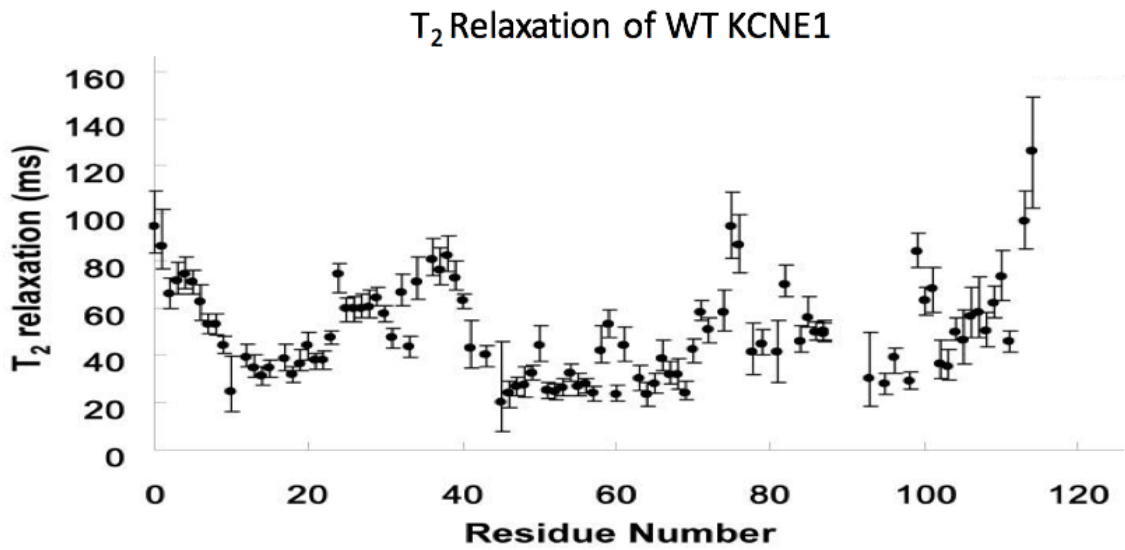


**Figure 30: T<sub>2</sub> Relaxation Data for Wild Type KCNE1**

This figure depicts T<sub>2</sub> relaxation data for WT KCNE1 in ms. The amino acid residues are on the x-axis and the relaxation times in ms are on the y-axis. Figure modified from reference 56

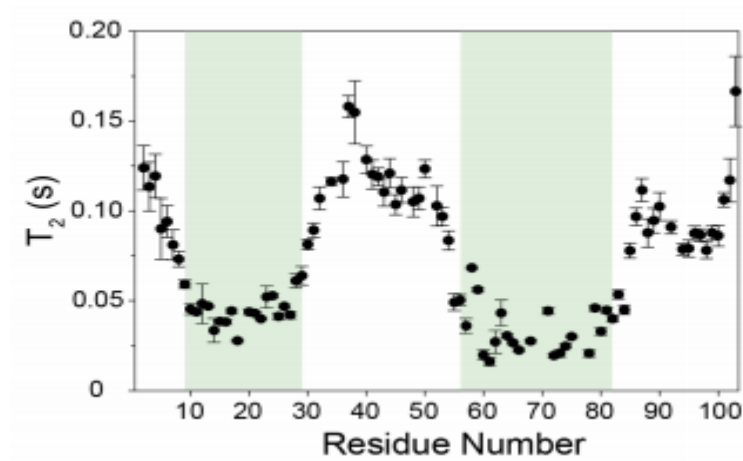


**Figure 31: T<sub>2</sub> Relaxation Data for Wild Type KCNE3**

This figure shows the T<sub>2</sub> relaxation data for KCNE3. The green blocks represent transmembrane regions. This data is from reference 53.

While figure 29 depicts only single-replicate data and the reliability of the data is not clear,  $T_2$  relaxation data show a general and similar pattern with wild type E1 (Figure 30). Both have a relatively rigid N-terminal helix, residues 9 to 20, followed by a short flexible region before the less flexible TM domain, residues 41 to 73. Wild type E1 data goes on to show a rigid C-terminal helix, residues 87 to 104, that is not seen in  $E1_{FTL \rightarrow TVG}$ . The noisy C-terminal data for the mutant could be a result both of not having replicated the experiments or even poor sample/spectral quality. These issues can be rectified with doing further replicates on stable  $E1_{FTL \rightarrow TVG}$ . Interestingly, E1 shows roughly 3 residues in the TM domain that are less rigid than the other TM residues located near the critical mutation substitution. Within that same region,  $E1_{FTL \rightarrow TVG}$  only shows 1 residue (T57) that is slightly more flexible. These data appear to be consistent with the TALOS-N data, where E1 shows a larger area with a break in helicity, while  $E1_{FTL \rightarrow TVG}$  shows a much smaller area. KCNE3 (Figure 31) shows similar results as  $E1_{FTL \rightarrow TVG}$  in that E3 only show 1 residues with increased flexibility in the TM region at residue T71. In  $E1_{FTL \rightarrow TVG}$  and E3, residues T57 and T71 show similarities in flexibility within the transmembrane region. Interestingly, these two residues are both Thr and are part of the FTL $\rightarrow$ TVG switch.

Again, this would suggest that  $E1_{FTL \rightarrow TVG}$  has a more rigid transmembrane helix similar to E3, and contributes to  $E1_{FTL \rightarrow TVG}$  and E3's functional similarities. The Thr residues may also play a key role in flexibility. Here I compare only  $T_2$  data because it is more informative than  $T_1$  and E1 WT only has  $T_2$  data published. Again, our  $E1_{FTL \rightarrow TVG}$  is in need of a much more rigorous study and future experiments completing ss-NOE experiments and plotting of  $1/T_1$  ( $R_1$ ) and  $1/T_2$  ( $R_2$ ) as they are much more reliable and will give better insight to flexible regions of  $E1_{FTL \rightarrow TVG}$ . In our future experiments, I hope that the  $T_1$  and  $T_2$  data will corroborate our preliminary data, and be more precise in residue flexibility and provide better resolution of the C-terminal helix. Re-analyzing the raw E1 relaxation data to compare  $T_1$  and  $T_2$  data to that of  $E1_{FTL \rightarrow TVG}$  would give more insight of the differences in flexibility of  $E1_{FTL \rightarrow TVG}$  and E1.

#### 4.2.2 Amide Hydrogen Exchange Measurements

To better understand what could be happening at the helical break and the possible flexible segment in the TM region, amide-water hydrogen exchange experiments might allow us to determine if these residues contain water-exposed amide sites not part of stable alpha helices. Experiments such as CLEANEX-PM can be a powerful tool for assessing structural information. While water exchange techniques are useful, many of them are plagued by artifacts that make interpreting data difficult or impossible. The Phase-Modulated CLEAN chemical EXchange (CLEANEX-PM) spin-locking sequence is unique because it eliminates artifacts that are often seen in traditional water-proton exchange experiments [63, 58]. The CLEANEX-PM spin-locking module is combined with an HSQC pulse sequence to create a 2D experiment useful for quantitating exchange rates. The CLEANEX-PM spin-locking module is applied after water is selectively excited and while amide protons and water are exchanging [58].

To test water accessibility, I conducted a preliminary test using  $^{15}\text{N}$ -E1<sub>FTL→TVG</sub> and  $^{15}\text{N}$ -E1 and ran a CLEANEX-PM module with delay times at 25ms and 100ms. To quantify this data, ratios of peak intensities for the 25 ms delay CLEANEX-PM spectrum against those from the reference sample for both WT E1 and E1<sub>FTL→TVG</sub> proteins were plotted (Figure 32, Figure 33). In WT E1 the transmembrane region, 47-74, I noticed that residues 56, 57, 58, 59, and 60 have a higher ratio suggesting the backbone amide protons are experiencing some exchange with water protons. Included in this region are mutated amino acids 57, 58, and 59. WT E1 residues 56, 57, and 58 have mild proton exchange while 59 and 60 have more significant exchange 4-6 times higher than that of 56 and 57 (Figure 32). In E1<sub>FTL→TVG</sub> the data show similar patterns to E1 with E1<sub>FTL→TVG</sub> water accessibility within the middle of a transmembrane helix. One notable difference is that E1<sub>FTL→TVG</sub> only shows water accessibility at residues 58 and 59 and their intensities are about half the amount of WT E1. While we do not have CLEAN-EX data for E3, hydrogen-deuterium exchange measurements show transient contact with water at residues T71, S74, and Leu 75. The residue T71 is part of the functionally critical E3 region and S74 and Leu 75 are in close proximity to that region [53]. Interestingly, E1<sub>FTL→TVG</sub>, E1, and E3 all experience contact with water within the transmembrane helix

and all are regions that are critical for their unique function. E3 NMR data-restrained molecular dynamics suggest that contact with water in the transmembrane helix at residues 71,74, and 75 stabilize E3 curved helix by decreasing the energetic cost of breaking backbone hydrogen bonds [53, 85]. Our lab has extensively shown that WT E1 helix is also curved [41, 86] and therefore I hypothesize that E1<sub>FTL→TVG</sub> is also curved and this curved nature of the helix for all 3 proteins is stabilized due to their contacts with water in the TM region. While E1<sub>FTL→TVG</sub> and E3 show water accessibility to 2 and 3 residues, respectively, E1 has 5 residues exposed to water in the TM region. This would suggest that simply having water accessibility is not a factor when differentiating function, but the amount of amino acids that interact with water might lead to both structural and functional differences.

Because CLEANEX-PM data has only been performed once and the data is very noisy, it is a bit premature to make a concrete conclusion that these sites in E1 have a higher water accessibility than E1<sub>FTL→TVG</sub>. Further, replicate experiments are required, but if confirmed, it would align with our TALOS-N and T2 relaxation data suggesting that E1 has a larger stretch of TM residues with reduced helicity and possibly more flexible, which allows more water penetration and exchange with more TM residues in wild type E1. E1<sub>FTL→TVG</sub> and E3 both experience water accessibility but to a lower degree which could possibly lead to a stronger helical structure in that region. It will be exciting if further CLEANEX-PM experiments validate our preliminary data.

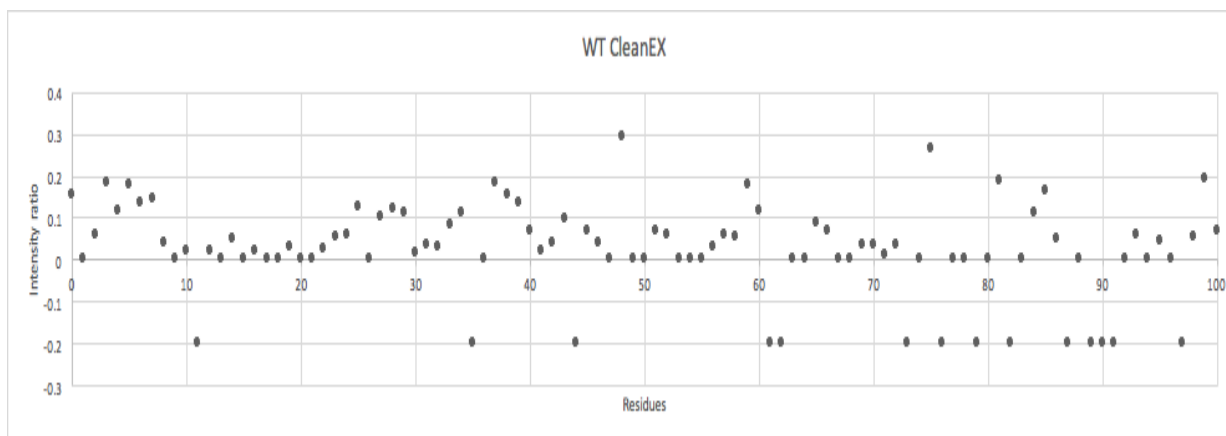


**Figure 32: CLEANEX-PM 25ms Data for WT E1**

This figure shows the CleanEX-PM (HSQC) of WT E1 with an exchange delay of 25ms. Residues with a high peak intensity ratio indicate high water-amide hydrogen exchange while low values indicate residues protected from exchange. Peaks located at -0.2 are for peaks that were missing or unassigned.

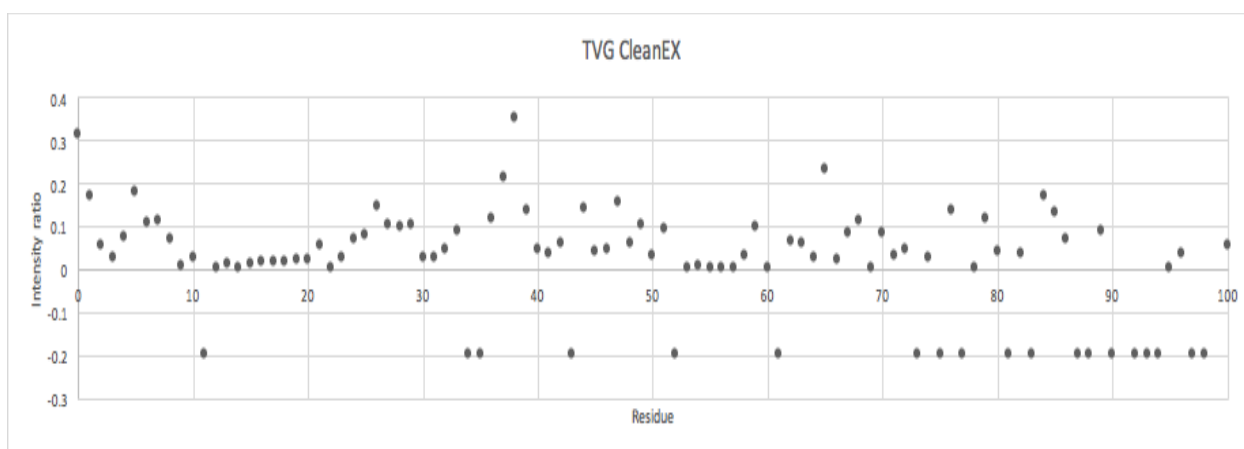


**Figure 33: CLEANEX-PM 25ms Data for E1<sub>FTL→TVG</sub>**

This figure shows the CLEANEX-PM (HSQC) of E1<sub>FTL→TVG</sub> with an exchange delay of 25ms. Residues with a high peak intensity ratio indicate water accessibility while low values indicate residues protected from water exchange. Residues fixed at -0.2 indicate residues that could not be assigned or for which the peak is missing.

#### 4.2.3 Comparison of E1, E3, and E1<sub>FTL→TVG</sub>

The highest degree of sequence identity between the 3 KCNE proteins occurs at the beginning and end of their TM domain, and E1, and E3 exhibit a curved or kinked TM helix yet they bind and modulate KCNQ1 in different manors. The first thing to make

notice of is the TM sequence surrounding the critically functional regions (Figure 34). These regions are 5 amino acids before the 3 residue functional region and 4 residues after it. The FTL amino acids of E1 and the TVG amino acids of E3 and E1<sub>FTL→TVG</sub> all have nonpolar Thr amino acids and beta-branched amino acid Leu and Val, respectively. All Thr residues are exposed to water molecules and exhibit some level of flexibility in E1, E3, and E1<sub>FTL→TVG</sub>. One significant thing that differentiates the FTL or E1 and the TVG of E3 and E1<sub>FTL→TVG</sub> is the large, bulky aromatic Phe of E1 and the flexible single hydrogen atom sidechain Gly in E3 and E1<sub>FTL→TVG</sub>. The removal of the large aromatic ring in the E1<sub>FTL→TVG</sub> could play a large factor leading to the structure, interactions, and function of E1<sub>FTL→TVG</sub>.

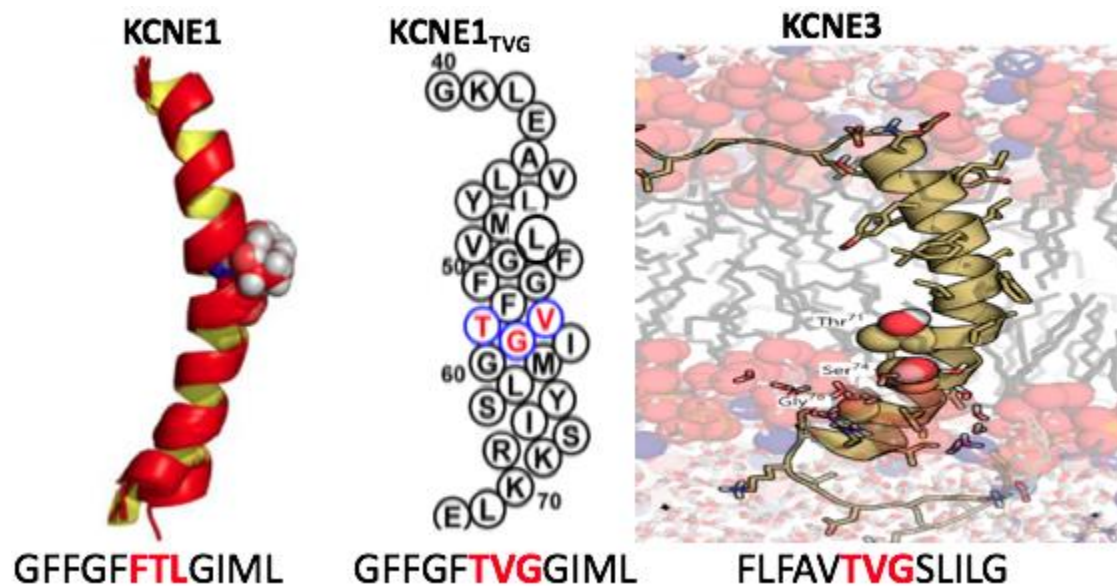


**Figure 34: Experimentally Determined KCNE1 and KCNE3 and Topology of E1<sub>FTL→TVG</sub>**  
 This figure show experientially determine KCNE1 (left) and KCNE3 (right) and E1<sub>FTL→TVG</sub> Topology (center) transmembrane regions. Highlighted in red is the functionally critical motif surrounded by 4 or 5 amino acids of the sequence on either side of the motif. The highlighted residue on KCNE1 indicates T57 while KCNE3 shows critical residues that sit on the concave face of the curve, T71, S74, G78.

In order to better understand the FTL→TVG mutation, it is helpful to understand the important interactions of WT E1 and WT E3. In WT E1, T58 (Figure 34, first panel) residues interacts directly with the S6 helix at residue F339 [87-89] to stabilize the closed state [47]. With the addition of the TVG mutation, the Thr residue is moved upwards by one residue. It is also likely that Q1 F339 plays a role in the gating of the channel. I hypothesize that this mutation eliminates the Thr and S6 F339 of interaction of E1 that stabilizes the closed state and makes the channel easier to open at initial and lower voltage potentials. It is possible this the T57/F339 interaction disruption also eliminate gating of the channel leading to a constitutively active channel. We also know that the bulky F57 residue helps stabilize the pre-open intermediate state is now missing from WT E1. These are 3 possible reason why the FTL→TVG mutation leads to an constitutively active E1 channel.

### **4.3 Future Experiments**

#### **4.3.1 Paramagnetic Probe Access Experiments**

When studying membrane proteins, it is often important to understand the membrane topology—how the protein sits and/or interacts in the membrane. To investigate membrane topology for a membrane protein in a model membrane environment, paramagnetic aqueous and lipophilic probes (Gd(III)-diethylenetriaminepentaacetic acid (Gd-DTPA) and 16 DOXYL-stearic acid (16-DSA), respectively) were used as relaxation-enhancement agents. Comparing the spectra of each paramagnetic probe to that for a reference sample in the absence of the probe allows us determine which residues lie within the membrane or are exposed to solution. These probes work by promoting the rapid NMR relaxation of nuclei that are in close proximity to the probe, resulting in line broadening. Those residues not close to the probe are unaffected. Gd-DTPA, a compound often used as a contrast agent, is a water-soluble paramagnetic probe based on the paramagnetic  $Gd^{3+}$  ion [63, 90]. Its presence will cause the signal of water-exposed residues to broaden. 16 DOXYL-stearic acid (16-DSA), also a contrast

agent, is a hydrophobic paramagnetic probe that partitions into the membrane and broadens NMR-active nuclei located on lipid-exposed hydrophobic segments [63, 91]. Sites buried deep in protein tertiary structure are protected from both probes.

Our preliminary studies used the same sample conditions previously used for KCNE3 [53] as a starting point for both 16-DSA at 0.7 mM and Gd-DTPA at 20 mM. Peak intensities for both 16-DSA and Gd-DTPA spectra were compared to the corresponding peaks in the reference sample absent of any paramagnetic agents. These probes work by relaxing NMR active nuclei that are within close proximity. While these experiments at the mentioned concentration did cause relaxation in a reasonable pattern, further experiments and possible varying concentrations are needed (preferably in triplicate) to better understand the topology. These data will be compared to the already published data for E3 [53]. Corresponding studies of E1 will also need to be performed to better understand if differences in the TM helix affect its position within the membrane phase. These data would provide information regarding whether E1, E1<sub>FTL→TVG</sub> and E3 have different residues, particularly in the ends of the transmembrane helix, that are sitting in the membrane or not.

#### **4.3.2 Structural Restraints**

To calculate a three dimensional E1<sub>FTL→TVG</sub> structure, it will be necessary to gather distance and orientational restraints. To gain distance restraints on the structure for membrane protein such as E1<sub>FTL→TVG</sub>, paramagnetic relaxation enhancement experiment (PRE) are often employed to gather short, medium, and long range distances. This experiment works by chemically attaching a single spin-label on E1<sub>FTL→TVG</sub> through selectively placed Cys residues. Based on the distance from the paramagnetic spin label, each NMR active nucleus will be affected differently, with sites close to the probe being strongly relaxed, leading to broadened resonance peaks.

To make these measurements, mutating out all wild type Cys residues in the sequence, then introduce a single Cys residue in specifically selected locations must be done.

Since our E1<sub>FTL→TVG</sub> construct has already removed all Cys residues to prevent dimerization, site-directed mutagenesis can easily be performed to incorporate additional cysteines. I have created 5 single-Cys constructs (A44C, Y46C, S64C, Y65C, Y74C) that were overexpressed and purified. These sites were selected because they lie in the juxtamembrane regions or only a few residues into the TM. These sites should be easy to label, but are located on relatively rigid parts of the protein, which will mean extracting distances from the associated PRE measurements easier. Preliminary 2D TROSY experiments were carried out. While generally of low quality due to low concentration and use of a low field magnet, the spectra do appear to be similar to the spectrum for the parent E1<sub>FTL→TVG</sub> mutant. Future samples will need to be purified to high enough concentrations and run on a high field magnet to ensure high quality NMR spectra. The resulting spectra should hopefully establish that the mutations have not affected the fold. If some spectra suggest a misfolded protein, further experiments would have to be carried out to identify more suitable residues for mutation to cysteine and spin labeling, located within the same area of the protein.

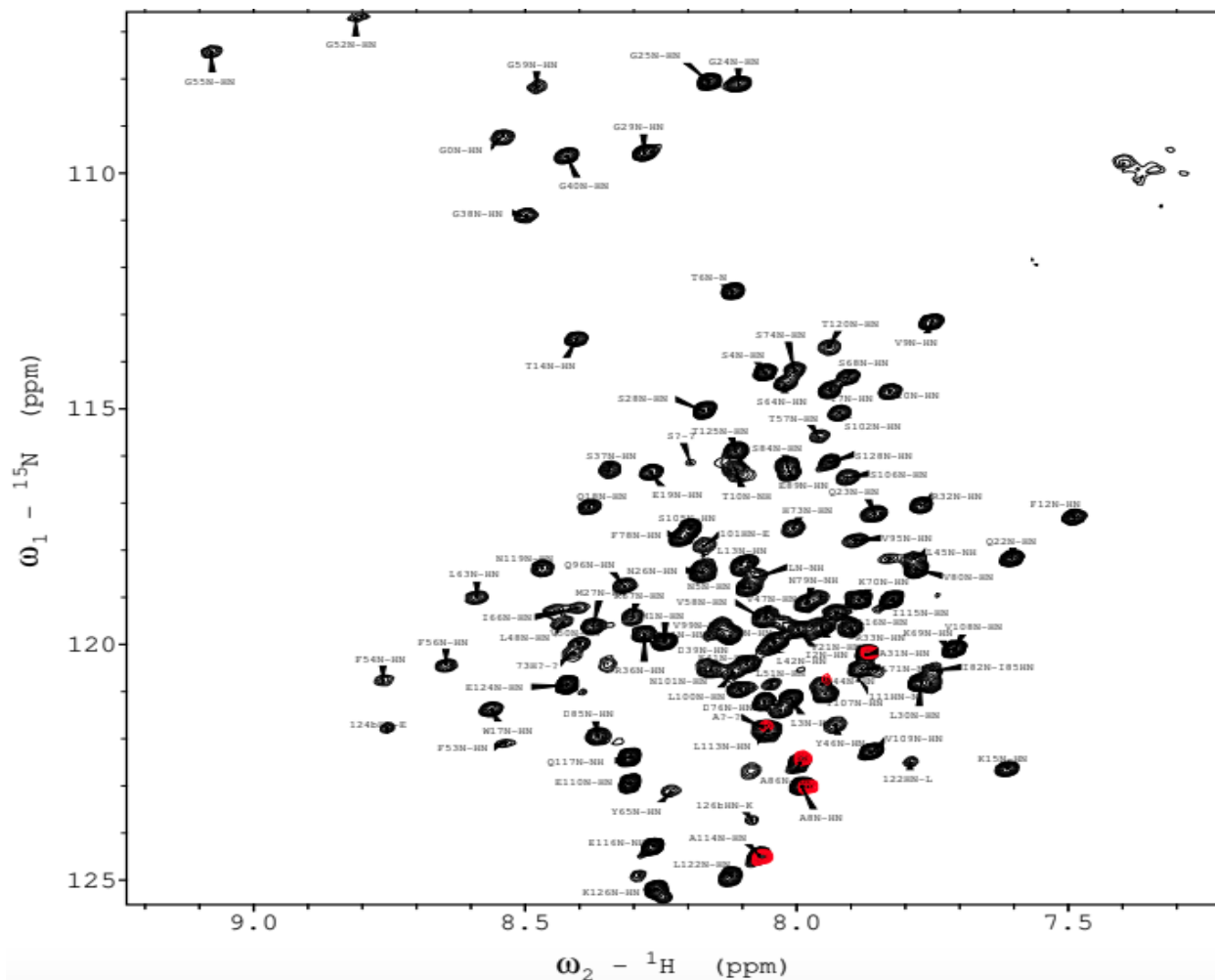
Once mutations are confirmed and are verified to not significantly alter the chemical shift profile, a thiol-reactive spin label probe, MTSL, would be attached to the single Cys residue and a pair of matched <sup>1</sup>H,<sup>15</sup>N-TROSY spectra would be acquired, one with the paramagnetic probe and then one in which the paramagnet has been quenched with ascorbic acid to convert the paramagnet to a diamagnet. The peak intensity ratios for the paramagnetic sample relative to those from the matched diamagnetic sample are used to assess distances between the paramagnetic probe and each amino acid residue [53, 92, 93]. Intensity ratios less than 0.15 are considered close in space (<12 angstroms between the probe and amide proton). Residues that experience moderate effect from the paramagnetic probe are medium in proximity (quantifiable in the 12-20 angstrom range), while those that exhibit little effect (less than 15% reduction in peak height due to broadening) are considered far (>20 angstroms) [94]. This anticipated data will provide distance restraints to aid in calculating our E1<sub>FTL→TVG</sub> structural ensemble. These experiments also will need to be done in triplicate as other experiments listed above to determine the most accurate structure calculation.

Other restraints used for calculating structure can be obtained from double electron-electron resonances (DEER) data and residual dipolar coupling (RDC) experiments. DEER experiments relate to long range distances between 18-80 angstrom by attaching spin labels at 2 locations and measuring the distance between the two probes [86]. This requires introducing 2 strategically placed Cys residues, then attaching spin labels to these Cys residues, and measuring the distance between the two. Previous DEER experiments have been performed on E1 [86], and the previous results would be compared to our DEER data. While providing distance information, the length of the TM of both E1 and E1<sub>FTL→TVG</sub> can also determine. Combined with 16-DSA and Gd-DTPA data this will shed light on if the TVG mutation substitution affects how the E1<sub>FTL→TVG</sub> sits in the membrane. RDC's provide structural restraints on the orientation of the bond vectors, typically the backbone amide HN, relative to the molecular frame. Using these restraints, the program Xplor-NIH can be employed [95] to begin calculating E1<sub>FTL→TVG</sub> structure. Observing the experimentally determined structures of E1, E3, and E1<sub>FTL→TVG</sub> will give us insight into how these protein are structurally different. Furthermore, computational docking of the E1<sub>FTL→TVG</sub> structure into the KCNQ1 structure can be employed to gain insight on how E1<sub>FTL→TVG</sub> modulates KCNQ1 differently from E1 and E3.

In this study, I reported the backbone NMR assignments and secondary structure of the E1<sub>FTL→TVG</sub> mutant that exhibits E3-like channel modulatory behavior. The results of this work provide a first step in comparing results for this mutant with the known NMR-determined structures of wild type E1 [56, 41] and wild type E3 [44, 53]. Our TALOS-N data show that the secondary structure of E1<sub>FTL→TVG</sub> at the mutation substitution site showed a slight decrease in helical structure relative to E3, but it was not as pronounced as that of E1. The completed backbone assignments for the E1<sub>FTL→TVG</sub> mutant also provide the basis for future studies of the 3D structure and dynamics of this membrane protein. I hypothesize that critical WT E1 contacts with Q1 that either gating or a pre-open state have been eliminated with the TVG substitution and leading to an Q1/E1 channel that behaves like an Q1/E3 channel. There is already much published information about the E1 and E3 structures and a number of studies have proposed models for how these

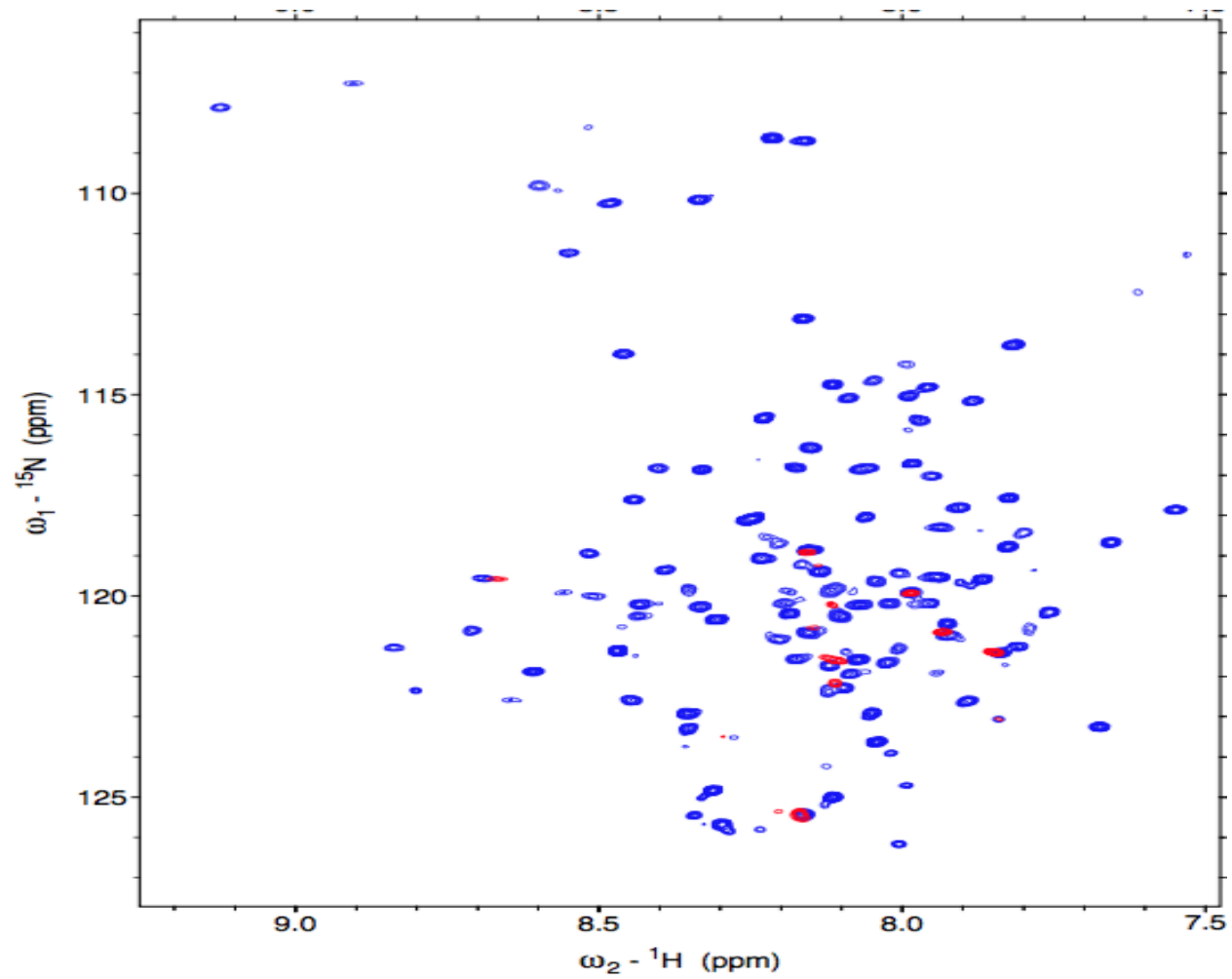
proteins bind Q1 and differentially modulate the function of this important channel. I hope this study will help contribute to the understanding of KCNQ1 and its ancillary KCNE family proteins. More specifically, I hope this work will allow others to better understand how critical amino acids and their interactions with the KCNQ1 channel can be manipulated to to modulate the channel in a different manner. This information can be useful when understanding how disease mutations alter the Q1 channel modulation and possibly be useful information for drug targets for modulating Q1 and its unique function when bound to KCNE family members.

## Supplemental Figures



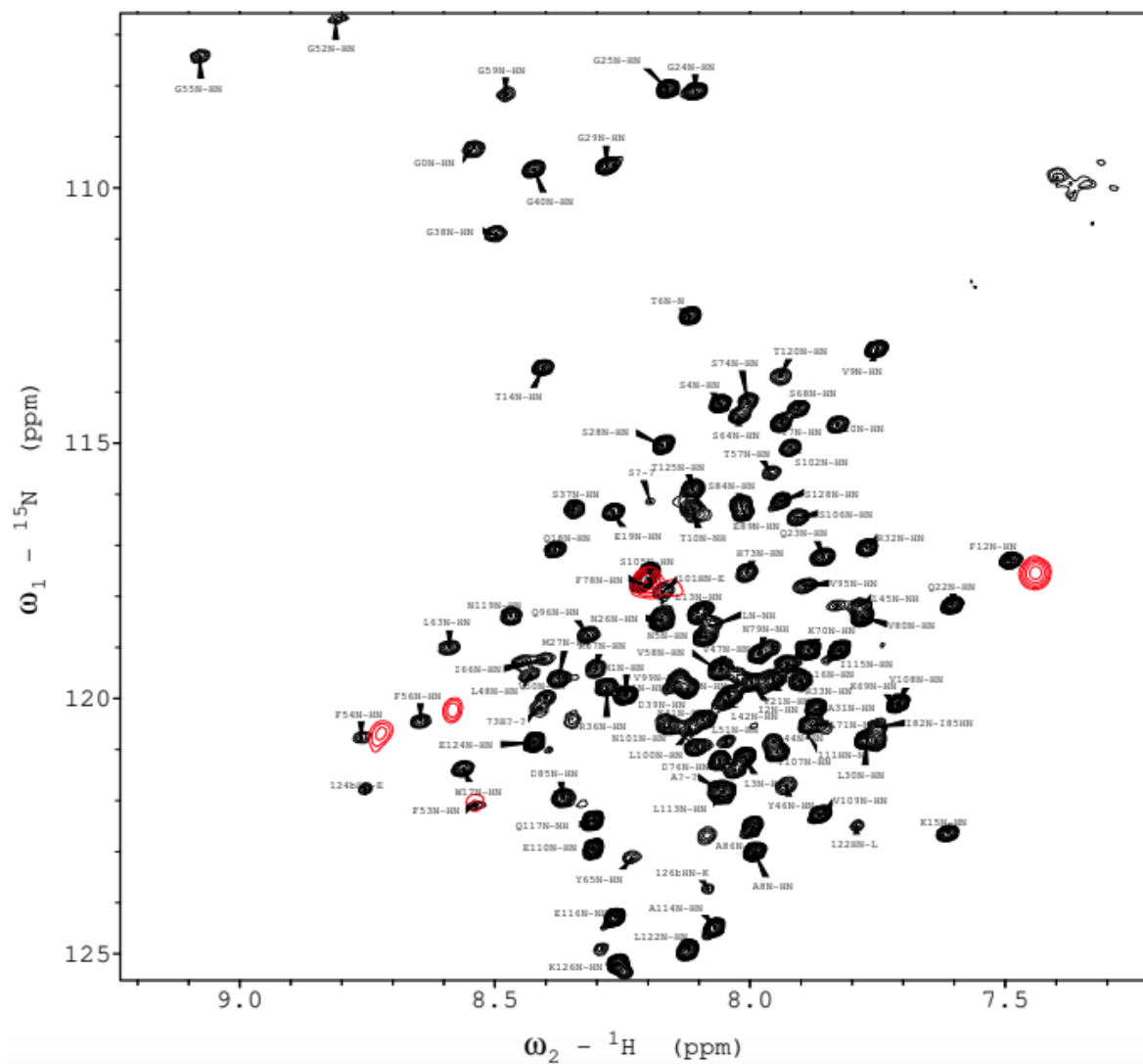
### Supplemental Figure 1: Specific Amino Acid Labeling of Ala

This figure depicts the specific amino acid labeling of Ala seen in red overlay with E1<sub>FTL-TVG</sub>. Of the 7 Ala residues in the sequence, 6 can be seen in this figure.



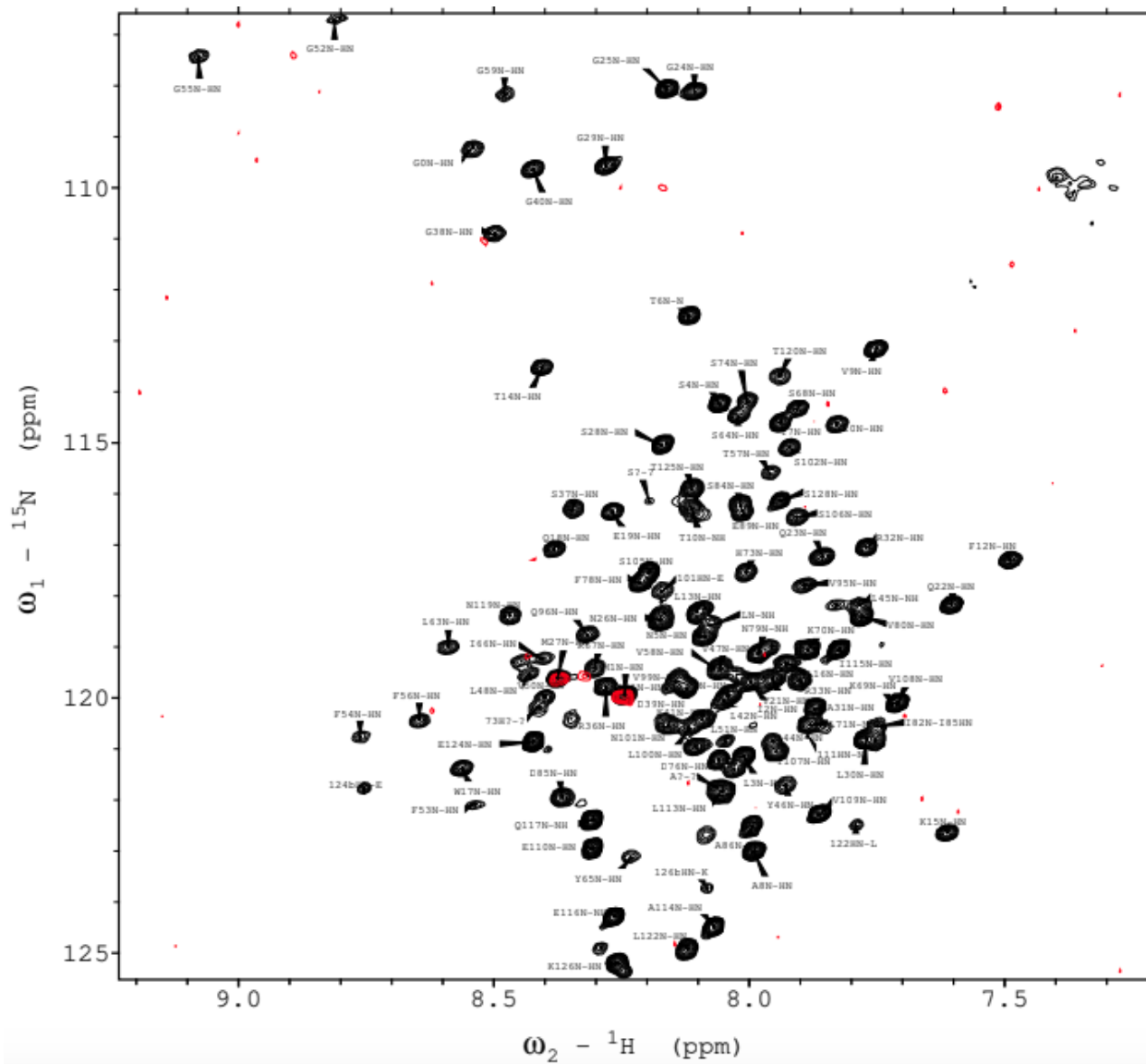
**Supplemental Figure 2: Specific Amino Acid Labeling of Leu**

This figure depicts the spectra of single amino acid labeling of Leu. Of the 13 residues in the E1<sub>FTL</sub>→TVG sequence, all 13 peaks can be seen in red.



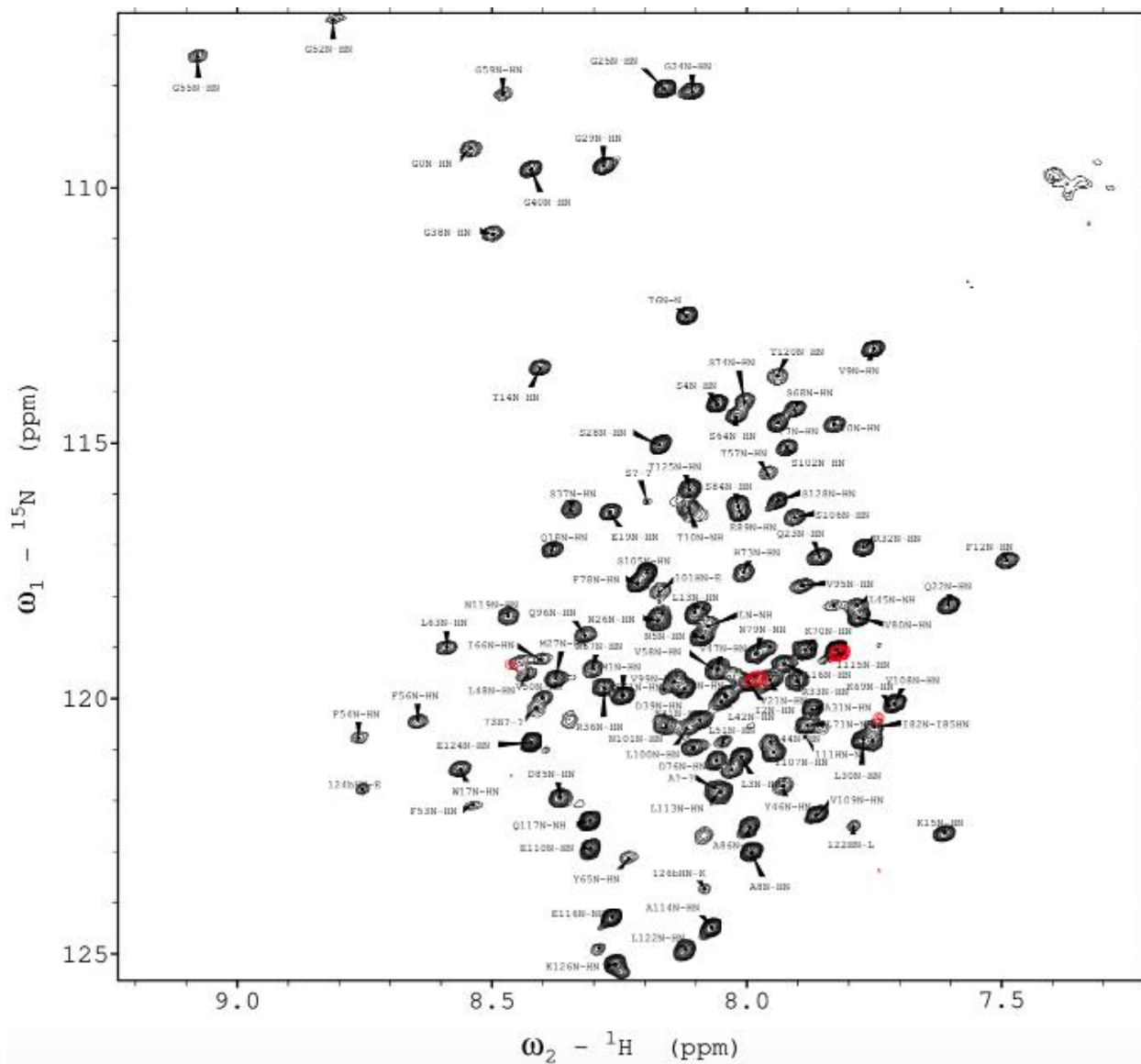
**Supplemental Figure 3: Specific Amino Acid Labeling of Phe**

This spectrum shows the specific amino acid labeling of Phe in red overlay with the E1<sub>FTL</sub>→TVG spectrum. Of the 5 residues in E1<sub>FTL</sub>→TVG sequence, all 5 can be observed.



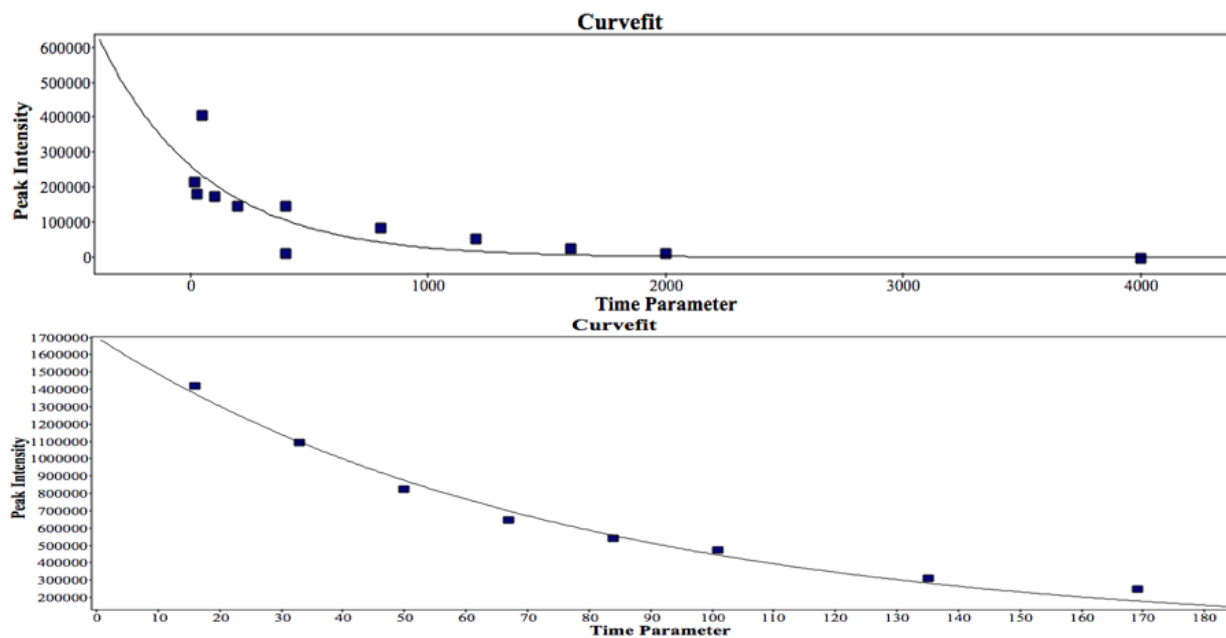
**Supplemental Figure 4: Specific Amino Acid Labeling of Met**

This figure depicts the single amino acid labeling of Met shown in the red peaks overlay with E1<sub>FTL</sub>→TVG spectrum. Of the 4 residues in the sequence, all 4 peaks can be observed.



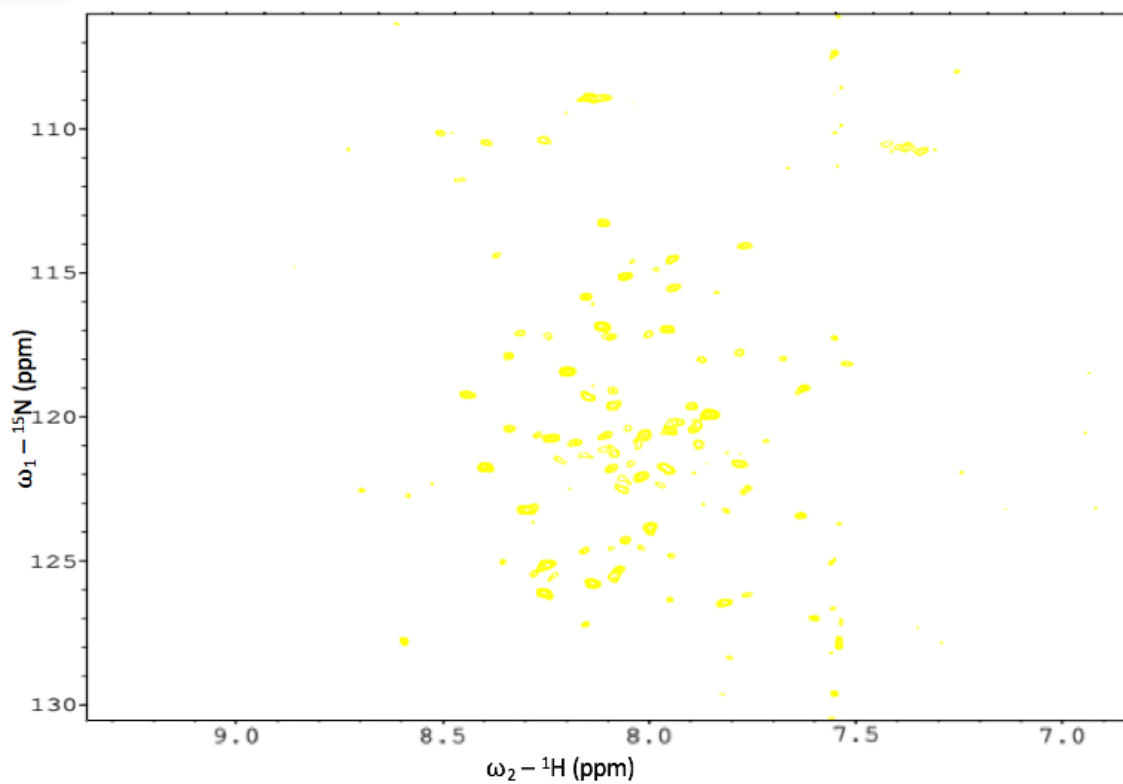
**Supplemental Figure 5: Specific Amino Acid Labeling of Ile**

This figure depicts the spectrum of the specific amino acid Ile seen in red that is overlaid onto E1<sub>FTL</sub>→TVG. Of the 5 residues in the E1<sub>FTL</sub>→TVG sequence, only 4 were visible in this spectrum.



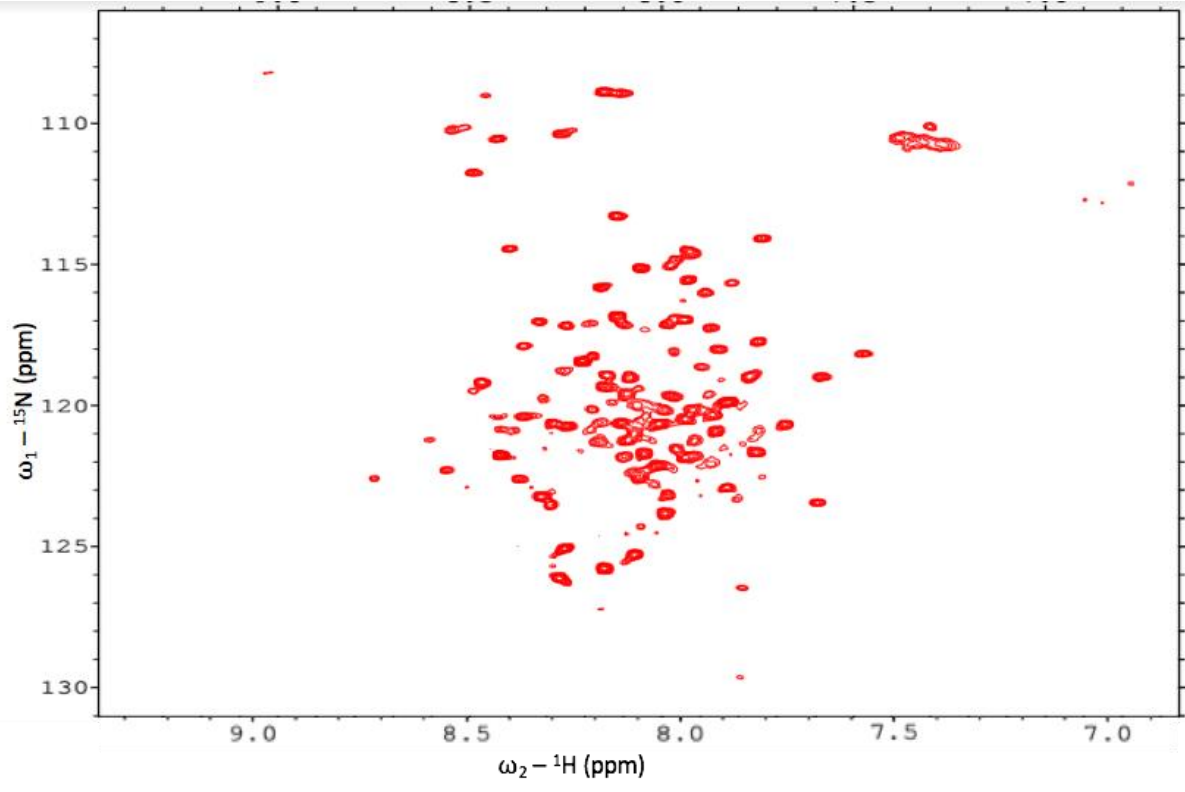
**Supplemental Figure 6:  $T_1$  and  $T_2$  of  $E1_{FTL \rightarrow TVG}$  Decay Curves**

The top panel shows the decay of a single peak from 2D TROSY spectra at various  $T_1$  tau times. The bottom panel displays the  $T_2$  decay curve of a single point from the 2D TROSY over the  $T_2$  tau times.



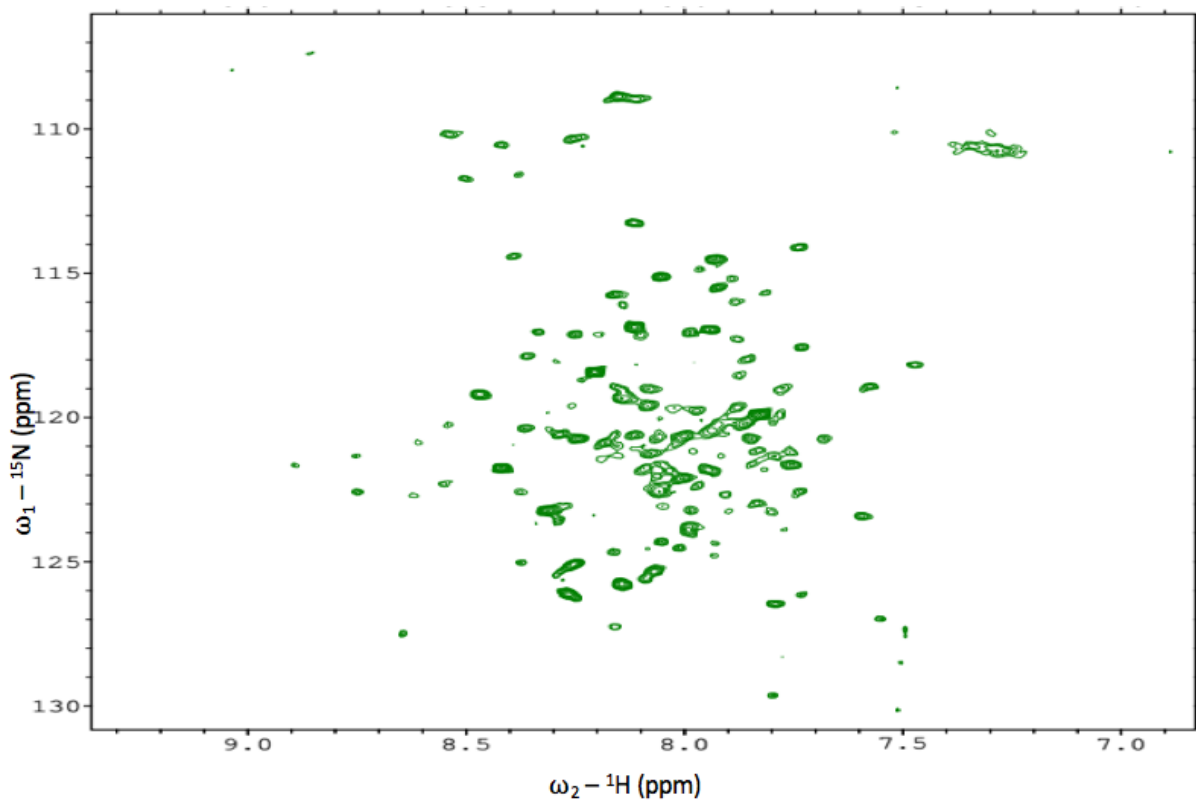
**Supplemental Figure 7: E1<sub>FTL→TVG</sub> Spectrum of Y74C Mutation**

This figure depicts the 2D TROSY spectrum of E1<sub>FTL→TVG</sub> with Y74C mutation at 50°C on a 600 MHz spectrometer.



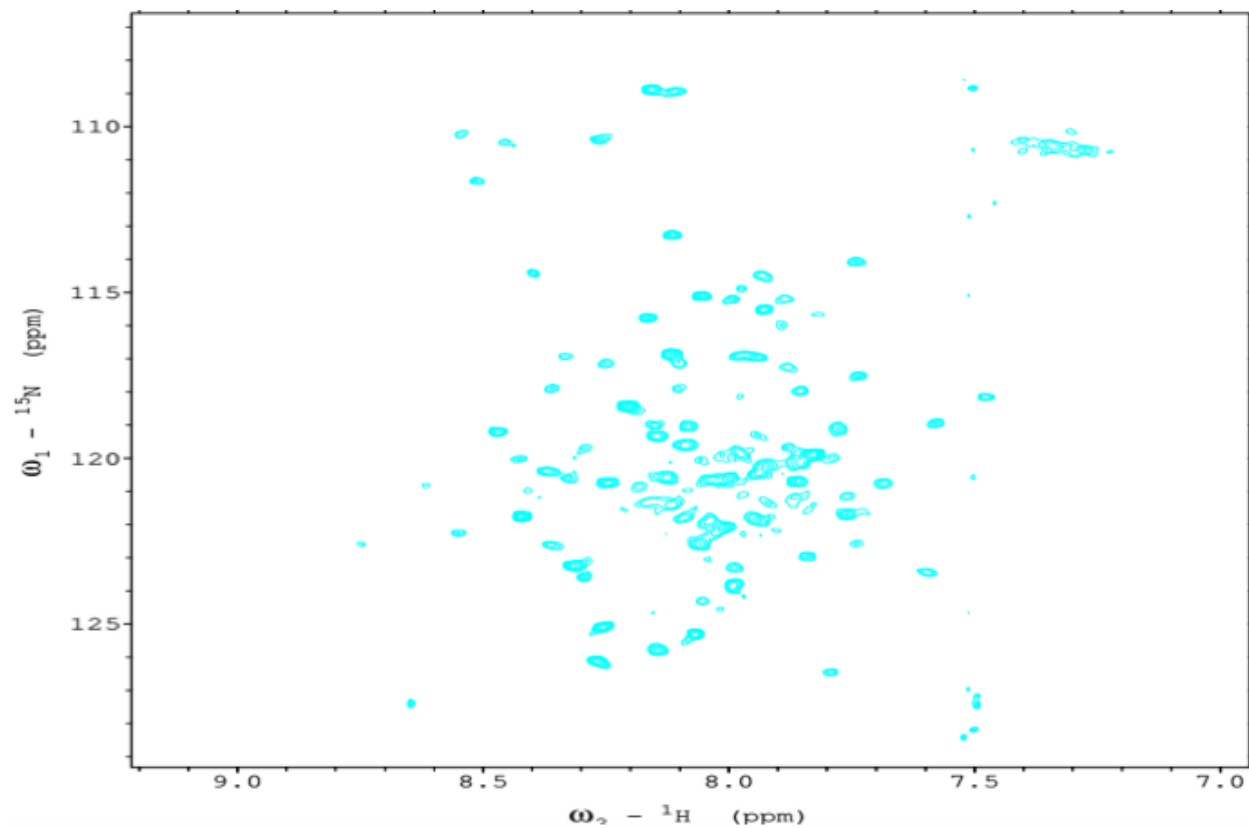
**Supplemental Figure 8: E1<sub>FTL→TVG</sub> Spectrum of Y65C Mutation**

This figure depicts the 2D TROSY spectrum of E1<sub>FTL→TVG</sub> with Y65C mutation at 50°C on a 600 MHz spectrometer.



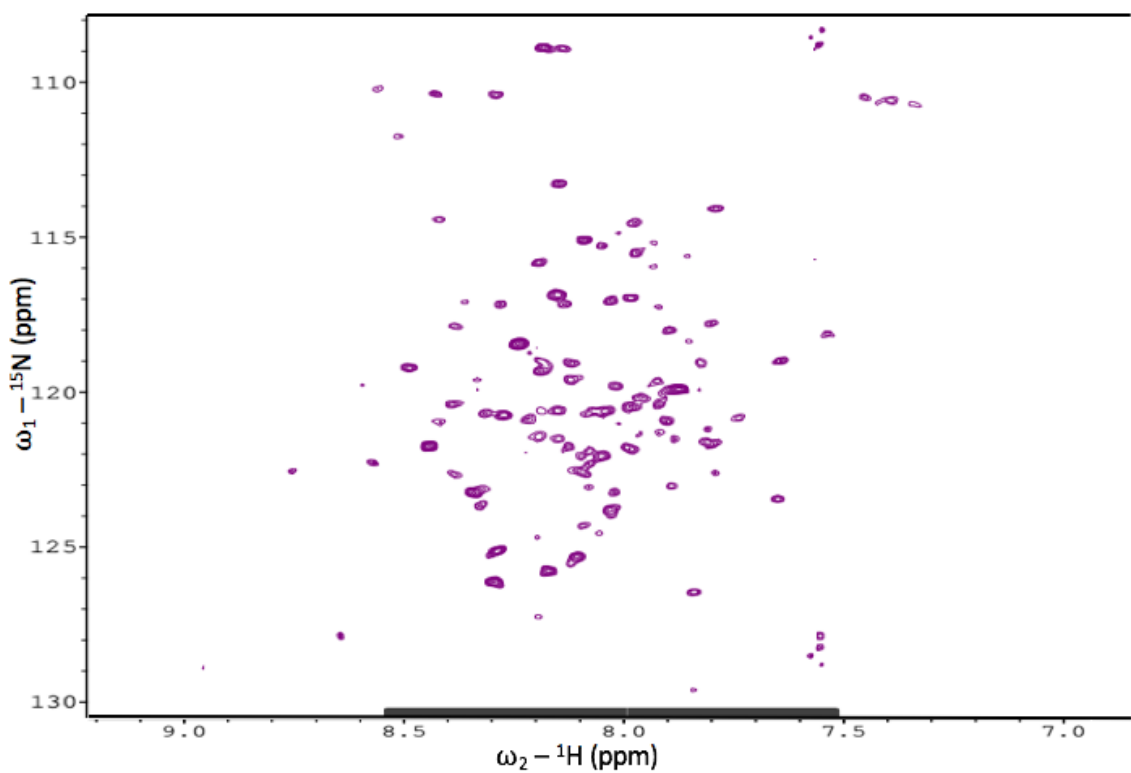
**Supplemental Figure 9: E1<sub>FTL</sub>→TVG Spectrum of S64C Mutation**

This figure depicts the 2D TROSY spectrum of E1<sub>FTL</sub>→TVG with S64C mutation at 50°C on a 600 MHz spectrometer.



**Supplemental Figure 10: E1<sub>FTL→TVG</sub> Spectrum of Y46C Mutation**

This figure depicts the 2D TROSY spectrum of E1<sub>FTL→TVG</sub> with Y46C mutation at 50°C on a 600 MHz spectrometer.



**Supplemental Figure 11: E1<sub>FTL→TVG</sub> Spectrum of A44C Mutation**

This figure depicts the 2D TROSY spectrum of E1<sub>FTL→TVG</sub> with A44C mutation at 50°C on a 600 MHz spectrometer.

## References

1. Fagerber L, Jonasson K, von Heijne G, Uhlen M, Berglund L (2010) Prediction of the human membrane proteome. *Proteomics* 10, 1141-1149.
2. Warschawski DE, Arnold AA, Beaugrand M, Gravel A, Chartrand E, Marcotte I (2011) Choosing membrane mimetics for NMR structural studies of transmembrane proteins. *BBA* 1808,1957-1974.
3. Seddon AM, Curnow P, Booth PJ (2004) Membrane proteins, lipids, and detergents: not just a soap opera. *BBA* 1666;105-117.
4. Kuo MM, Haynes WJ, Loukin SH, Kung C, Saimi Y (2005) Prokaryotic K(+) channels: from crystal structures to diversity. *FEMS Microbiol Rev* 29(5):961-985.
5. Buckingham SD, Kidd JF, Law RJ, Franks CJ, Sattelle DB (2005) Structure and function of two-pore-domain K<sup>+</sup> channels: contributions from genetic models organisms. *Trends Pharmacol Sci* 26(7):361-367.
6. Kuang Q, Purhonen P, Hebert H (2015) Structure of potassium channels. *Cell Mol Life Sci* 72:3677-3693.
7. Sanson MSP, Shrivastave IH, Bright JN, Take J, Capener CE, Biggin PC (2002) Potassium channels: structure, models, simulations. *BBA Biomembranes* 1565(2);294-307.
8. Doyle DA, Morais-Cabral JH, Pfuetzner RA, Kou A, Gulbis JM, Cohen SL, Chait BT, MacKinnon R (1998) The structure of the potassium channel: molecular basis of K<sup>+</sup> conduction and selectivity. *Science* 208(5360): 69-77.
9. Morais-Cabral JH, Zhou Y, MacKinnon R (2001) Energetic optimization of ion conduction rate by the K<sup>+</sup> selectivity filter/ *Nature* 414(6859):37-42.
10. Zhou Y, Marais-Cabral JH, Kaufman A, MacKinnon R (2001) Chemistry on ion coordination and hydration revealed by a K<sup>+</sup> channel-Fab complex at 2.0 resolution. *Nature* 414(6859)43-48.
11. Zhou Y, MacKinnon R (2003) The occupancy of ions in the K<sup>+</sup> selectivity filter: charge balance and the coupling of ion binding to a protein conformational change underlie high conduction rates. *J Mol Biol* 333(5):965-975.

12. Gutman GA, Chandy KG, Grissmer S, Lazdunski M, McKinnon D, Pardo LA, Robertson GA (2005) International union of pharmacology. LIII. nomenclature and molecular relationships of voltage-gated potassium channel. *Pharmacol Rev* 57(4);473-508.
13. Pal SK, Takimoto K, Aizenman E, Levitan ES (2006) Apoptotic surface delivery of K<sup>+</sup> channels. *Cell death Differ.* 13(4);661-667.
14. Deutsch C, Chen LQ (1993) Heterologous expression of specific K<sup>+</sup> channels in T lymphocytes: functional consequences for volume regulation. *PNAS USA* 90(21);10036-10040.
15. Wang Q, Curran ME, Splawski I, Burn TC, Millholland JM, VanRaay TJ, Shen J, Timothy KW, Vincent GM, de Jager T, Schwartz PJ, Toubin JA, Moss AJ, Atkinson DL, Landes GM, Connors TD, Keating MT (2006) Positional cloning of a novel potassium channel gene: KVLQT1 mutations cause cardiac arrhythmias. *Nat Genet* 12(1);17-23.
16. Curlo LG, Romera JG, Cortes DM, Perozo E (1998) pH-dependent gating in *Streptomyces lividans* K<sup>+</sup> channel *Biochem* 37(10);3220-3236.
17. Heginbotham L, LeMasurier M, Kolmakova-Partensky L, Miller C (1999) Single *streptomyces lividans* K(+) channels: Functional asymmetries and sidedness of proton activation. *J Gen Physiol* 114(4);551-560.
18. Shrivastava IH, Capener CE, Forrest LR, Sansom MSP (2000) Structure and dynamics of K channel pore-lining helices: A comparative simulation study. *J Biophys* 78(1);79-92.
19. Zhou M, MacKinnon R (2004) A mutant KcsA K(+) channel with altered conduction properties and selectivity filter ion distribution. *J Mol Biol* 338(4);839-846.
20. Shrivastava IH, Capener CE, Forrest LR,
21. Kerr ID, Son HS, Sankararamakrishnan R, Sansom MSP (1996) MOlecular dynamics simulations of isolated transmembrane helices of potassium channels. *Biopolymers* 39;503-515
22. Tieleman PD, Shrivastava IH, Ulnschneider MR, Sansom MSP (2001) Proline-induced hinge in transmembrane helices: Possible roles in ion channel gating. *Protein: Structure, Function, and Bioinformatics* 44(2);63-72.

23. Camino DD, Holmgren M, Liu Y, Yellen G (2000) Blocker protection in the pore of a voltage-gated K<sup>+</sup> channel and its structural implications. *Nature* 403(6767);321-215.
24. Del Camino D, Yellen G (2001) Tight steric closure at the intercellular activation gate of the voltage-gated K(+) channel. *Neuron* 32(4);649-656.
25. Schrodeder BC, Waldegger S, Fehr S, Bleich M, Warth R, Greger R, Jentsch TJ (2000) A constitutively open potassium channel formed by KCNQ1 and KCNE3. *Nature* 403(6766):196-9.
26. Campbell CM, Campbell JD, Thompson CH, Galimberti ES, Darbar D, Vanoye CG, George AL Jr (2013) Selective targeting of gain-of-function KCNQ1 mutations predisposing to atrial fibrillation. *Circ Arrhythm Electrophysiol* 6(5):960-966.
27. Neyroud N, Tesson F, Denjoy I, Leibovici M, Donger C, Barhanin J, Faure S, Gary F, Coumel P, Petit C, Schwartz K, Guicheney P (1997) A novel mutation in the potassium channel gene KVLQT1 causes the Jervell and Lange-Nielsen carioauditory syndrome. *Nat Genet* 15; 186-189.
28. Casimiro MC, Knollmann BC, Ebert SN, Vary JC Jr, Greene AE, Franz MR, Grinberg A, Huang SP, Pfeifer K (2001) Targeted disruption of the Kcnq1 gene produces a mouse model of Jervell and Lange-Nielsen Syndrome. *PNAS* 98; 2526-2532.
29. Lee MP, Ravenel JD, Hu RJ, Lustig LR, Tomaselli G, Berger RD, Brandenburg SA, Litzl TJ, Bunton TE, Limb C, Francis H, Gorelikow M, Gu H, Washington K, Argani P, Goldenring JR, Coffey RJ, Feinberg AP (2000) Targeted disruption of the Kvlqt1 gene causes deafness and gastric hyperplasia in mice. *J Clin Invest* 106;1447-1455.
30. Jespersen T, Grunnet M, Olesen SP. (2005) The KCNQ1 Potassium Channel: From Gene to Physiological Function. *Physiology* 20;408-416.
31. Robbins J. (2001) KCNQ Potassium Channels: Physiology, Pathophysiology, and Pharmacology. *Pharmacol. Ther.* 90:1–19.
32. Wrobel E, Tapken D, Seeböhm G (2012) The KCNE Tango- how KCNE1 interacts with Kv7.1. *Front Pharmacol.* 3;142.

33. McCrossan ZA, Abbott GW. (2004) The MinK-related Peptides. *Neuropharmacology* 47, 787-821. 10.1016/j.neuropharm.2004.06.018.
34. Nakajo K, Ulbrich MH, Kubo Y, Isacoff EY (2010) Stoichiometry of KCNQ1 - KCNE1 ion channel complex. *Proc Natl Acad Sci USA* 107(44): 18862-18867
35. Nakajo K, Ulbrich MH, Kubo Y, Isacoff EY (2010) Stoichiometry of KCNQ1 - KCNE1 ion channel complex. *Proc Natl Acad Sci USA* 107(44): 18862-18867
36. Wang KW, Goldstein SA (1995) Subunit composition of mniK potassium channels. *Neuron* 14;1303-1309.
37. Chen H, Kim LA, Rajan S, Xu S, Goldstein SA (2003) Charybdotoxin binding in the I<sub>Ks</sub> pore demonstrates two minK subunit in each channel complex. *Neuron* 40;15-23.
38. Morin TJ, Kobertz WR (2008) Counting membrane-embedded KNCE subunits in functioning K<sup>+</sup> channel complexes. *Proc Natl Acad Sci USA* 105;1478-1482.
39. Plant LD, Xiong D, Dai H, Goldstein SA (2014) Individual I<sub>Ks</sub> channels at the surface of mammalian cells contain two KCNE1 accessory subunits. *Proc Natl Acad Sci USA* 111;E1438-1446
40. Melman YF, Um SY, Krumerman A, Kagan A, McDonald TV (2004) KCNE1 binds to the KCNQ1 pore to regulate potassium channel activity. *Neuron* 42(6);927-937.
41. Kang C, Tian C, Sonnichens FD, Smith JA, Meiler J, George AL Jr, Vanoye CG, Kim HJ, Sanders CR (2008) Structure of KCNE1 and Implications for how it Modulates the KCNQ1 Potassium Channel. *Biochem.* 5;47(31):7999-8006. 10.1021/bio800875q.
42. Van Horn WD, Vanoye CG, Sanders CR (2011) Working model for the structural basis for KCNE1 modulation of the KCNQ1 potassium channel. *Curr Opin Struct Biol* 2;283-291.
43. Barhanin J, Lesage F, Guillemare E, Fink M, Lazdunski M, Romey G. (1996) K(V)LQT1 and IsK (minK) Proteins Associate to form the I(K<sub>s</sub>) Cardiac Potassium Current. *Nature* 384, 78–80. 10.1038/384078a0.
44. Abbott GW. (2016) KCNE1 and KCNE3: The Yin and Yang of Voltage-gated K<sup>+</sup> Channel Regulation. *Gene* 576:1-13. 10.1016/j.gene.2015.09.059.

45. Organ-Darlin LE, Vermon AN, Giovanniello JR, Lu Y, Moshal K, Roder K, Li W, Koren G. (2013) Interactions Between hERG and KCNQ1  $\alpha$ -subunits are Mediated by their COOH Termini and Modulated by cAMP. *Am. J Physiol Heart Circ Physiol* 304(4):H589-99. 10.1152/ajpheart.00385.2012.
46. Abbott GW (2015) The KCNE2 K<sub>v</sub> channel regulatory subunit: Ubiquitous influence, complex pathobiology. *Gene* 569(2):162-172.
47. Barro-Soria R, Ramentola R, Liina SI, Perez ME, Kass RS, Larsson PH. (2017) KCNE1 and KCNE3 Modulate KCNQ1 Channels by Affecting Different Gating Transitions. *PNAS* 114(35): E7367-E7376. 10.1073/pnas.1710335114.
48. Panaghi G, Tai KK, Abbott GW (2006) Interactions of KCNE subunits with the KCNQ1 K<sup>+</sup> channel pore. *J Physiol* 570; 455-467.
49. Peng D, Kim J, Kroncke BM, **Law CL**, Xia Y, Droegge KD, Van Horn WD, Vanoye CG, Sanders CR (2014) Purification and structural study of the voltage-sensor domain of the human KCNQ1 potassium ion channel. *Biochem* 53 (12), 2032-2042.
50. Osteen JD, Gonzalez C, Sampson KJ, Iyer V, Rebolledo S, Larsson HP, Kass RS (2010) KCNE1 alters the voltage sensor movements necessary to open KCNQ1 channel gate. *PNAS* 107(52);22710-22715.
51. The KCNQ1 Channel-Remarkable flexibility in gating allows for functional versatility (2015) *J Physio* 593(pt 12);2605-2615.
52. Kronke BM, Van Horn WD, Smith J, Kang C, Welch R, Song Y, Nannermann DP, Taylor KC, Sisco NJ, George AL, Meiler J, Vanoye CG, Sanders CR (2016) Structural basis for KCNE3 modulation of potassium recycling in epithelia. *Sci Adv* 2(9);e1501228.
53. Melman YF, Krumerman A, McDonald TV. (2002) A Single Transmembrane Site in the KCNE-encoded Proteins Controls the Specificity of KvLQT1 Channel Gating. *J. Biol. Chem.* 277, 25187-25194.
54. Melman Y, Domenech A, Luna S, McDonald TV (2000) Structural Determinants of KvLQT1 Control by the KCNE Family of Proteins. *J. Biol. Chem.* 276(9), 6439-6444.

55. Tian C, Vanoye CG, Kang C, Welch RC, Kim HJ, George AL, Sanders CR (2007) Preparation, functional characterization, and NMR studies of human KCNE1, a voltage-gated potassium channel accessory subunit associated with deafness and long QT syndrome. *Biochem* 46(41); 11459-11472.
56. Ohori Y, Okazaki H, Wantabe S, Tochio N, Arai M, Kigawa T, Nishimura C (2013) Flexible and ridged structure in HIV-1 p17 matrix protein monitored by relaxation and amide proton exchange with NMR. *BBA* 1844; 520-526.
57. Hwang T, Zijl PCM, Mori S (1998) Accurate quantitation of water-amide proton exchange rates using the Phase-Modulated CLEAN chemical EXchange (CLEANEX-PM) approach with a Fast-HSQC (FHSQC) detection scheme. *J Biomolec NMR*. 11; 221-226.
58. Wallin E, von Heijne G. (1998) Genome-wide analysis of integral membrane proteins from eubacterial, archaean, and eukaryotic organisms. *Protein Sci*. 7:1029–1038.
59. Ahram M, Litou ZI, Fang R, Al-Tawallbeh G (2006) Estimation of membrane proteins in the human proteome. *In Silico Biol*. 6:379–386.
60. Verardi R, Traaseth NJ, Masterson LR, Vostrikov VV, Veglis (2012) Isotope labeling for solution and solid-state NMR spectroscopy of membrane proteins. *Adv Exp Med Biol* 992; 35-62.
61. Whittaker JW (2007) Selective isotopic labeling of recombinant proteins using amino acid auxotroph strains. *Pichia Protocols* 389; 175-187.
62. Kim HJ, Howell SC, Van Horn WD, Jeon YH, Sanders CR (2009) Recent advances in the application of solution NMR spectroscopy to multi-span intergral membrane proteins. *Prog Nucl Magn Reson Spectrosc*. 55, 335-360.
63. Law CL, Sanders CR (2019) NMR resonance assignments and secondary structure of a mutant form of the human KCNE1 channel accessory protein that exhibits KCNE3-like function. *Biomolecular NMR Assignments*.  
<https://doi.org/10.1007/s12104-018-09867-6>.
64. Harbers M (2008) The current status of cDNA cloning. *Genomics* 91(3);323-242.
65. Rosano GL, Ceccarelli EA (2014) Recombinant protein expression in *Escherichia coli*: advances and challenges. *Front Microbiol* 17, 172.

66. Tian C, Karra MD, Ellis CD, Jacob J, Oxeniod K, Sonnichsen F, Sanders CR (2005) Membrane proteins preparation for TROSY NMR screening. *Methods in Enzymology* 394,321-334.
67. Nilsson J, Persson B, von Heijne G (2005) Comparative analysis of amino acid distributions in integral membrane proteins from 107 genomes. *Proteins: Struct., Funct, Bioinf* 60(4);606-616.
68. Raschle T, Hiller S, Etkorn M, Wagner G (2010) Non-micellar systems for solution NMR spectroscopy of membrane proteins. *Curr Opin Struct Biol* 20(4);471-479.
69. Zhang R, Sahu ID, Lui L, Osatuke A, Comer RG, Dabney-Smith C, Lorigan GA (2014) Characterizing the structure of lipodisq nanoparticles for membrane protein spectroscopic studies. *BBA* 1848, 329-333.
70. Sahu ID, McCarrick M, Troxel KR, Zhang R, Smith HJ, Dunagan MM, Swartz MS, Rajan PV, Kroncke BM, Sanders CR, Lorigan GA (2013) DEER EPR measurements for membrane protein structure via bifunctional spin labels and lipodisq nanoparticles. *Am Chem Soc.* 52, 6627-6632.
71. Sanders CR, Oxenoid (2000) Customizing model membranes and samples for NMR spectroscopic studies of complex membrane proteins. *BBA* 1508, 129-145.
72. Bornhorst JA, Falke JJ (2010) Purification of proteins using polyhistidine affinity tags. *Method Enzymol* 326, 245-254.
73. Marion D (2013) An introduction to biological NMR spectroscopy. *Mol Cell Proteomics* 12(11) 3006-3025.
74. Fernandez C, Wider G (2003) TROSY in NMR studies of the Structure and Function of large biological macromolecules. *Curr Op Struc Bio* 13,570-580.
75. Pervushin K, Riek R, Wider G, Wuthrick K (1997) Attenuated T2 relaxation by mutual cancellation of dipole-dipole coupling and chemical shift anisotropy indicates an avenue to NMR structures of very large biological macromolecules in solution. *PNAS USA* 94 (23), 12366-12371.

76. Salzmann M, Wider G, Pervushin K, Senn Hans, Wuthrich K (1999) TROSY-type triple-resonance experiments for sequential NMR assignments of large proteins. *JACS* 12(4); 844-848.
77. Frueh DP (2014) Practical aspects of NMR signal assignment in large and challenging proteins. *Progress in Nuclear Magnetic Resonances Spectroscopy* 78;47-75.
78. Omasits U, Ahrens CH, Muller S, Wollscheid B (2014) Protter: interactive protein feature visualization and integration with experimental proteomic data. *Bioinformatics* 30(6): 884-886.
79. Shen Y, Bax A (2013) Protein backbone and sidechain torsion angles predicted from NMR chemical shifts using artificial neural networks. *J Biomol NMR* 56(3); 227-241.
80. Peng D, Kim J, Kroncke BM, Law CL, Xia Y, Droege KD, Van Horn WD, Vanoye CG, Sanders CR (2014) Purification and structural study of the voltage-sensor domain of the human KCNQ1 potassium ion channel. *Biochem* 53 (12), 2032-2042.
81. Dong H, Sharma M, Zhou H, Cross TA (2012) Glycines: Role in  $\alpha$ -helical membrane protein structure and a potential indicator for native conformations. *Biochem* 51(24); 4779-4789.
82. Kimple ME, Brill AL, Pasker RL (2013) Overview of affinity tags for protein purification. *Curr Protoc Protein Sci* 73,9.9.
83. Zhu G, Xia Y, Nicholson LK, Sze KH (2000) Protein dynamics measurements by TROSY-based NMR experiments. *J Magn Reson* 143(2);423-426.
84. Cao Z, Bowie JU (2012) Shifting hydrogen bonds may produce flexible transmembrane helices. *PNAS* 109;8121-8126.
85. Sahu ID, Kronke BM, Zhang R, Dunagan MM, Smith HJ, Craig A, McMarrick RM, Sanders CR, Lorigan GA (2014) Structural investigation of the transmembrane domain of KCNE1 in proteoliposomes. *Biochem* 53(40); 6392-640
86. Melman YF, Domenech A, de la Luna S, McDonalds TV (2001) Structural determinants of KvLQT1 control by the KCNE family of proteins. *J Biol Chem* 276;6439-6444

87. Melam YF, Um SY, Krumerman A, Kagen A, McDonald TV (2004) KCNE1 binds to the KCNQ1 pore to regulate potassium channel activity. *Neuron* 42; 927-937.
88. Panaghie G, Tai KK, Abbott GW (2006) Interactions of KCNE subunits with the KCNQ1 K<sup>+</sup> channel pore *J Physiol* 570;455-467.
89. Petros AM, Muller L, Kopple KD (1990) NMR identification of protein surfaces using paramagnetic probes. *Biochem* 29(43);10041-10048.
90. Beel AJ, Mobley CK, Kim HJ, Tian F, Hadziselimovic A, Jap B, Prestegard JH, Sanders CR (2008) Structural Studies of the transmembrane C-terminal domain of the amyloid precursor protein (APP): Does APP function as a cholesterol sensor? *Biochem* 47(36) 9428-9446.
91. Deatherage CL, Lu Z, Kronke BM, Ma S, Smith JA, Voehler M, McFeeters RL, Sanders CR (2017) Structural and biochemical differences between the Notch and the amyloid precursor protein transmembrane domains. 3(4);e1602794.
92. Coey AT, Sahu ID, Gunasekera TS, Troxel KR, Hawn JM, Swartz MS, Wickenheiser MR, Reid R, Welch RC, Vanoye CG, Kang C, Sanders CR, Lorigan GA (2011) Reconstruction of KCNE1 into lipid bilayers: Comparing the structural dynamics, and activity differences in micelle and vesicle environments. *Biochem* 50(50);10851-10859.
93. Battiste JL, Wagner G (2000) Utilization of site-directed spin labeling and high-resolution heteronuclear nuclear magnetic resonance for global fold determination of large proteins with limited nuclear overhauser effect. *Biochem* 39(18);5355-5365.
94. Schwieters CD, Kuszewski JJ, Tjandra N, Clore GM (2003) The Xplor-NIH NMR molecular structure determination package. *J Magn Res* 160(1); 65-73.
95. Sanders CR, Sonnichsen F (2006) Solution NMR of membrane proteins: practice and challenges. *Magn Recon Chem* 44.S24-S40.

